Review

Recent development in graphitic carbon nitride based photocatalysis for hydrogen generation

Muhammad Salman Nasir[a], Guorui Yang[a,b,*], Iqra Ayub[c], Silan Wang[a], Ling Wang[a], Xiaojun Wang[a], Wei Yan[a,*], Shengjie Peng[d], Seeram Ramakarishna[d]

[a] Department of Environmental Science & Engineering, State Key Laboratory of Multiphase Flow in Power Engineering Xi'an Jiaotong University, Xi'an 710049, China
[b] Xi'an Jiaotong University Suzhou Institute, Suzhou 215123, China
[c] School of Chemical Engineering and Technology, State Key Laboratory of Multiphase Flow in Power Engineering Xi'an Jiaotong University, Xi'an 710049, China
[d] Department of Mechanical Engineering, National University of Singapore, 117574 Singapore

ABSTRACT

The future energy crisis and environmental degradation can only mitigate by harvesting solar energy into renewable, safe, economical and clean technology like water splitting. The graphitic carbon nitride has an attractive band structure, good chemical stability, earth-abundant and significantly easily fabricated which makes an application for the generation of hydrogen by water splitting. In this paper, we try to critically focus on the current progress and future development of the different strategies of water splitting using graphitic carbon nitride (g-C_3N_4) for hydrogen generation. In this context, we discuss recent strategies like metal and non-metal doping (electronic structure), morphology tuning (geometric structuring), use of mediators (Z-scheme technology), defects engineering, plasmonic materials, dye-sensitization, perovskite oxides, carbon nitrides, carbon dots, metal organic framework, and a bimetallic cocatalyst. Finally, we summarize the recent advances and future developments of g-C_3N_4 bases photocatalysis.

1. Introduction

The energy crises have been a great challenge for increasing population and industrialization in recent decades. The energy demand of the world is mostly depending on non-renewable sources (coal, fossil fuels, petrol, oil, etc.) which are depleting day by day. [1] It reported that the energy required by the world is about two times of its existing energy supply by 2050 [2]. These energy sources are also the primary source of greenhouse gases after consumption that is detrimental to the environment [3]. The renewable energy sources are the best alternative that can address these issues. There are so many environment-friendly energy resources like hydroelectricity, biomass, wind, geothermal energy and solar light (solar drying, solar cooking), etc [4,5]. To alleviate the future energy crisis and environmental degradation, the conversion of solar energy into chemical energy via photosynthesis is a sensible approach. The harvesting of solar light can produce environment-friendly hydrogen gas because it only produces water or water vapors after burning with oxygen. Accordingly, the production of hydrogen gas as an energy source can help to meet the future energy demand and address the environmental problems.

Hydrogen is considered as a clean source of solar energy having heat value 120–142 MJ kg^{-1} among other hydrocarbon fuels. [6] At present, the worldwide production of hydrogen is more than 44.5 million tons [7], and it will be the primary source of energy up to 2080 [8].Although there are many techniques to produce hydrogen, photocatalytic water splitting is a promising approach as it has gained significant devotion for its different potential in environment and energy applications [9–20]. The artificial photosynthesis is one of the only green solutions to deliver the future crisis of energy and environment. [21–32]

1.1. Photocatalytic water splitting

Photocatalysis is the chemical process of harvesting solar energy which considered renewable, safe, economical and clean technology mainly includes water splitting, [33–37] reduction of CO_2, [38–42] degradation of pollutants [43–50], bacterial disinfection [51–53] and organic synthesis [54–57]. In semiconducting photocatalyst, after the light incident electron jumps to the conduction band (CB) while hole generates at valence band (VB), and then they transfer to the photocatalyst surface for the redox reaction [58]. The water splitting consists

of two half-reactions, water oxidation which produces oxygen (OER) and water reduction which produce hydrogen (HER) Eqs. (1)–(3). To sustain the water splitting process, the two reactions OER and HER should co-occur for the flow of electron.

Overall water splitting:

$$2H_2O + hv \rightarrow 2H_2 + O_2 \qquad (1)$$
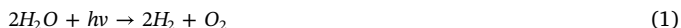
Oxygen evolution Reaction (OER)

$$2H_2O \rightarrow 4H^+ + 4e^- + O_2 \qquad (2)$$

Hydrogen evolution reaction (HER)

$$4H^+ + 4e^- \rightarrow 2H_2 \qquad (3)$$

Moreover, for photocatalytic water splitting the change of Gibbs free energy $+237.2\,kJ\,mol^{-1}$ is required for the splitting of one molecule of water into H_2 and $\frac{1}{2}O_2$ having 1.23 V required potential while the potential of the highest level of photocatalyst VB should be more positive than 1.23 V vs. Normal hydrogen electrode (NHE) and the potential of the CB should be more negative than 0 V vs. NHE. Fig. 1 shows the different bandgaps as well as VB and CB positions of the selected oxides, nitrides and chalcogenides semiconductor photocatalyst which are suitable for OER and HER [59].

The overall photocatalytic reaction takes place in six steps include photon absorption, separation of an electron-hole pair, carrier diffusion, transport carriers, catalytic reaction, and mass transfer. These six steps can be divided into three main categories: light absorption, charge separation and transport, and surface reaction. [60] To get maximum solar conversion efficiency, the material should meet the three requirements. Firstly, it is essential to harvest a visible portion of light that is about 45% of the total solar spectrum [58]. Secondly, it should be more electrically conductive (EC) otherwise more electron-hole recombines at the surface during transportation.

Moreover, due to the dominance of charge recombination that takes place on the surface of the semiconductor (Fig. 2), it is estimated that only 10% of photogenerated electron-hole pairs are available for water splitting. [61] Third, the surface of the catalyst should be more active for the redox reaction. So, our principal focused on three main aspects: enhanced the light absorption, reduce charge recombination and surface kinetics.

If we talk solar conversion efficiency by visible light harvesting than an essential requirement for photocatalyst should a low electronic band gap, long carrier lifetime, earth-abundant, chemically stable and non-toxic. Unfortunately, many prominent semiconductors have a wide band gap and absorb light below 400 nm as shown in Fig. 2. The conversion efficiency can be increased by 16% if there is a possibility to harvest solar light up to 600 nm and can be further expanded up to 32% if 800 nm range light can capture. To solve this issue doping is an efficient technique which discuss in detail in section 2.

Apart from light absorption, charge recombination is also the main

factor that decreases the photocatalytic action. After absorption of light, electron holes generated which takes part in redox reaction as it transfers to the surface and at that time it recombines with each other which affect the efficiency of solar conversion. To overcome this issue, many strategies have been used to shorten the transfer distance and increase the EC of material or by forming a heterojunction with other noble metals. [62] At last, all the charge carriers accumulate at the surface of a photocatalyst that shows the low activity of water splitting. These accumulations also increase the charge recombination as well as damage the stability of photocatalyst [63]. It found that particular kind of catalyst namely bimetallic co-catalyst can be useful for accelerating surface kinetics. [64].

Furthermore, the charge recombination also retarded the hydrogen evolution which can be accomplished by using electron donor molecules or hole scavenger. It has been studied by many researchers that the overall water splitting using different photocatalyst is difficult without using sacrificial agents because the splitting of water is an uphill reaction and these agents help to prevent the recombination by holes depletion or providing the hydrogen atoms for the hydrogen production [65–69]. Guzman et al., studied the role of methanol as sacrificial agent for the hydrogen production and they found that CH_3OH has an ability to produce an electron donor and inoculate it to the conduction band that enhance the hydrogen evolution potential [70]. A very recent study has revealed the importance of different sacrificial agents for the photocatalytic hydrogen production. The authors concluded that the selection of sacrificial agents for specific photocatalyst is very imperative. Table 1 also shows the importance and comparison of different sacrificial agents regarding hydrogen evolution with g-C_3N_4 as photocatalyst. Till now only Zhang et al has reported the water splitting without use of sacrificial agent by g-C_3N_4 conjugated polymer via four electron pathways modified with Pt for the hydrogen and oxygen generation in a 2:1 stoichiometric molar ratio [71]. The nanocomposite had TON of 3.1 mol of hydrogen and oxygen per mole of g-C_3N_4 photocatalyst and it remain stable in water and under visible light.

1.2. Graphitic carbon nitride (g-C_3N_4)

To satisfy the requirements of solar energy conversion efficiency the large band gap and charge recombination is remain the bottleneck for the researchers. Therefore, in search of the active photocatalyst, an active polymeric semiconductor named as graphitic carbon nitride (g-C_3N_4) has provoked a new wave of excitement in the future research generation. The graphitic carbon nitride has alluring band structure, good chemical stability, earth-abundant [72–76] and significantly easily manufactured from nitrogen-rich precursor-like melamine [77–85], cyanamide [86–90], dicyandiamide [82,91–98], thiourea [99–102], urea [103–106], and ammonium thiocyanate [107].

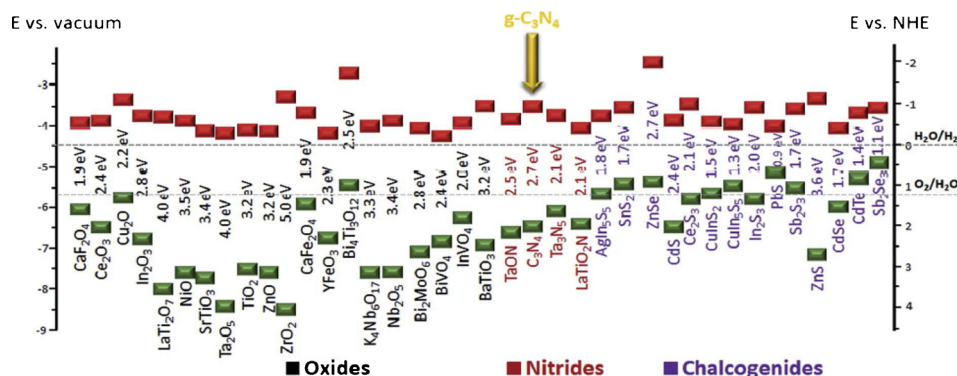Among the synthetic polymers, it is the oldest in the scientific

Fig. 1. Bandgap, CB (green) and VB (red) positions of the different oxides, nitrides and chalcogenides w.r.t the vacuum level of NHE. The two dashed line indicates the water redox reaction potentials. Reproduced with permission. [59] Copyright 2015 Wiley.
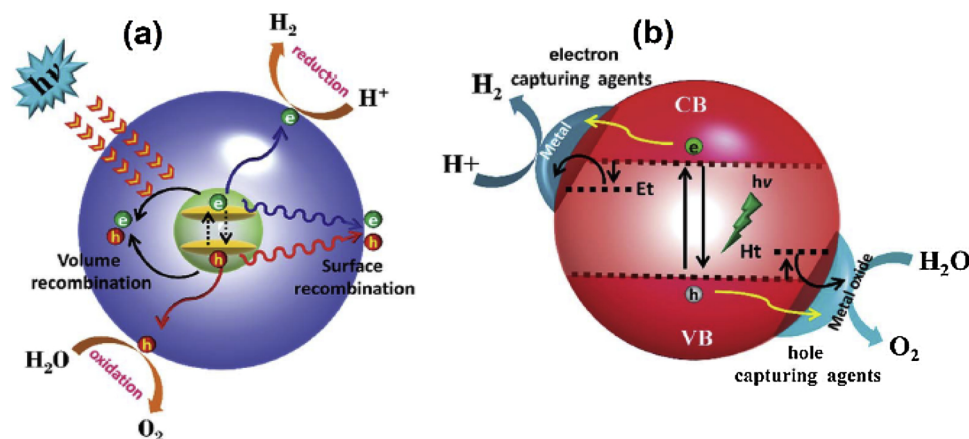
Fig. 2. (a) Schematic illustration of the Charge generation, separation, recombination, and conversion process in photocatalyst and (b) facilitation of charge separation by electron and hole capturing agents. Reproduced with permission [61] Copyright 2015 Royal Society of Chemistry.

research history. The first polymer and precursor of C_3N_4 discovered by Berzelius and called by Liebig (Fig. 3) in 1834 which is an embryonic form of melon and interconnected with tri-s-triazine using nitrogen. [108,109] From 2006 the use of carbon nitride started in the field of heterogeneous catalysis [110]. Wang et al. in 2009, first discovered g-C_3N_4, a non-metal conjugated semiconductor photocatalyst for hydrogen generation. [111] There are seven different phases of g-C_3N_4 as α-C_3N_4, cubic C_3N_4, β-C_3N_4, pseudo-cubic C_3N_4, g-o-triazine, g-h-triazine, and g-h-heptazine having bandgap 5.49, 4.13, 4.85, 4.30, 0.93, 2.97 and 2.88 eV, respectively. [112] To establish g-C_3N_4 allotropes, the basic tectonic units are triazine (C_3N_4), and tri-s-triazine/heptazine (C_6N_7) rings as shown in Fig. 4. [113,114] The most favorable and energetically stable phase of C_3N_4 among all of these is tri-s-triazine-based g-C_3N_4 at ambient conditions. [115].

Most of the works indicated that most suitable patterns were tecton because the polycondensation of cyanamide, melamine, dicyandiamide made a polymer of melon from melem. [116–120] It has the lowest bandgap due to the existence of sp^2 hybridized nitrogen and carbon which established the π-conjugated band structures. [86] The graphitic carbon nitride has a band gap of 2.7–2.8 eV and has an excellent visible light response up to 460 nm [121]. Despite all the exciting properties of g-C_3N_4, the practical application still obstructed by numerous complications and inadequacies of pristine g-C_3N_4 like lacking solar light absorption, low surface area and the fast recombination of charges. Therefore, there are different modification techniques such as doping, [122–126] heterojunctions [127–132], morphological tuning [133–139], perovskite type oxide [140–144], metal-organic framework [145–147], defects engineering [148–151], Z-scheme technology [139,152–156], Dye-sensitization of g-C_3N_4, [157–160] Co-catalyst [161–165] and surface plasmon resonance are adopted to enhance the photocatalytic activity.

Till now there have been many exciting reviews about the history, synthesis method, properties, applications and strategies for improving photocatalysis performance of g-C_3N_4. However, there is a quick advancement in this area, but a comprehensive review about water splitting using g-C_3N_4 and focusing on hydrogen production still lacks to deliver the readers a complete picture of the recent improvement in this area. Herein, we try to critically focus on the current progress and development of the different strategies of water splitting by g-C_3N_4 and hydrogen generation. In this context, we divide the article into different categories like, metal and non-metal doping (electronic structure), morphology tuning (geometric structuring), use of mediators (Z-scheme technology), defects engineering, plasmonic materials, dye-sensitization, perovskite oxides, carbon nitrides, carbon dots, metal organic framework, and bimetallic cocatalyst. We hope that this review will provide a comprehensive detail about g-C_3N_4 photocatalyst to the

readers from every perspective.

2. Reduced bandgap

2.1. Doping (electronic structure)

The semiconductor photocatalysts have affected by different parameters like wide bandgap limit the absorbance of visible light and the redox potential. The doping is one of the techniques to tune the band gap of semiconductor photocatalyst and enhance the visible light absorption. [62,72,166–168] The introduction of metallic and non-metallic impurities in the system endows the photocatalytic properties which lower the band gap energy, tune the harvesting of sunlight and other physical properties [115,169–171]. There have been different research conducted to reduce the bandgap of g-C_3N_4 material. [62] The doping of metal and non-metal such as iron (Fe) [172–174], Iodine (I) [92,175,176], Sodium (Na) [177–180], Lithium (Li) [178], Carbon (C) [181–183], Zinc (Zn) [184,185], Fluorine (F), Oxygen (O) [186–189], Nitrogen (N) [190,191], Sulphur (S) [192,193], Phosphorus (P) [126,178,194,195], Boron (B) [196–198], and some combinations have been widely investigated [199–203].

As we concern the metal doping, the soluble salt is always homogeneously mixed with the g-C_3N_4 precursor so that impurities will equally be doped into the g-C_3N_4 during the thermal condensation process. Metal doping techniques have been proven effective to enhance the light absorption, reduce the band gap and increase the photocatalytic performance. [62,204] It could bind the structure of g-C_3N_4 through weak ligation and forming a strong hybrid material which made it an excellent photocatalytic material. There is a strong interaction between metal cations and the electron-rich sp^2 nitrogen in the nitrogen pots of g-C_3N_4. [172,177] The metal doping increases the photocatalytic activity because it acts as an electron and improve the charge movement rate and efficiently control the electron-hole separation [205]. The Fe ions help to customize the electronic properties of g-C_3N_4 [206] Gau et al. [207], prepared iron doped novel 2D carbon nitride (Fe-g-CN) by using the mild one-pot method. After mixing the precursors formamide and citric acid with a metal salt, the reagents are preorganized into the polymeric structure. The as-prepared photocatalyst showed hydrogen production approximately 16.2 mmol $g^{-1} h^{-1}$ and AQE of 0.8%. It also investigated that iron doping with carbon nitride formed a unique structure that favors the charge transfer process and it will increase the generation efficiency of hydrogen. In this system, the unique electronic structure of two-dimensional materials and strong electron coupling between metal dopant and g-C_3N_4 planar delocalized electrons facilitated the electron transfer and enhances the hydrogen generation. In another study, iron is doped by one

Table 1
Comparison and Summary of the photocatalytic performance of g-C_3N_4 based photocatalytic water splitting.

	Photocatalyst	Co-catalyst	Reaction Condition or sacrificial agent	Light Source	Reaction rate (H_2 evolution)	Stability	AQY (%)	Ref.
Heteromolecular Doping	$(FeTPP)_2O/$ g-C_3N_4	$(FeTPP)_2O$ (5 wt%)	10 mL of TEOA	300 W Xe lamp with a 420 nm cutoff filter	14.5 µmolh^{-1}	N/A	0.04 (420 nm)	[105]
	ABN- g-C_3N_4	ABN (5 wt%) Pt (3 wt%)	100 m L of TEOA (10 vol %)	300W Xe lamp with Cutoff filter ($\lambda > 420$ nm)	147 µmol h^{-1}	> 20h	N/A	[429]
	ABN/g-C_3N_4	N/A	TEOA	300W Xe lamp with Cutoff filter ($\lambda > 455$ nm)	260 µmol h^{-1}	N/A	N/A	[430]
	ADHP/g-C_3N_4	N/A	TEOA	300 W Xe lamp with a 420 nm cutoff filter	204 µmol h^{-1}	N/A	3.4	[431]
	ATCN modified g-C_3N_4	Pt (3 wt%)	100 m L of TEOA (10 vol %)	300W Xe lamp with Cutoff filter ($\lambda > 420$ nm)	85 µmolh^{-1}	N/A	8.8 (420 nm)	[431]
	ATCN modified hollow g-C_3N_4 nanosphere	ATCN (5 wt%) Pt (3 wt%)	100 m L of TEOA (10 vol %)	300W Xe lamp with Cutoff filter ($\lambda > 455$ nm)	278 µmol h^{-1}	> 16h	N/A	[430]
	P_3HT/g-C_3N_4	P_3HT (3 wt%)	10 mL of water containing AA	300W Xe lamp with Cutoff filter ($\lambda = 420$ nm)	3045 µmolh^{-1}	70% activity after 23 days	77.4 (420 nm)	[432]
	BA/g-C_3N_4	N/A	TEOA	300W Xe lamp with Cutoff filter ($\lambda > 455$ nm)	240 µmol h^{-1}	N/A	N/A	[430]
	BA-modified g-C_3N_4	BA (5 wt%), Pt (3 wt%)	100 m L of TEOA (10 vol %)	500W Xe lamp with Cutoff filter ($\lambda > 300$ nm)	253.1 µmol h^{-1}	> 25h	N/A	[433]
	DAMN/g-C_3N_4	N/A	TEOA	300 W Xe lamp with a 420 nm cutoff filter	350 µmol h^{-1}	N/A	N/A	[430]
	DCDA/ATCN/Pt	ATCN (0.01 g), DCDA (3 g) Pt (3 wt%)	100 m L of TEOA (10 vol %)	300W Xe lamp with water cooling filter ($\lambda > 420$ nm)	131 µmol h^{-1}	N/A	N/A	[434]
	Ppy/ g-C_3N_4	Ppy (1.5 wt%)	100 m L of DI water	300W Xe lamp with Cutoff filter ($\lambda = 400$ nm)	385.15 µmol	N/A	N/A	[435]
Hybrids	C, N-TiO_2/ g-C_3N_4	C, N-TiO2 (3.0 wt %)	100 m L of TEOA (10 vol %)	300 W Xe lamp with a 400 nm cutoff filter	39.18 µmolg^{-1} h^{-1}	> 32h	N/A	[436]
	C_2/ g-C_3N_4	N/A	5 vol% TEOA AA	300W Xe lamp with Cutoff filter ($\lambda = 400$ nm)	281 TON	N/A	N/A	[437]
	C_3N_4/Ni-Tu-TETN	N/A	70 mL water and 10 mL	300W Xe lamp with a solar simulator filter	51 µmol h^{-1}	N/A	0.2 (420 nm)	[438]
	CdS/ g-C_3N_4	g-C_3N_4 (2 wt%)	80 m L of 0.35 M Na_2S and 0.25 Na_2SO_3	300 W Xe lamp with a 420 nm cutoff filter	4152 µmolg^{-1} h^{-1}	> 12h	4.3 (420 nm)	[439]
	CdS/g-C_3N_4	N/A	Lactic acid	300 W Xe lamp with a 420 nm cutoff filter	22.5 µmolh^{-1}	> 16h	N/A	[440]
	CdS/g-C_3N_4	N/A	0.35 M Na_2S and 0.25 M Na_2SO_3	300 W Xe lamp with a 420 nm cutoff filter	83 µmolh^{-1}	N/A	N/A	[441]
	CNS/g-C_3N_4	N/A	TEOA	300 W Xe lamp with a 420 nm cutoff filter	50 µmol h^{-1}	> 16h	N/A	[442]
	CoPi/g-C_3N_4	N/A	120 m L of solution containing 25% methanol by volume	300W Xe arc lamp with UV Cutoff filter ($\lambda > 400$ nm)	194.8 µmolg^{-1} h^{-1}	> 48h	N/A	[443]
	CoPi/mpg-CNx	Co (10% w/w)	20 m L phosphate buffer solution	Visible light ($\lambda > 400$ nm)	626.4 µmolg^{-1} h^{-1}	> 24h	N/A	[444]
	CoS/mpg-CN	CoS content	100 m L of TEOA (10 vol %)	300 W Xe lamp with a 420 nm cutoff filter	36.5 µmolh^{-1}	> 20h	N/A	[445]
	C-PDA/ g-C_3N_4	C-PDA (1.5 wt%) Pt (1.5 wt%)	300 m L of TEOA (10 vol %)	300 W Xe lamp with a 400 nm cutoff filter	81.1 µmol h^{-1}	> 10h	2.3 (420 nm)	[446]
	CQD/ g-C_3N_4 nanosheets	CQD (1.0 wt%)	10 mL of solution containing methanol (20 vol%)	1000 W Xe lamp with a 420 nm cutoff filter	50.5 µmolg^{-1} h^{-1}	N/A	1.4 (405 nm)	[447]
	Cu (OH)$_2$/ g-C_3N_4	Cu (OH)$_2$ (0.34 mol %)	80 m L mixed solution of methanol and water (1:3)		48.7 µmol h^{-1}	> 28h	N/A	[448]

4

(*continued on next page*)

Table 1 (*continued*)

Photocatalyst	Co-catalyst	Reaction Condition or sacrificial agent	Light Source	Reaction rate (H_2 evolution)	Stability	AQY (%)	Ref.
			300 W Xe lamp with a 400 nm cut off filter				
Fluorinated polymeric g-C_3N_4	NH$_4$F (2.0 g) Pt (3 wt%)	100 m L of TEOA (10 vol %)	500 W Xe lamp with a 420 nm cutoff filter	12.8 µmol h^{-1}	N/A	N/A	[120]
g-C_3N_4 quantum dots	Pt (1.0 wt%)	100 m L of TEOA (10 vol %)	300 W Xe lamp with a 420 nm cutoff filter	137.84 µmol h^{-1}	N/A	N/A	[449]
g-C_3N_4/ nanocarbon/ ZnIn$_2$S$_4$	ZnCl2 (0.136 g) InCl$_3$ (0.586 g) g-C_3N_4 (0.047 g)	80 m L of 0.35 M Na$_2$S and 0.25 M Na$_2$SO$_3$	Four low power UV-LEDs (3 W, 420 nm)	29.97 µmol h^{-1}	N/A	N/A	[424]
g-C_3N_4/ hydrogenase /NiP	Hydrogenase	Solution of EDTA (0.1 M, 3 mL)	1000 W halogen lamp with a AM 1.5 G filter (100 mW/cm2, λ > 300 nm)	9135 TON	N/A	0.07	[450]
g-C_3N_4/KCl	N/A	100 m L of TEOA (10 vol %)	300 W Xe lamp with a water cooling filter (λ > 420 nm)	0.332 mmolg^{-1}-h^{-1}	N/A	7.2 (420 nm)	[451]
g-C_3N_4/NiS/ carbon black	Carbon black (0.5 wt %) NiS (1.5 wt%)	100 m L of TEOA (15 vol %)	300 W Xe lamp with a 420 nm cutoff filter	992 µmolg^{-1}h^{-1}	> 15h	N/A	[452]
g-PAN/ g-C_3N_4/Pt	g-PAN (5 wt%)	300 L of TEOA (10 vol %)	300W X lamp with Cutoff filter (λ = 400 nm)	37.0 µmol h^{-1}	N/A	N/A	[446]
MgFe$_2$O$_4$/ g-C_3N_4	Pt (1.0 wt%) MgFe (150 mg)	100 m L of TEOA (10 vol %)	300 W Xe lamp with a 430 nm cutoff filter	30.09 µmolh^{-1}	N/A	1.8 (420 nm)	[453]
MWCNT/ g-C_3N_4	MWCNT(0.5 wt%)	10 mL of water and 3 mL of methanol	300 W Xe lamp with a 395 nm cutoff filter	42 µmolg^{-1}h^{-1}	N/A	N/A	[454]
MWCNT/ g-C_3N_4	MWCNT (0.2 wt%) Pt (1.2 wt%)	10 mL of TEOA	300 W Xe lamp with a 420 nm cutoff filter	39.4 µmol h^{-1}	> 40h	N/A	[345]
Pure g-C_3N_4	Phenyl urea (70 mg) Pt (3 wt%)	100 m L of TEOA (10 vol %)	300 W Xe lamp with a 420 nm cutoff filter	535 µmolh^{-1}	> 24h	N/A	[92]
RP/g-C_3N_4	N/A	Lactic acid	300 W Xe lamp with a 400 nm cutoff filter	10 µmol h^{-1}	N/A	N/A	[455]
Surface H-bonding network/ g-C_3N_4	NaOH (0.1 m M)	100 m L of TEOA (10 vol %)	300 W Xe lamp with a 420 nm cutoff filter	73 µmolh^{-1}	> 28h	N/A	[456]
TiO$_2$/g-C_3N_4	N/A	TEOA	500 W Xe lamp with a 420 nm cutoff filter	178 µmol h^{-1}	N/A	N/A	[457]
TiO$_2$/In$_2$O$_3$/ g-C_3N_4	g-C_3N_4 (0.5 g) TBOT (0.2 mL) In(NO$_3$)$_3$ (0.5 mmol)	80 m L solution containing 25 vol% methanol	Four low power UV-LEDs (3 W,420 nm)	6.2 µmol h^{-1}	N/A	N/A	[458]
UiO-66 10 /g-C_3N_4	N/A	l-Ascorbic acid	300W Xe lamp with Cutoff filter (λ = 400 nm)	14 µmol h^{-1}	N/A	N/A	[459]
WO$_3$/ g-C_3N_4/rGO	Pt (1.0 wt%) g-C_3N_4.rGO (1 g)	100 m L of water 10 mL of TEOA	250 W iron doped metal halide UV − vis lamp with a 420 nm cutoff filter	2.84 µmol	N/A	0.9 (420 nm)	[460]
WS$_2$/ g-C_3N_4	WS$_2$ (0.3 wt%)	10 mL of lactic acid (10 vol%)	300 W Xe lamp with a 420 nm cutoff filter	12 µmol h^{-1}	> 4h	N/A	[461]
Zn/ g-C_3N_4	Zn (10 wt%) Pt (0.5 wt%)	50 mL of methanol and 220 mL of water	200 W Xe lamp with a 420 nm cutoff filter	59.5 µmolh^{-1}	> 48h	3.2 (420 nm)	[201]
ZnFe$_2$O$_4$/ g-C_3N_4	Pt (1.0 wt%) ZnFe$_2$O$_4$ (50 wt%)	180 m L of TEOA (10 vol %)	300 W Xe lamp with a 430 nm cutoff filter	200 µmolg^{-1}h^{-1}	> 40h	N/A	[462]
Zn-tri-PcNc/ g-C_3N_4	Pt (1.0 wt%)	10 mL of water, and 88 mg of AA (50 mM)	300 W Xe lamp with a 420 nm cutoff filter	68 µmol h^{-1}	> 30h	1.85 (700 nm)	[463]
Nano-InVO$_4$/ g-C_3N_4	InVO$_4$ (20 wt%)	200 m L of methanol (20%)	300 W Xe lamp with a 420 nm cutoff filter	212 µmolg^{-1}h^{-1}	> 20h	4.9 (420 nm)	[464]
N-CeOx/ g-C_3N_4	Pt (1.0 wt%)	200 m L of TEOA (10 vol %)		292.5 µmolg^{-1}-h^{-1}	> 40h	N/A	[465]

Table 1 (*continued*)

	Photocatalyst	Co-catalyst	Reaction Condition or sacrificial agent	Light Source	Reaction rate (H_2 evolution)	Stability	AQY (%)	Ref.
Co catalyst	N-deficient g-C_3N_4 (g-C3N4 − x)	N/C	100 m L of TEOA (10 vol %)	300 W Xe lamp with a 420 nm cutoff filter	31.6 μmolh^{-1}	> 30h	N/A	[466]
	MoS$_2$/g-C_3N_4	N/A	TEOA	300 W Xe lamp with a 420 nm cutoff filter	27 μmol h^{-1}	> 12h	2.1 (420 nm)	[467]
	MoS$_2$/g-C_3N_4	N/A	TEOA	300 W Xe UV lamp with a 400 nm cutoff filter	23.1 μmol h^{-1}	> 24h	N/A	[468]
	CdS/Au/ g-C_3N_4	Pt (1.0 wt%) Au/g C_3N_4 (0.5 g) S8 (2.0 mmol) Cd (ClO4)$_2$ (4.0 mmol)	10 mL methanol and 50 mL water	300 W Xe UV lamp with a 420 nm cutoff filter	19.02 μmolg^{-1} h^{-1}	N/A	N/A	[469]
	Ag/g-C_3N_4	N/A	MeOH	300 W Xe UV lamp with a 420 nm cutoff filter	10.10 μmol h^{-1}	> 16h	N/A	[470]
	Ag$_2$O/ g-C_3N_4	Ag$_2$O (0.83 wt%)	100 m L of TEOA (10 vol %)	300 W Xe lamp with a 420 nm cutoff filter	32.88 μmolg^{-1} h^{-1}	> 8h	N/A	[471]
	Au/ g-C_3N_4	N/A	100 m L of TEOA (10 vol %)	500 W HBO lamp with a water filter ($\lambda > 420$ nm	10.70 μmol h^{-1}	> 15h	N/A	[472]
	Ni (OH)$_2$/ g-C_3N_4	Ni (OH)$_2$ (0.5 mol %)	80 m L of TEOA (10 vol%)	350 W Xe lamp with a 400 nm cutoff filter	7.60 μmol h^{-1}	> 12h	1.1 (420 nm)	[473]
	Ni(dmgH)$_2$/ g-C_3N_4	Ni(dmgH)$_2$ (3.5 wt %)	10 mL of TEOA (15 vol%)	300 W Xe lamp with a 420 nm cutoff filter	1.18 μmol h^{-1}	> 18h	N/A	[441]
	[Ni (TEOH)$_2$] Cl$_2$/ g-C_3N_4	NiCl2 (1 wt%)	5 m L of TEOA (10 vol%)	500 W Xe lamp with a water cooling filter ($\lambda > 400$ nm)	TOF 12.4 molh^{-1}	N/A	1.51 (400 nm)	[474]
	Ni(OH)$_2$/ CdS/g-C3N4	Ni (OH)2 (4.76 wt %) g-C_3N_4/ CdS (4%)	20 m L of 0.5 M Na$_2$S and 0.7 M Na$_2$SO$_3$	300 W Xe lamp with a 420 nm cutoff filter	115 μmolmg^{-1}-h^{-1}	> 40h	16.7 (450 nm)	[475]
	Ni/ g-C_3N_4	Ni (0.1 wt%)	50 mL of TEOA (10 vol%)	Xe lamp (125 mW/cm2) with a 420 nm cutoff filter	5.5 μmolh^{-1}	> 24h	2.6 (420 nm)	[476]
	Ni/NiO/ g-C_3N_4	Ni/NiO (2 wt%)	100 m L of TEOA (10 vol %)	300 W Xe lamp with a 420 nm cutoff filter	10 μmol h^{-1}	> 16h	N/A	[477]
	NiS/ g-C_3N_4	NiS (1 wt%)	50 mL of TEOA (10 vol%)	350 W Xe lamp with a 420 nm cutoff filter	4.20 μmol h^{-1}	> 24h	1.4 (420 nm)	[478]
	NiS/ g-C_3N_4	NiS (1.5 mol%)	100 m L of TEOA (10 vol %)	300W Xe lamp with Cutoff filter ($\lambda = 420$ nm)	44.77 μmol h^{-1}	> 15h	N/A	[422]
	NiS/ g-C_3N_4	NiS (1.1 wt%)	100 m L of TEOA (15 vol %)	150 W Xe lamp with a 400 nm cutoff filter	48.2 μmol h^{-1}	> 30h	1.9 (440 nm)	[479]
	NiS/mpg-C_3N_4/ CNT	NiS (1 wt%)	10 mL of TEOA	300 W Xe lamp with a 420 nm cutoff filter	521 μmolg^{-1} h^{-1}	> 15h	N/A	[480]
	NiS$_2$/ g-C_3N_4	NiS$_2$ (2 wt%)	10 mL of TEOA (15 vol%)	300W Xe lamp with Cutoff filter ($\lambda = 420$ nm)	4.06 μmolh^{-1}	> 4h	N/A	[481]
	Pt/g-C_3N_4	N/A	TEOA	300W Xe lamp with Cutoff filter ($\lambda = 420$ nm)	10 μmol h^{-1}	N/A	N/A	[111]
	g-C_3N_4 Polymers	Pt	No sacrificial agent	300 W Xe lamp with a 420 nm cutoff filter	3.1 TON	> 510h	0.3 (405 nm)	[71]
	Pt-TiO2/ g-C_3N_4-MnOx	Pt (1.0 wt%) MnO (1.0 wt%)	300 m L isopropanol/H$_2$O (1:11)	300 W Xe UV lamp with a 420 nm cutoff filter	7.6 mmolg^{-1} h^{-1}	N/A	N/A	[482]
	P$_3$HT/ g-C_3N_4/Pt	P$_3$HT (3 wt%) Pt (1 wt%)	600 m L Na$_2$S (0.25 M) and Na$_2$SO$_3$ (0.25 M)	300W Xe Hg lamp with Cutoff filter ($\lambda = 420$ nm)	550 μmol h^{-1}	50% after 15h	2.9 (420 nm)	[483]
	PEDOT/ g-C_3N_4/ Pt	PEDOT (2 wt%)	30 m L of TEOA (10 vol%)	300W Xe lamp with Cutoff filter ($\lambda > 400$ nm)	32.7 μmol h^{-1}	N/A	N/A	[297]
	PMDA/ g-C_3N_4/Pt	Pt (1 wt%)			20.6 μmolh^{-1}	> 30h		[484]

Table 1 (*continued*)

	Photocatalyst	Co-catalyst	Reaction Condition or sacrificial agent	Light Source	Reaction rate (H_2 evolution)	Stability	AQY (%)	Ref.
			400 m L of methanol (10 vol%)	300W Xe lamp with Cutoff filter ($\lambda > 420$ nm)			0.3 (420 nm)	
Heteroatom Doping	S-doped and N deficient g-C_3N_4	S/C (0.012) N/C (1.239)	TEOA	Visible light ($\lambda > 420$ nm)	121 µmol h^{-1}	> 30h	N/A	[485]
	S-doped g-C_3N_4	Thiourea (10 wt%) Pt (1 wt%)	120 m L solution containing methanol (25 vol%)	300 W Xe lamp with a 400 nm cutoff filter	12.16 µmolh^{-1}	> 8h	2.6 (420 nm)	[486]
	S-doped g-C_3N_4	S (0.5 wt%) Pt (3 wt%)	100 m L of TEOA (10 vol %)	300 W Xe lamp with a 420 nm cutoff filter	140.5 µmolh^{-1}	N/A	N/A	[487]
	S-doped g-C_3N_4 ($C_3N_4 - xSx$)	Pt (6 wt%)	300 m L of TEOA (10 vol	300 W Xe lamp	160 µmol	N/A	N/A	[199]
	S-doped g-C_3N_4 microrods	Pt (1 wt%)	50 mL of TEOA (10 vol%)	500 W Xe lamp with a 400 nm cutoff filter	5000 µmolg^{-1}-h^{-1}	> 60h	N/A	[167]
	S-doped mpg-CN	S (0.8 wt%) Pt (3 wt%)	100 m L of TEOA (15 vol %)	300 W Xe lamp with a 420 nm cutoff filter	136.0 µmol h^{-1}	> 72h	5.8 (440 nm)	[238]
	S-doped/g-C_3N_4	N/A	TEOA	300 W Xe lamp with a 420 nm cutoff filter	100 µmol h^{-1}	N/A	N/A	[199]
	P-doped g-C_3N_4	HCCP, GndCl (10 wt%) Pt (3 wt%)	100 m L of TEOA (10 vol %)	300 W Xe lamp with a 420 nm cutoff filter	50.6 µmolh^{-1}	> 15h	N/A	[228]
	P-doped g-C_3N_4	Melamine: HEDP mass ratio (12:1)	100 m L of TEOA (10 vol %)	300 W Xe lamp with a 420 nm cutoff filter	104.1 µmol h^{-1}	> 16h	N/A	[236]
	O-doped g-C_3N_4	O (7.98 at%) Pt (1.2 wt%)	100 m L of TEOA (10 vol %)	300 W Xe lamp with a 420 nm cutoff filter	37.5 µmolh^{-1}	> 24h	N/A	[186]
	O-doped g-C_3N_4	O (1.5 at%) Pt (3 wt%)	120 m L of TEOA (10 vol %)	300 W Xe lamp with a 420 nm cutoff filter	60.2 µmol h^{-1}	N/A	7.8 (420 nm)	[202]
	N-vacant/ g-C_3N_4	Pt (3 wt%)	300 m L of TEOA (10 vol %)	300 W Xe lamp with a 400 nm cutoff filter	123 µmolg^{-1} h^{-1}	N/A	N/A	[488]
	N self-doped g-C_3N_4	Pt (3 wt%)	100 m L of TEOA (10 vol %)	300 W Xe lamp with a 400 nm cutoff filter	44.28 µmol h^{-1}	> 16h	N/A	[81]
	I-doped g-C_3N_4	Ammonium iodine conc (1.0 g)	100 m L of TEOA (10 vol %)	300 W Xe lamp with a 420 nm cutoff filter	38 µmol h^{-1}	> 20h	2.4 (420 nm)	[434]
	I-doped g-C_3N_4 nanosheets	I (0.34 wt%)	100 m L of TEOA (10 vol %)	300 W Xe lamp with a 420 nm cutoff filter	44.5 µmolh^{-1}	> 12h	3.0 (420 nm)	[176]
	I-doped/g-C_3N_4	N/A	TEOA	300 W Xe lamp with a 420 nm cutoff filter	38 µmol h^{-1}	N/A	2.4	[209]
	K/ g-C_3N_4	KCl/ g-C_3N_4 wt (10:1)	100 m L of TEOA (10 vol %)	300 W Xe lamp with a 420 nm cutoff filter	102.8 µmol h^{-1}	> 16h	N/A	[489]
	F-doped g-C_3N_4	F (0.5 at%)	200 m L of methanol (20 vol%)	300 W Xe lamp (UV − vis)	0.327 mmolh^{-1}	> 32h	4.1 (420 nm)	[490]
	F-doped/g-C_3N_4	N/A	TEOA	300 W Xe lamp	12 µmol h^{-1}	N/A	N/A	[120]
	Fe/P/ g-C_3N_4	Fe (0.5%)	100 m L of methanol (10 vol%)	250 W high pressure Na lamp ($\lambda = 400 − 800$-nm)	150.6 µmolh^{-1}	N/A	8.5 (400 nm)	[491]
	Carbon black/ g-C_3N_4	Carbon black (0.5 wt %) Pt (3.0 wt%)	100 m L of solution containing methanol	300 W Xe lamp with a 420 nm cutoff filter	68.9 µmolh^{-1}	N/A	N/A	[492]
	C-doped g-C_3N_4	C/N (0.766)	methanol (25 vol %)	300W Xe lamp with Cutoff filter ($\lambda > 400$ nm)	N/A	> 250min	N/A	[181]
	B-doped g-C_3N_4	Ph$_4$BNa (5 mg) Pt (3 wt%)	100 m L of TEOA (10 vol %)	300W Xe lamp with Cutoff filter ($\lambda > 420$ nm)	278 µmol h^{-1}	> 24h	N/A	[241]

(FeTPP)$_2$O: µ-oxo dimeric iron(III) porphyrin; AA: acetonitrile aqueous; CoPi: cobalt-oxide-phosphate; ABN: 2-aminobenzonitrile; ATCN: 2-aminothiophene-3-car-bonitrile; BA: barbituric acid; PEDOT: poly(3,4-ethylenedioxythiophene); PMDA: pyromellitic dianhydride; Ppy: polypyrrole; DI: denionized; g-PAN: graphitized polyacrylonitrile; TEOA: triethanolamine; P3HT: poly-3-hexylthiophene; AA: ascorbic acid; Ni-Tu-TETN: nickelthiourea- N(CH2CH3)$_3$; C1: carboxy-functionalized cobaloxime; C$_2$: pyrene-functionalized cobaloxime; C$_3$: nonfunctionalized cabaloxime; DCDA: dicyandiamide; EDTA: ethylenediaminetetraacetic acid; HER: hy-drogen evolution rate; mpg-CN: mesoporous graphitic carbon nitride; e-C_3N_4: exfoliated graphitic carbon nitride; HCCP: hexachlorotriphosphazene; GndCl: gua-nidiniumhydrochloride; HEDP: (hydroxyethylidene) diphosphonic acid; MWCNT: multiwalled carbon nanotube; CQD: carbon quantum dot; EQE: external quantum efficiency; C-PDA: carbonized polydopamine;; Zn-tri-PcNc: zinc phthalocyanine.

step synthesis method into nanosheet of g-C_3N_4 which improved the surface area about 2.5 times that is 236.52 $m^2 g^{-1}$, than that of g-C_3N_4. [208]. The hydrogen generation was also increased about 6 time than bulk g-C_3N_4 and rate was 536 mmolh^{-1} g^{-1} as shown in Fig. 5b.

The Fe ions synchronized with aromatic rings and made a new impurity bond that not only reduced the band gap but also separates the photogenerated charges and eventually increases the photocatalytic performance.

Among the transition material results, Zn doped material harvest the visible light and produce hydrogen energy ten times more than pure g-C_3N_4 that are about 59.5 μmol.h^{-1}. [201]. The study depicts that by increasing the concentration of Zn doping the absorption edge of both materials' Zn/g-C_3N_4 was enhanced. The impregnation of cobalt ions into the g-C_3N_4 by soft chemical synthesis liberate oxygen from water. [209] Zhang et al. prepared Na doped carbon nanotubes (CNNTs) by a simple method and applied in water splitting [180]. The Na$^+$ doping alters the band structure and porous structure of the CNNTs also help to increase the surface area. It also enhanced the hydrogen production rate as high as 143 μmol.h^{-1}. They also compared the other alkali metals like Lix-CNNTs and Kx-CNNTs but found that the hydrogen production rate is low than Na doping. In another study, they synthesized sodium and g-C_3N_4 by ball milling and calcination process. [210] SEM images show the tightly packed layer with a smooth surface (Fig. 6). The hydrogen production rate after doping was increased up to 9.5 times than pure g-C_3N_4 that are about 169.0 mol h^{-1} g^{-1}. In this case, Na$^+$ doping and synergistic effect by high surface area could enhanced the hydrogen evolution. Apart from this, there are many other metals like Zr, W, Pd, Cu have also been doped to alter the photocatalytic activity. [205,211–214].

There are numbers of alkali metals that have incorporated into g-C_3N_4. [180,215,216] Moreover, K^{+-}, Na^{+-}, and Li^{+-} introduced into carbon nitride nanotubes through a molten salt, which improved the hydrogen generation rate of 346 μmol.h^{-1} [77]. These ions unusually amend the transfer rate and charge separation efficiency to generate spatial charge delivery for enhanced photocatalytic reaction. The larger diameter of heptazine units shows a strong binding between alkali cations and nitrogen pots of g-C_3N_4. Noble metals like Pt and Pd were also used to improve the photocatalytic activity of g-C_3N_4, but it is scarce and quite expensive. [217]

Although many researchers studied different metal doping on g-C_3N_4 and the calculations concluded that metal doping creates a new energy band which might be work as a recombination center and the thermal stability of ion is poor. [214] So, non-metal doping has studied because they have high ionization energy and high electronegativity. Thus, it controls the thermal changes of doped metal ions and maintains the metal free property of the material [218,219]. The non-metal doping method is like that of metal doping [220,221]. The researchers studied different non-metals doping including Sulphur [101,192,199,222–224], carbon [181,225,226], phosphorus [42,188,203,227,228], iodine [176,209], boron [196–198,229,230], nitrogen [81], oxygen [188,202,231–233], fluorine [120], and halogen [234] have been employed for doping on g-C_3N_4.

Zhang et al. claimed that the phosphorus doping of g-C_3N_4 prepared by polycondensation of a mixture with dicyandiamide and a source of heteroatom namely phosphorus containing ionic liquid. [235] The results showed that after doping there is an improvement in the photocatalytic properties, especially in the photocurrent generation. In another study, phosphorus doping done by using (NH$_4$)$_2$HPO$_4$ (diammonium hydrogen phosphate) and dicyandiamide for g-C_3N_4 [220]. The atom of phosphorus doped into the lattice of g-C_3N_4 and make a P−N bond. The results told that there is no specific change in reaction mechanism by altering the doping site, but photocatalytic efficiency can be improved by interstitial P doping rather than by substitutional P doping. The corresponding results have also been reported by Ma et al., as their study based on the electronic structure and various doped position of phosphorus doping in g-C_3N_4 to calculate the dopant

formation energies [192].

The substitutional doping of P has been studied in plane mesoporous nanostructures flower using hydroxyethylidene diphosphonic acid HEDP without any template in Fig. 7a. The resulting flower-like structure (Fig. 7b) helps to increase the surface area due to high porosity and superior charge transfer for water reduction. [236]. In this work, P doping offers a direction towards the modification in the texture and altering the electronic structure of g-C_3N_4 that showed great potential to enhance the photocatalytic hydrogen evolution performance under visible light. The C_3N_4 hexagonal tube fabricated which helps to reduce band gap and absorb more light for better hydrogen evolution. [237] Sulfur doping is also used to enhance the photocatalytic activity of g-C_3N_4. [101,199,221,223,224,238] Liu et al., prepared S- doped g-C_3N_4 by treating gaseous H$_2$S with pure g-C_3N_4 at 450 ^{0}C. [199] This unique electronic structure evolved H$_2$ rate of 7.2 and 8.0 times more than pure g-C_3N_4. It displayed an increased in the width of VB minimized the CB elevation at the same time and reduced the absorbance.

Zhang et al. prepared sulfur mediated synthesis to examine the physicochemical properties of the g-C_3N_4. [239] They found that water oxidation reaction improved due to significant modification in the optical, textural and electronic properties. The study was done to investigate the sulfur doping effect on the geometric and electronic structure of g-C_3N_4. In another study, S-doped micro-rods synthesized by condensation of melamine and tri-this cyanuric acid supramolecular co-crystal under N$_2$ atmosphere. [167] It increased the surface area and improved the light absorption that helped to increase hydrogen evolution by 9.3 times. The S-doping decrease the band gap energy by contributing the valence charge densities [193]. It stated that Sulfur and Nitrogen have similar electronegativities and mostly literature said that S doping replaces lattice N atoms instead of C atoms [101,224]. Ma et al. investigated that this replacement of N atoms with S atoms was practically promising [192]. So, the substitution of N atoms by S doping in g-C_3N_4 enhanced the photocatalytic properties and helped to evolve more hydrogen.

Porous oxygen doped g-C_3N_4 prepared with thermal polycondensation of melamine and polyvinylpyrrolidone as shown in Fig. 8. [240] The TEM images show that there is lamellar structure over CN 0 and CN 0.1 while EM indicates that O element homogeneously doped on g-C_3N_4. After modification in PVP, there is a reduction of 0.2 eV in band gap and the expansion in the surface area. These factors exhibit remarkable improvement in the hydrogen evolution which is about five times more from pure g-C_3N_4. The photocatalytic activity of ultra-thin O-doped g-C_3N_4 nanosheets for H$_2$ development is nearly 5.2 times more than that of the pure g-C_3N_4. Iodine doped g-C_3N_4 nanosheets prepared by ball milling techniques as shown in Fig. 9. The TEM and EM images revealed the presence of iodine. It enhances the area of the surface and reduces the bandgap which helps to evolved hydrogen using visible light with a rate of 44.5 mmolh^{-1}. [176] The study showed that doping with nanosheet enables the redshift of spectrum to utilize more visible light. In another study for iodine doping the results showed I doping increased surface area, enhances the light absorption and produce the H$_2$ about 14 μmol h^{-1} more than g-C_3N_4. [92] Further, halogen element like fluorine doped g-C_3N_4 prepared from NH$_4$F using a thermal condensation process. [120] The doped fluorine makes a bond with carbon instead of Nitrogen and this C–F bonding helps in reduction of bandgap from 2.69 to 2.63 eV and enhanced the photocatalytic properties.

Lin and Wang prepared boron-doped g-C_3N_4 samples using polymerization of urea and Ph$_4$BNa for photocatalytic water splitting. [241] The B doped graphitic carbon nitride shows a great hydrogen evolution activity. They suggested that the specific surface area increases by B-doping and it also changes the electronic structure by creating polar surface docking sites. From these studies, we can say that doping can help to alter the photocatalytic properties of g-C_3N_4, but some issues still exist like the presence of surface trapping center, doping site, lower
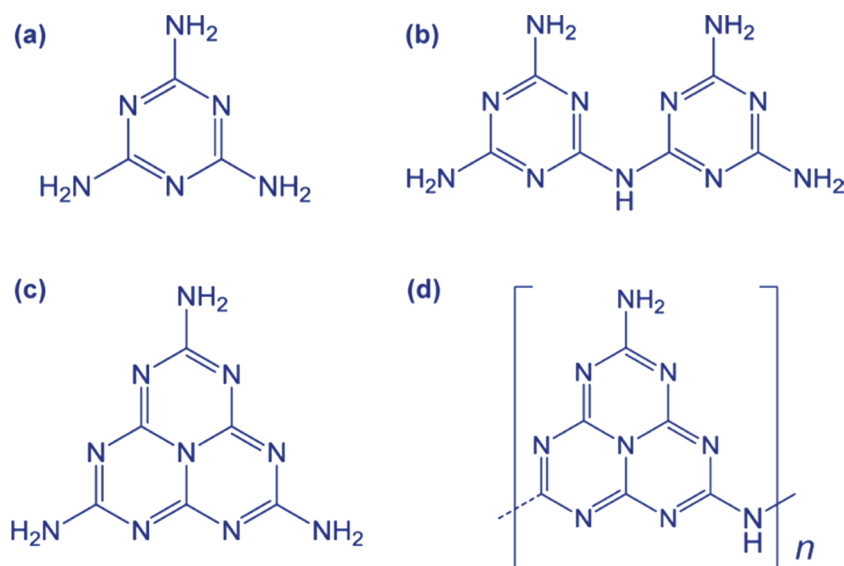
Fig. 3. Carbon and Nitrogen containing materials: (a) melamine, (b) melam, (c) melem and (d) melon obtained from the thermolysis of mercury II thiocyanate by Liebig [108].
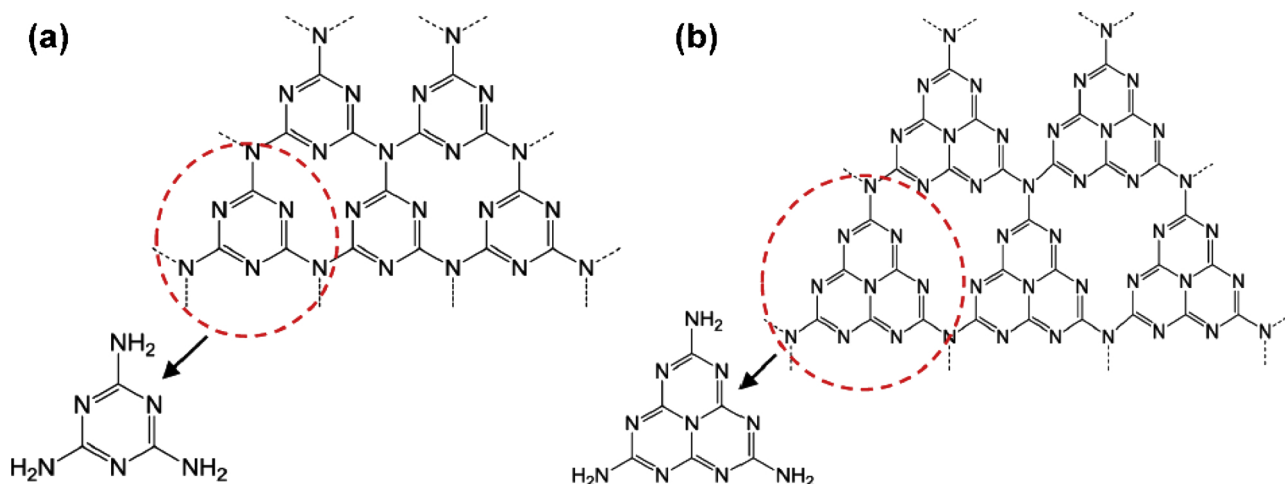

Fig. 4. Triazine and (b) tri-s-triazine (heptazine) structures of g-C_3N_4 [113].

oxidizing and reducing ability. Also, the results revealed that the excessive doping of metals and non-metals is detrimental due to the formation of more defects in the charge separation because of doping asymmetry. [181,242,243] So, there is a need to further studies new doping methods that can achieve higher photocatalytic activity.

2.2. Defects engineering

In addition to doping, defects in the photocatalytic material is another strategy to enhance the photocatalytic activity namely called defect engineering. The defects mostly carry derogatory implications that emanate their role of providing trap spots for Shockley-Read-Hall type charge recombination. Though, many recent studies depict a positive influence to balance the losses by recombination. The studies includes the introduction of nitrogen and carbon vacancies, [244–246] reducing defects [247], cyanamide defects [248,249], dye [250], protonation [251], oxygenation [252], alkalinized treatment [253], amorphization [254], vacuum heat-treatment [255], and hydrogen bonds breaking [256], have also been examined in the past few years [257].

The oxygen vacancies help to absorb the wide bandgap into visible range and provide inter-band state like in case of TiO_2, the formation of additional donor energy state below the conduction band shifts the absorption from 400 nm to 530 nm. [258] The oxygen vacancies related to electron traps in the oxide semiconductors while with hole traps in the hydroxyl group. [259]. The free charges contributed to the redox reaction by capturing at or near the surface that acts as a reaction center in the defect system and provides further electron accepting and donating state in the bandgap. Carbon vacancies on g-C_3N_4 generated by applying hot argon gas. The results proved that it reduces the band gap energy by providing more electron and the hydrogen production rate was 14 times higher. [260] A very recent Liu et al. studied N deficient g-C_3N_4 prepared by a molten salt post-treatment method. [261] It enhances the visible light absorbance and slightly lower the band gap which evolved H_2 at a rate 403.1 µmol h^{-1}, that is about 2.2 times of pure g-C_3N_4. Nitrogen deficiency alters the electronic structure of graphitic carbon nitride and enhances the separation of charge carriers by improving photocatalytic performance.

The cyanamide defects in g-C_3N_4 yielded the H_2 evolution rate about 16 times more than unmodified melon. [249] The findings in this study provide the rationale for the extensive disparity in the synthesis process of photocatalytic activity and find a way to explore the new avenues to expand intrinsic photocatalytic properties. The density of these defects associates with photocatalytic performance. Tay et al.
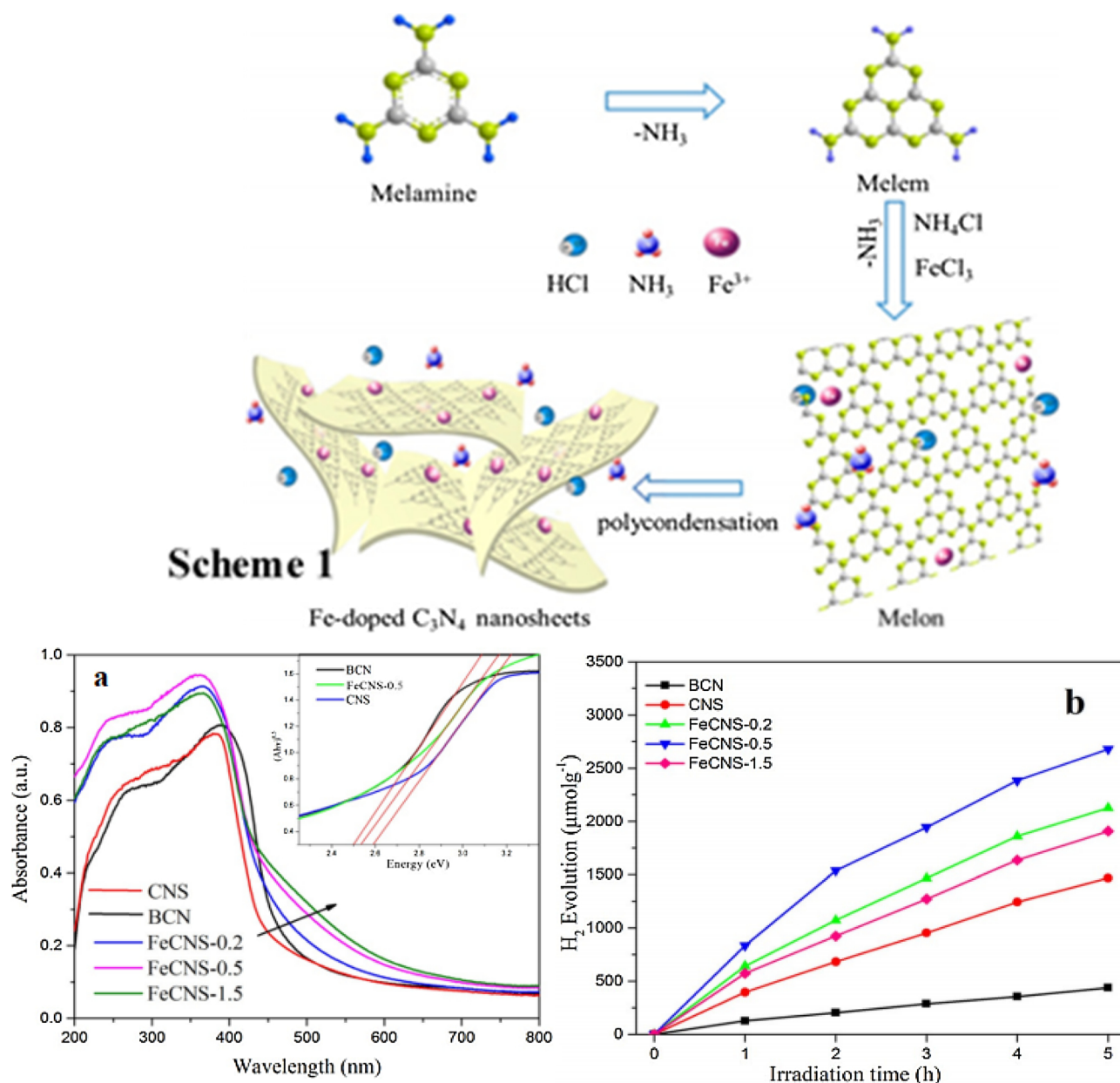
Fig. 5. Scheme 1: Schematic illustration of the synthesis process of Fe-doped g-C_3N_4 sheet (a) Uv/Vis. Absorption spectrum (b) Photocatalytic hydrogen evolution. Reproduced with permission [208]. Copyrights 2017 Wiley.

introduced a defect in g-C_3N_4 by synthesized hydrogen gas and bandgap reduced from 2.7 to 2.0 eV. [248] The reduction of bandgap and enhancement in the solar absorption is due to the formation of two co-ordinated nitrogen vacancies in the graphitic carbon nitride.

The proton concentration could be increased if the hydrogen atom would occupy these vacancies. The partially crystalline g-C_3N_4 (GCN) having a band gap of 2.82 eV was merely heated to get an amorphous g-C_3N_4 (ACN) with a band gap of 1.90 eV. It has shifted the light range, reduce the charge separation and enhance the H_2 evolution rate. [254] The introduction of carbon-rich structure in this work reduced the bandgap of g-C_3N_4 nanosheet and enhanced the electron delocalization without any other heterojunction material. Wu et al. reported facial melamine defect improving approach and prepared a C_3N_4 high-performance photocatalyst (R-C_3N_4) as shown in Fig. 10.

The melamine remediation stimulated the development of g-C_3N_4/mpg-C_3N_4 junctions which reduce the recombination of charges. The results showed that the H_2 evolution rate by R-C_3N_4 reaches 2700 μmol/g that is 6.5 times higher than pristine g-C_3N_4. [247] Kang

et al. prepared a g-C_3N_4 modified by the hydrogen bond breaking and found that there is an improvement in hydrogen generation under visible light. [256]. As a result of breaking of intralayer atomic order, the band tail or localized state have been increased near the band edges and the formation of pores due to shrinkage of volume that not only help to improve the absorption of visible light portion but also reduce the electron-hole recombination by providing charge trapping sites (Fig. 10b–c) A very recent Han et al. synthesized defect-rich amorphous carbon nitride (DACN) by calcination of urea as shown in Fig. 11. [262] The entrance of nitrogen into the disturbed structure and destruction of long-range atomic order produced a wide range of visible light and helped to deliver a high rate of hydrogen about 37,680 μmol h^{-1} g^{-1}.

3. Reduced charge recombination

3.1. Metal-organic framework (MOF)

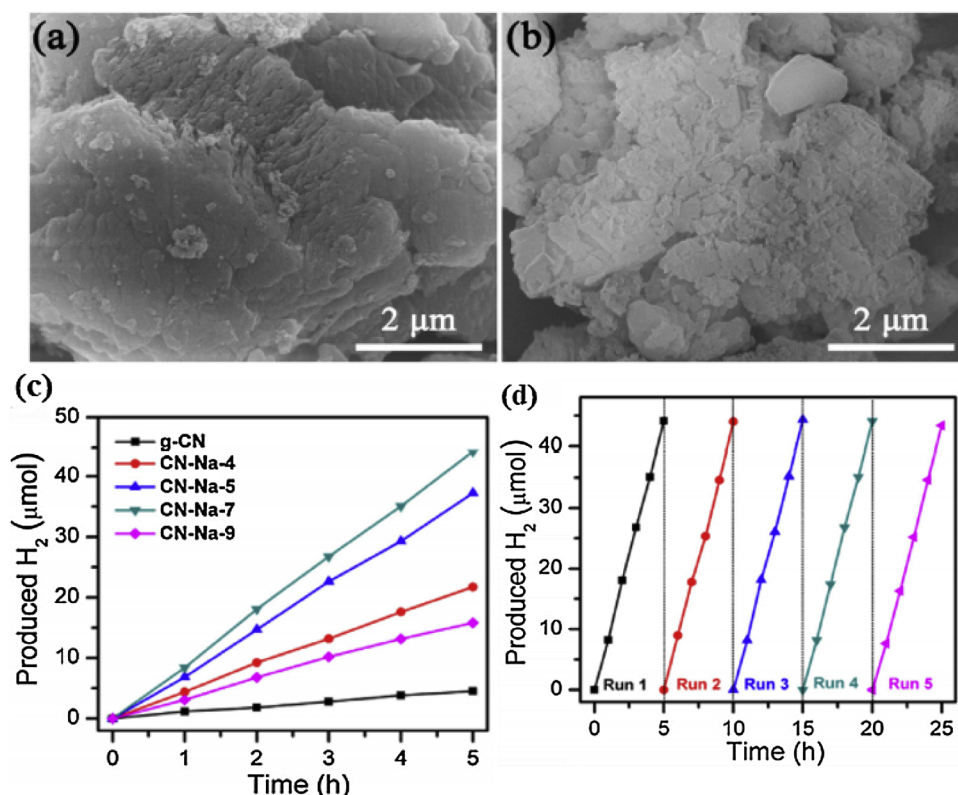The metal-organic framework is a family of crystalline porous solid

Fig. 6. SEM image of (a) pure g-C_3N_4 (b) CN-Na-7. (c) The plots of photocatalytic H_2 evolution amount to time. (d) Long-term H_2 evolution by CN-Na-7 under visible light irradiation. Reproduced with permission [210] Copyrights Elsevier.

connected by a strong linkage of organic and inorganic units. It has a unique structure and excellent properties that made MOF's hotspot material for the photocatalytic application. [263–269] There is remarkably a fast development related to MOF based photocatalysis in the past few years. There are numbers of reviews in this specific area that have given the impression over the past several years [18,36,270–281]. It is the ideal material for light absorption and energy generation, so the researchers mostly focus on its light catalytic reaction. A very recent Wang et al. synthesized g-C_3N_4 and MOF (ZIF-67) by the hydrothermal condensation method and MoS_2 decorated on their surface. [282] As MoS_2 is a strong cocatalyst used to enhance the photocatalytic performance of hydrogen production. [283,284].

The introduction of these two materials helps to evolve maximum hydrogen about 321 mmol that is 30 times higher than pure g-C_3N_4. [282]. This study shows the improvement of electron transfer by

restraining the electron-hole recombination due to the synergistic effect between Co and Mo. The MoS_2 as charge transmission provide more active sites on the surface and change the route of charge transmission. The most common used Zn MOF material is Zeolitic imidazolate framework-8 (ZIF-8), has been proved it's potential in the different applications. [277,286–289] In another study, ZIF-8 is anchored with a modified rod-like g-C_3N_4 material by self-assembly and thermal treatment process as shown in Fig. 12. [285] The SEM images show that ZIF-8 is evenly distributed on the g-C_3N_4 surface. The integration of g-C_3N_4 with MOF leads to absorb visible light portion, reduce charge separation and suppressed recombination of electron holes that result in the evolution of hydrogen that is approximately 15 μmol/L under illumination. The composite photocatalyst $Ni_xMo_{1-x}S_2$/MOF-5@g-C_3N_4 prepared by the hydrothermal method and photocatalytic improvement was observed. [290] The maximum hydrogen evolution was 319 mmol
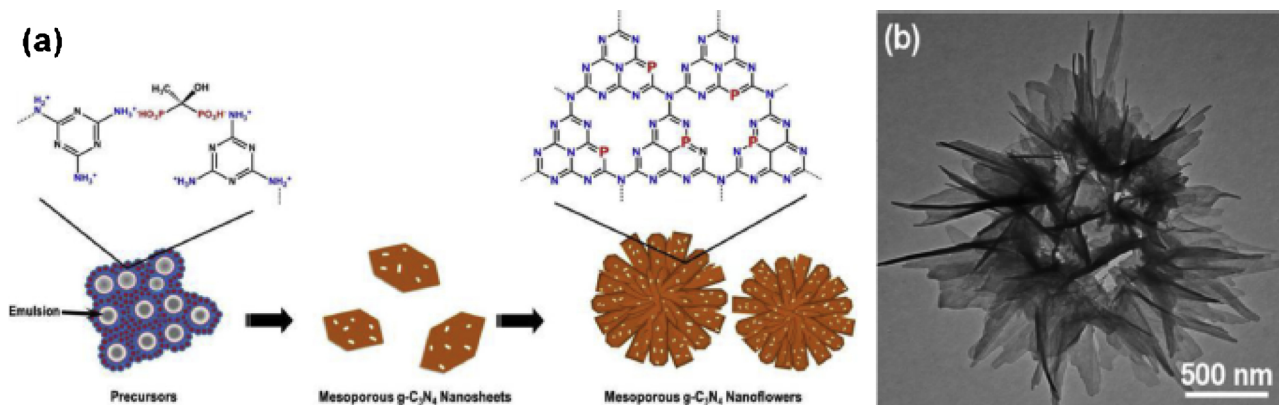

Fig. 7. (a) Formation mechanism of mesoporous P-doped g-C_3N_4 flower-like morphology and (b) TEM image of that morphology. Reproduced with permission [236] Copyrights 2015 American Chemical Society.
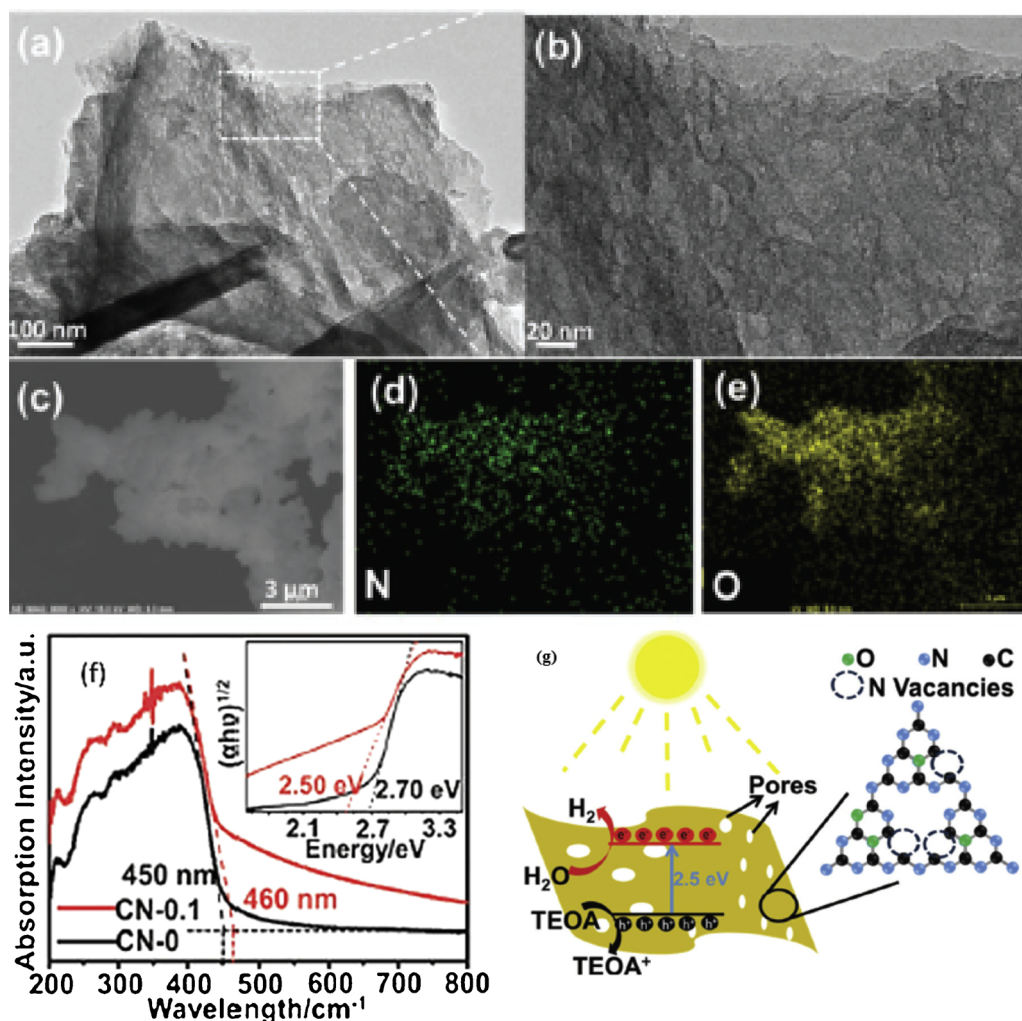
Fig. 8. TEM (a) and HR-TEM (b) images of CN-0.1. (c–e) Elemental mapping of CN-0.1. NAD isothermal curves, (f) UV–vis diffuse reflection spectra and corresponding Tauc plots (inset), (g) Photocatalytic reaction of the prepared porous oxygen-doped and feeble nitrogen-vacancy g-C3N4 (l4420 nm). Reproduced with permission [77]. Copyrights 2016 Royal Society of Chemistry.

that is 30 times more than that of the bulk g-C_3N_4 photocatalyst.

3.2. Z-scheme technology

The essential requirement for photocatalysis reaction is light absorption and strong redox ability, but it is challenging for a single material to possess both at the same time. For the full range of light absorption, the bandgap should narrow while for strong redox ability positive valence band (VB) and negative conduction band (CB) requires (Fig. 13). Further, light efficiency also decreased by the recombination of electron holes on the surface. [291,292]. The heterojunction type systems are widely used to separate the photoinduced charges, but due to the potential differences between CB and VB, the photogenerated electron and holes transfer into CB and VB respectively, shows results in low redox ability [43,293–296]. This problem can solve by mediator molecules which perform two functions, one is to collect the charge at surface and second is to release the charges. In the last few years [71,297–300], the growing number of studies is done using the Z-scheme system to increase the efficiency of g-C_3N_4 with different material like WO_3, [301] Ag_3PO_4, [302] $BiVO_4$, [303] $BiOI$, [304] MoO_3, [305] TiO_2, [306] and many more. [307–312].

Xiao et al. synthesized $C_3N_4@Ag–Bi_2WO_6$ by a photo deposition method. [313] The Z-scheme technology enhances the photocatalytic performance especially the hydrogen evolution. The different semiconductors distributed the photogenerated electrons and holes that

increase the charge separation and transfer process by reducing the charge recombination process, corresponding to increase photocatalytic performance. In another study, 2D hybrid solid state Z-scheme junction of a small amount of α-Fe_2O_3 nanosheets is prepared that promote exfoliation of g-C_3N_4 and produce a high rate of H_2 evolution approximately 31,400 μmolg^{-1}h^{-1} [314]. There is fast electron transfer between VB of α-Fe_2O_3 and CB of g-C_3N_4 due to tight bonding between both the materials and the Z-scheme suppressed the recombination process. Han et al. reported that Z-scheme $Co_3(PO_4)_2$/α-Fe_2O_3 is an excellent structure for water splitting under visible light. The synergetic effect of $Co_3(PO_4)_2$ and α-Fe_2O_3 in the Z-scheme structure enhanced the photocatalytic activity which results in the evolution of hydrogen about 0.63 μmol h^{-1} which is 35 times higher than pure $Co_3(PO_4)_2$ catalyst. [315]. The $Co_3(PO_4)_2$ have a narrow bandgap but suffers from fast recombination process while Fe_2O_3 also have low band gap, but conduction band is low enough to reduce hydrogen from water. So, by combining these two semiconductors in a Z-scheme pattern, a synergistic effect has been realized which enhance the photocatalytic behavior. In another work, Z-scheme g-C_3N_4/Au/C-TiO_2 hollow spheres prepared with Au nanoparticles as the electron mediator. The results showed the improved photocatalytic hydrogen production under the visible light that is 86 and 42 times higher than those of pure C-TiO_2 and g-C_3N_4, respectively. [316].

The light response has primarily increased in this Z-Scheme structure due to the SPR effect of Au particles that allowed the maximum
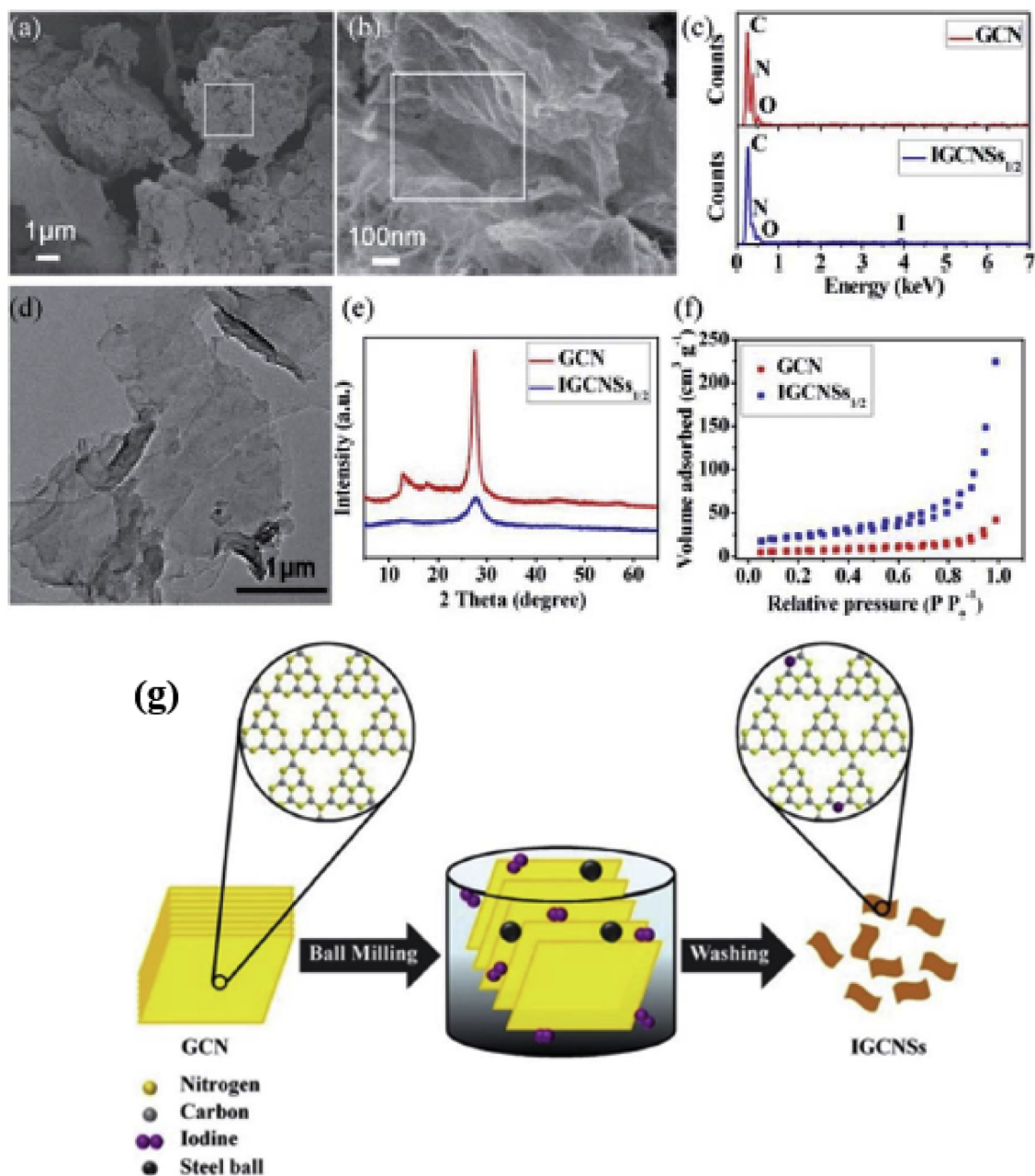
Fig. 9. (a). High-magnification SEM image of IGCNSs1/2 (b). (c) EDX spectra obtained from the rectangle areas of (a) and (b). (d) TEM image of IGCNSs1/2. (e) XRD patterns of the bulk GCN and IGCNSs1/2. (f) Nitrogen adsorption–desorption isotherms of the bulk GCN and IGCNSs1/2. The scale bars are 1 mm for (a) and (d) but 100 nm for (b). (g) Schematic of ball-milling process of bulk GCN and iodine resulting in the formation of IGCNSs. Yellow, gray, purple and black spheres stand for nitrogen atoms, carbon atoms, iodine atoms and steel balls, respectively. SEM images of the bulk GCN Reproduced with permission [176]. Copyrights 2015 Royal Society of Chemistry.

reflection of light in the inner cavity of semiconductors. A plasmonic photocatalyst g-C$_3$N$_4$/Ag/MoS$_2$ in all solid-state Z-scheme prepared in a flowerlike structure of diameter about 0.4–0.6 μm. [317] Fig. 14A shows the schematic illustration of preparation methods and Fig. 14B–f shows the morphology of the sample. The SEM images g-C$_3$N$_4$/Ag/MoS$_2$ microspheres have shown in Fig. 14F.

For the same study, the TEM images of MoS$_2$ that show an agglomerated structure while a few dark spots on the nanosheet surface indicating the formation of Ag/MoS$_2$ samples. Fig. 15A shows the TEM images of MoS$_2$ that show an agglomerated structure while few dark spots on the nanosheet surface indicating the formation of Ag/MoS$_2$ samples. The poor transparency reveals in the TEM image of g-C$_3$N$_4$/Ag/MoS$_2$ (Fig. 15G) after the amendment of Ag nanoparticles and g-

C$_3$N$_4$ on MoS$_2$ surface. The high-resolution TEM (Fig. 15J) show that MoS$_2$, g-C$_3$N$_4$, and Ag coexist in the composites. This study proves an exceptional photocatalyst for the visible light absorption, charge separation, pollutant degradation and hydrogen evolution which is about 8.78-fold and 2.08-fold of Ag/MoS$_2$ and g-C$_3$N$_4$/MoS$_2$ systems, respectively. Shi et al. prepared Z-scheme g-C$_3$N$_4$/nanocarbon/ZnIn$_2$S$_4$ photocatalyst which enhances the hydrogen evolution by 3.4 times of pure ZnIn$_2$S$_4$ and 3.2 times ZnIn$_2$S$_4$/g-C$_3$N$_4$. [318].

3.3. Carbonaceous materials

The metal-free compounds or carbonaceous materials employed for the modification of g-C$_3$N$_4$. There are different materials that have been
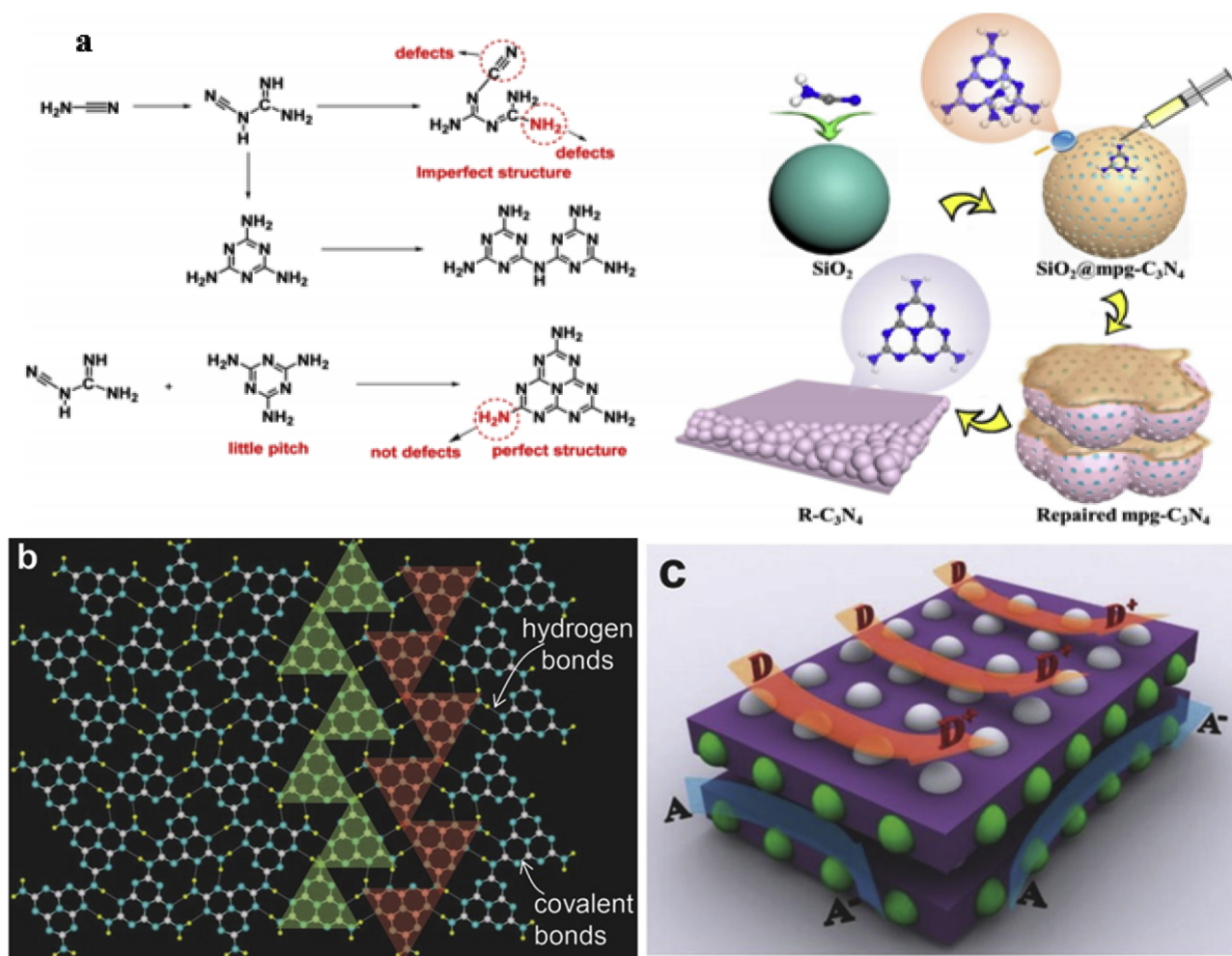
Fig. 10. a) Schematic illustration of repairing defects of mpg-C$_3$N$_4$ to R-C$_3$N$_4$. Reproduced with permission [247]. Copyrights 2016 American Chemical Society. b–c) top view of the atomic structure of layered carbon nitride. H, C, and N atoms are denoted by small yellow, large white, and light blue balls, respectively. Two nearest neighboring melon strands within the basal plane of monolayer carbon nitride are masked by solid green and red triangles in (b). the pristine layered carbon nitride and Electrons and holes are labeled by green and white spheres in (c) and (d), respectively. D: donor of electrons and A: acceptor of electrons. Reproduced with permission [256]. Copyrights 2016 Wiley.
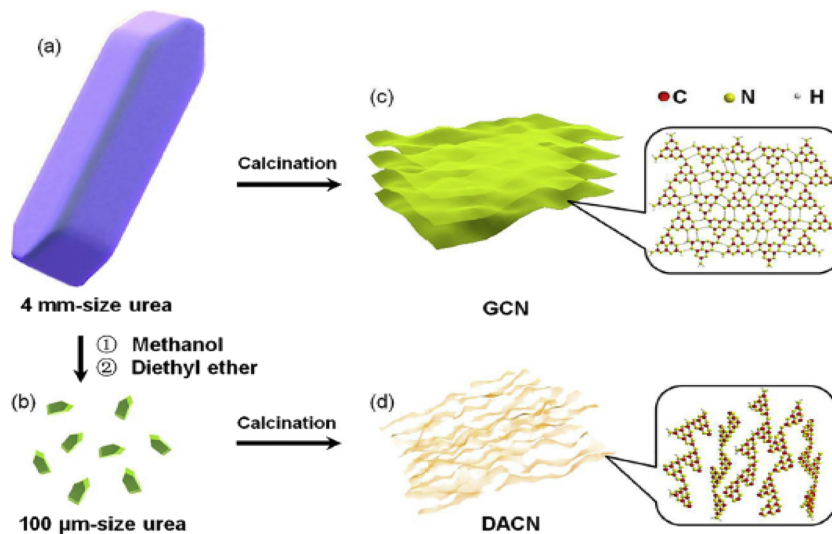

Fig. 11. Preparation process of DACN. (a) Pristine urea, (b) size-reduced urea, (c) GCN, and (d) DACN. Reproduced with permission [262]. Copyrights 2018 American Chemical Society.
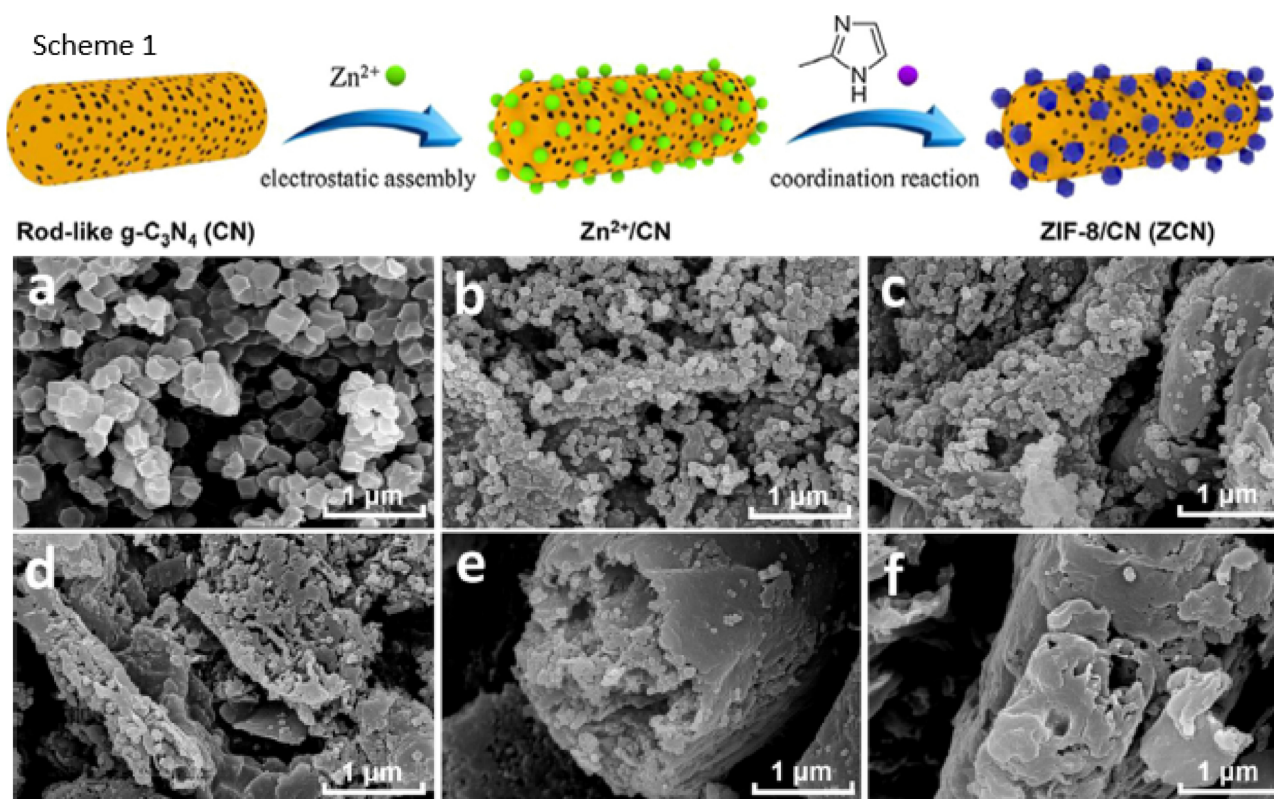
Fig. 12. Scheme 1: Schematic diagram of synthesis for ZIF-8/modified rod-like g-C$_3$N$_4$ composites, SEM images of (a) ZIF-8, (b) ZCN100, (c) ZCN200, (d) ZCN400, (e) ZCN800, (f) modified g-C$_3$N$_4$ sample CN. Reproduced with permission [285]. Copyrights 2018 Elsevier.

utilized to enhance the photocatalytic behavior of water splitting include g-C$_3$N$_4$, carbon nanodots, carbon nanotubes, (CNTs) carbon fiber, graphene, graphene quantum dots and other forms of carbon-containing materials [319–323]. The carbon dots consist of functional groups such as −OH, −COOH and −CHO having sp^2 bonded graphitic carbon less than 10 nm in diameter. It has very excellent optical features, diverse structure, good thermal and electrical conductivity. [324] The different synthesis methods regarding g-C$_3$N$_4$/carbon dots have already been discussed. [325–330]. A very recent Gogoi et al. [331] reported noble metal free ternary Cd$_{0.5}$Zn$_{0.5}$S-g-C$_3$N$_4$-MoS$_2$ composite for photocatalytic properties and evaluated for measuring the rate of

photocatalytic hydrogen evolution (Fig. 16). The loading of MoS$_2$ and carbon nitride onto Cd$_{0.5}$Zn$_{0.5}$S enhanced the hydrogen evolution by 197% and 120% respectively from the bare Cd$_{0.5}$Zn$_{0.5}$S. The average length of Cd$_{0.5}$Zn$_{0.5}$S is 100 nm (Fig. 16a,b). The FSEM images indicate that the structures are flat and porous (Fig. 16c,d). The MoS$_2$ has a large surface area which provides an excellent environment for hydrogen production. The FSEM image (Fig. 16e, f) of MoS$_2$ shows porous bunched structure about 500 nm diameter. The three materials are seen very close proximate to each other which are very helpful for charge migration (Fig. 16g, h, I, j). The improvement in the photocatalytic performance can be ascribed by the interfacial charge transfer of
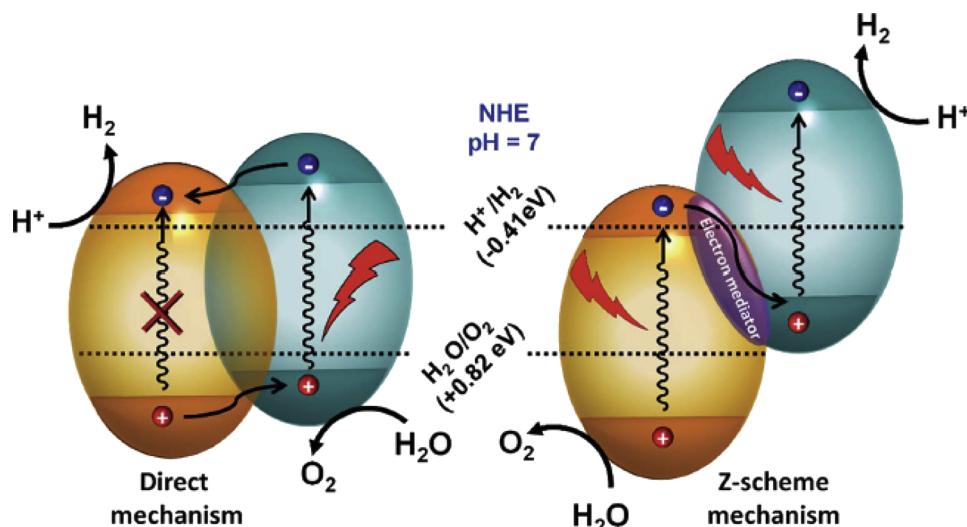

Fig. 13. Mechanistic representation of direct and Z-schemes of photocatalysis on two different bandgap semiconductors for overall water splitting. Reproduced with permission [6]. Copyright 2018 Royal Society of Chemistry.
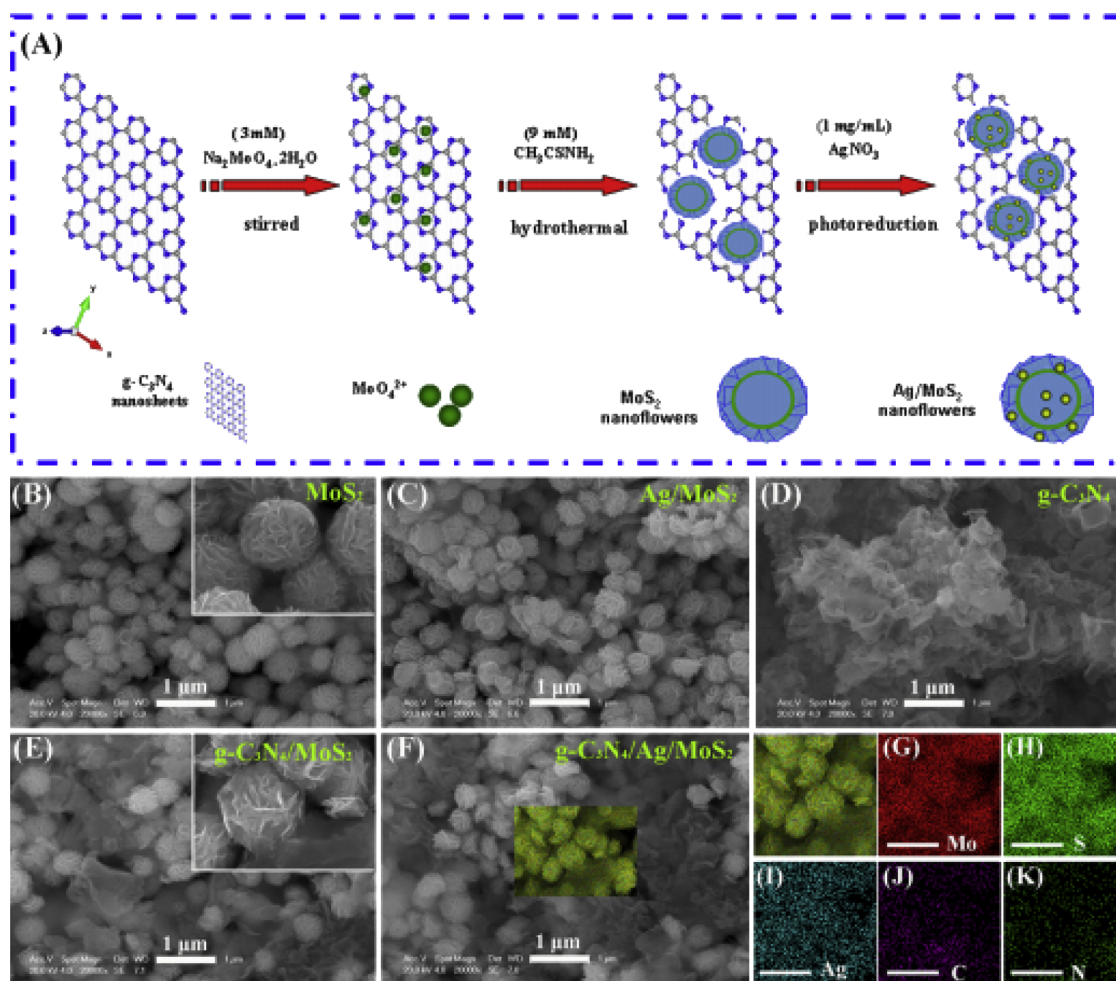
Fig. 14. (A) Schematic illustration of g-C$_3$N$_4$ and Ag co-modified MoS$_2$ microspheres synthesized by a novel process. SEM images of (B) MoS$_2$, (C) Ag/MoS$_2$, (D) g-C3N4, (E) g-C3N4/MoS$_2$, and (F) g-C$_3$N$_4$/Ag/MoS$_2$. (G–K) Corresponding elemental mapping images of the Mo, S, Ag, C, and N elements in the g-C$_3$N$_4$/Ag/MoS$_2$ microspheres. Reproduced with permission. [317] Copyrights 2017 American Chemical Society.
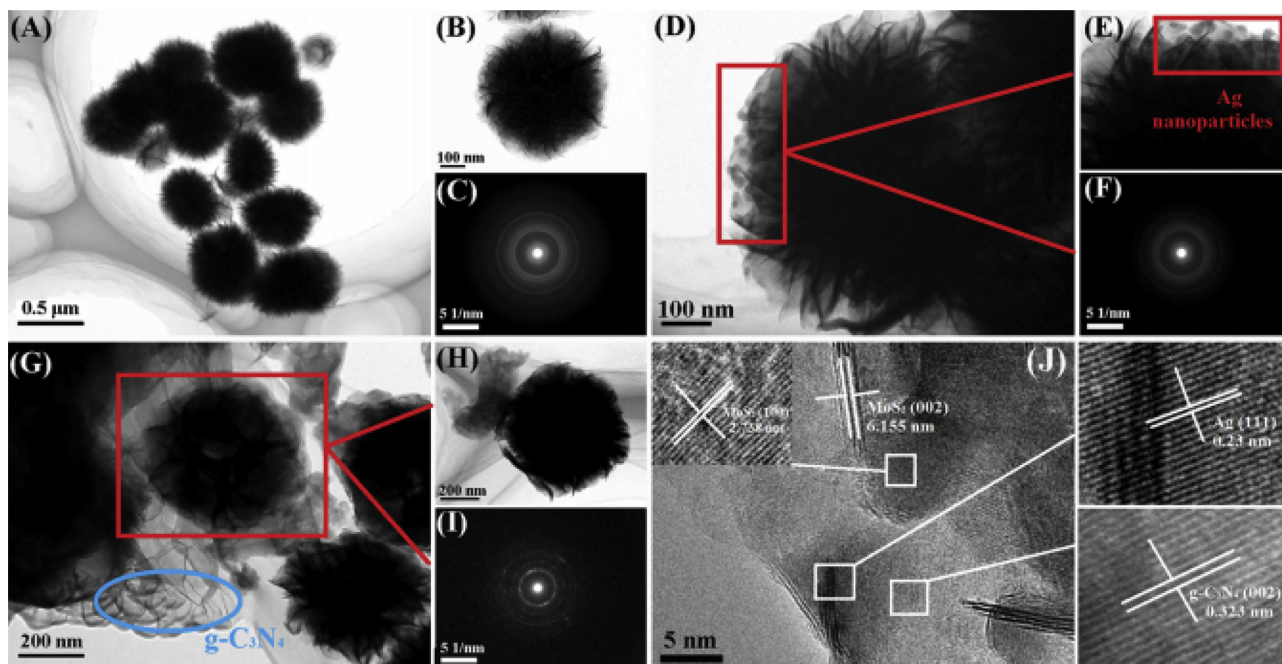

Fig. 15. TEM images and SAED patterns of (A–C) MoS$_2$, (D–F) Ag/MoS$_2$, and (G–I) g-C$_3$N$_4$/Ag/MoS$_2$. (J) High-resolution TEM of g-C$_3$N$_4$/ Ag/MoS$_2$. Reproduced with permission. [317] Copyrights 2017 American Chemical Society.
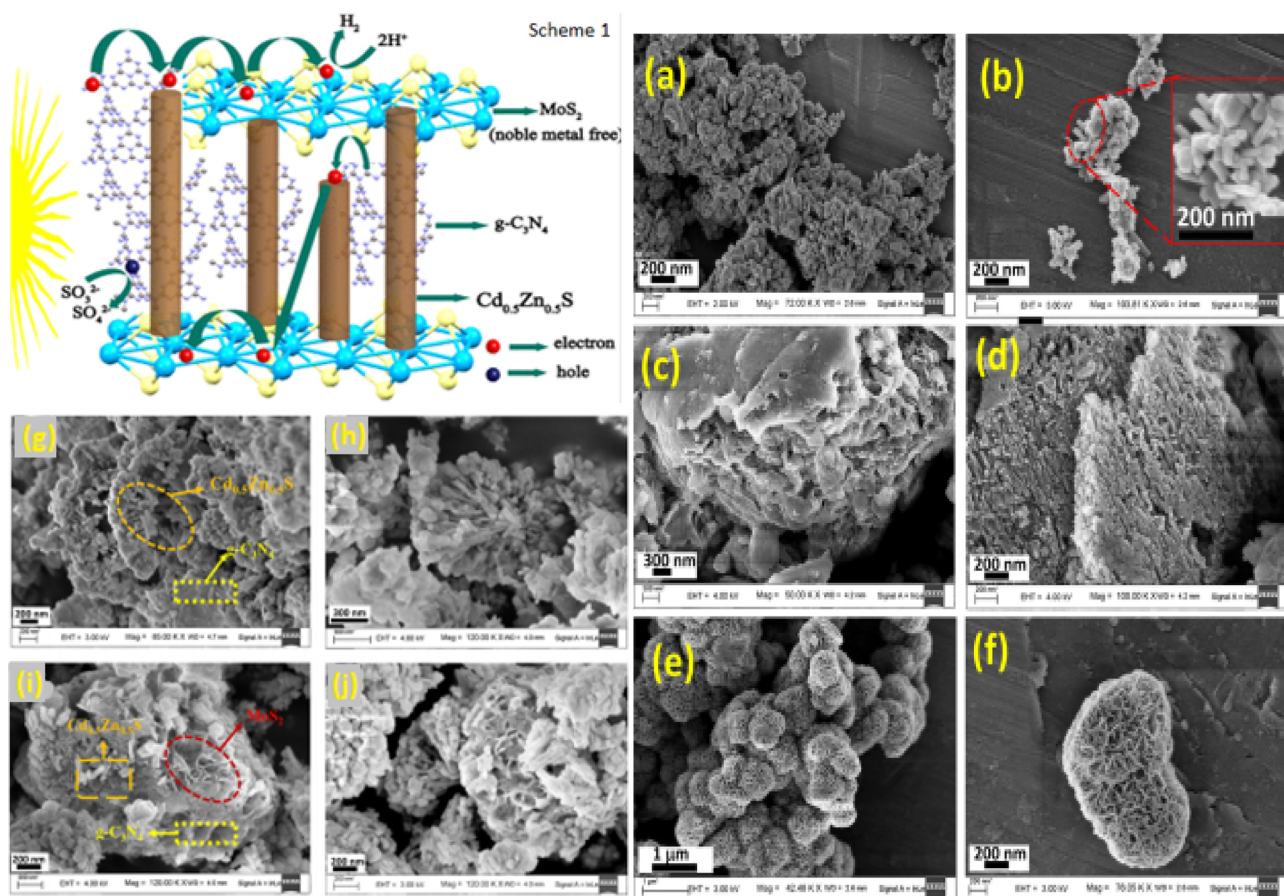
Fig. 16. Schematic 1: A schematic diagram of H_2 evolution process for the $Cd_{0.5}Zn_{0.5}S$-g-C_3N_4-MoS_2. Field-emission scanning electron microscopy (FESEM) images of (a, b) $Cd_{0.5}Zn_{0.5}S$, (c, d) g-C_3N_4, (e, f) MoS_2 (g, h) $Cd_{0.5}Zn_{0.5}S$-g-C_3N_4, (i, j) $Cd_{0.5}Zn_{0.5}S$-g-C_3N_4-MoS_2 at different magnifications. Reproduced with permission. [331] Copyrights 2018 American Chemical Society.

electrons from graphitic carbon nitride to $Cd_{0.5}Zn_{0.5}S$. MoS_2.

Li et al., employed deposition carbon QDs on g-C_3N_4 nanosheets to enhance the hydrogen evolution and the resulted rate was 116.1 mmol h^{-1} that is about three times higher than g-C_3N_4 nanosheets. [332]. Graphene is a single atom thick sheet of sp^2 hybridized carbon atom arranged in hexagonally. [2,333–335] There are different methods for the synthesis of graphene from graphitic such as epitaxial growth, mechanical exfoliation, chemical vapor deposition, chemical/electro-chemical reduction, etc. but exfoliated graphene oxide is mostly used [336–341]. The excellent conductivity, absorptivity, high thermal stability, flexibility, and specific surface area of graphene make it suitable for photocatalysis.

Zou et al. reported a different non-metal N-GQDs/g-C_3N_4 catalyst that shows better performance for hydrogen evolution from water splitting. [323]. The study shows there is absorbance of visible light region due to red shift by making a composite. The photogenerated electrons transferred from carbon nitride to CdS QDs and then after got maximum energy it accumulates at Pt where it played a role for the hydrogen generation. In another work by Qiu et al., the Nanoporous graphene was synthesized by Ni dopant using the CVD method. The results of DFT calculation and experimental studies show the remarkable increase in the hydrogen evolution. [342]. The chemical bonding between the nickel dopant and the carbon adjacent maintain the Ni species due to charge transfer and interplay between them caused the hydrogen evolution reaction. Yan et al. employed NGQDs-$ZnNb_2O_6$/g-C_3N_4 heterostructures for efficient photocatalytic performance as the hydrogen evolving catalysts. The results showed a higher amount of hydrogen evolution rate about 340.9 μmol h^{-1} g^{-1}. [343]. The NGQDs and heterostructure showed supportive effect that engendered more

electron-hole pairs and augmented the interfacial charge transfer.

Carbon Nanotubes (CNT's) comprising of carbon hexagons arranged concentrically, which represent carbon 1D structured allotropes. The CNT's can transfer superior electron that helps to improve the photocatalytic hydrogen evolution in g-C_3N_4. [344] In addition to it, nanocomposites of CNT's have the high surface area, active morphology and structure improve optical absorption rather than pure g-C_3N_4. [345]

Ge and Han synthesis multi-walled MWCNT/ g-C_3N_4 composites to enhance the photocatalytic performance for hydrogen generation. [346] The results showed a 3.7-fold higher evolution as compared to pure g-C_3N_4. In another study, MWCNT/g-C_3N_4 prepared with cyanamide. There is an increase of 2.4-fold in the production of hydrogen with respect to bulk g-C_3N_4. [345] A very recent study investigated the effect of coupling carbon nitride with different types of CNT's on the photocatalytic hydrogen evolution [347]. They used (single (SWCNTs), double (DWCNTs) and multi-walled (MWCNTs) CNTs) to improve the photocatalytic effect in CN. The result concludes that the composite of CN with SWCNT's was most functionalized and evolved hydrogen about 2–5 times more than DWCNTs and MWCNTs.

3.4. Surface plasmon resonance

Another method for improvement in the efficiency of the photocatalytic material is Surface plasmon Resonance (SPR). It is the joint oscillations of the metal-free NPs cloud that caused due to the contact of the electromagnetic waves. It helps to sensitize the wide band gap of semiconductors by using metals like Au and Ag. [348–350] The SPR effect is one of the most effective and common strategies to enhance the photocatalytic activity for hydrogen evolution [351–354]. The different
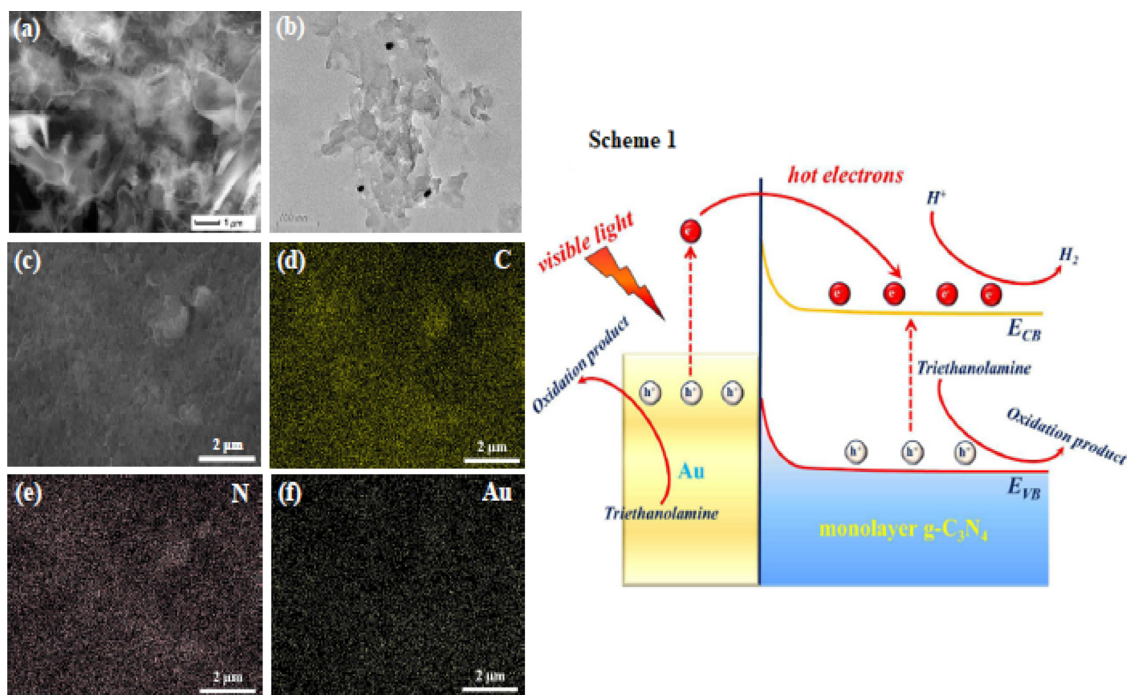
Fig. 17. (a) SEM image of monolayer g-C_3N_4. (b) TEM image of 1%bAu/monolayer g-C_3N_4. (c) SEM image of 1% Au/monolayer g-C_3N_4. Chemical element mapping images of 1% Au/monolayer g-C_3N_4 C 1s (d) N 1s (e), and Au 4f (f). Scheme 1: Schematic illustration of the proposed mechanism for photocatalytic H_2 evolution over the Au/monolayer g-C_3N_4 composites. Reproduced with permission. [377] Copyrights 2018 Elsevier.
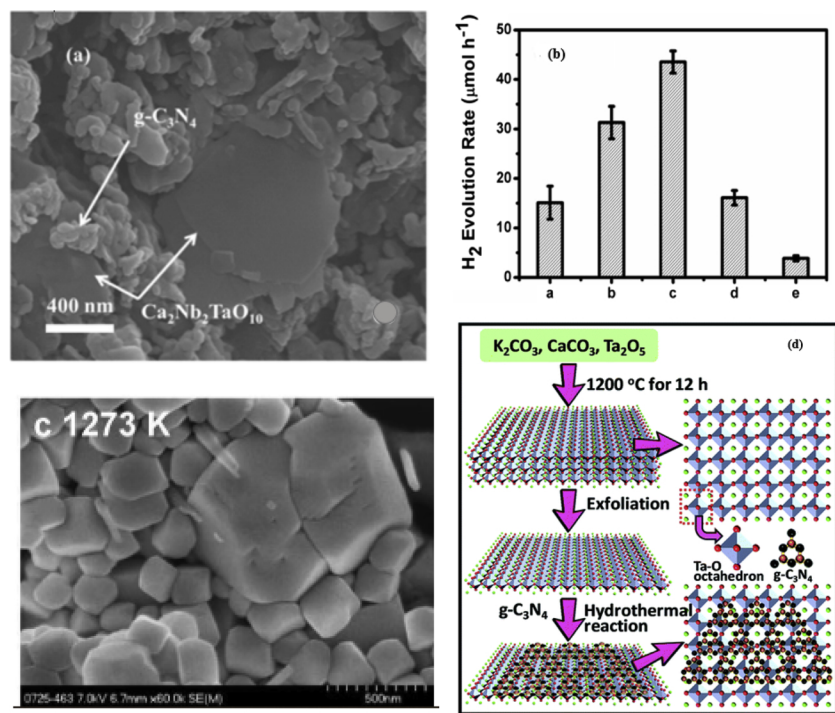

Fig. 18. a) SEM image of g-C_3N_4/$Ca_2Nb_2TakO_{10}$, b) Hydrogen Evolution Rate of different samples. Reproduced with permission [419]. Copyrights 2017 Elsevier. c) $BaTaO_2N$ samples obtained by nitriding amorphous $A_2Ta_2O_7$ 1273 K for 20 h under NH_3 flow. Reproduced with permission [420]. Copyrights 2009 American Chemical Society. (d) Schematic diagram of the synthetic process of the CN/KCTO heterojunctions. Reproduced with permission [421]. Copyrights 2009 American Chemical Society.

studies reported [355–361] that hot electrons are generated in the plasmonic metal when it coupled with semiconductors by suppressing the Schottky barrier under visible light portion and after that these hot electron flows towards CB of the semiconductor to activate the reduction reaction which enhances the photocatalytic activity.

The generation of heat near the NPs surface due to strong light absorption enhance the photochemical transformation. [362,363] There are three different methods to use plasmonic NPs for photocatalytic reactions [360,364–366]. (a) Direct, hot electron-induced photocatalysis on plasmonic NP surface (b) hot-electron transfer from plasmonic NP to nearby semiconductor or metal (c) SPR-induced electromagnetic field enhancement [367–372]. Cheng et al., used Au (Gold) nanoparticles on graphitic carbon nitride nanosheets by green photoreduction of Au (III) under visible light radiation. [373] Another study by Tonda et al. also used Au NPs on the mesoporous g-C_3N_4 sheet and both the studies showed SPR absorption in Au NPs which lead to improving the photocatalytic efficiency. [374]

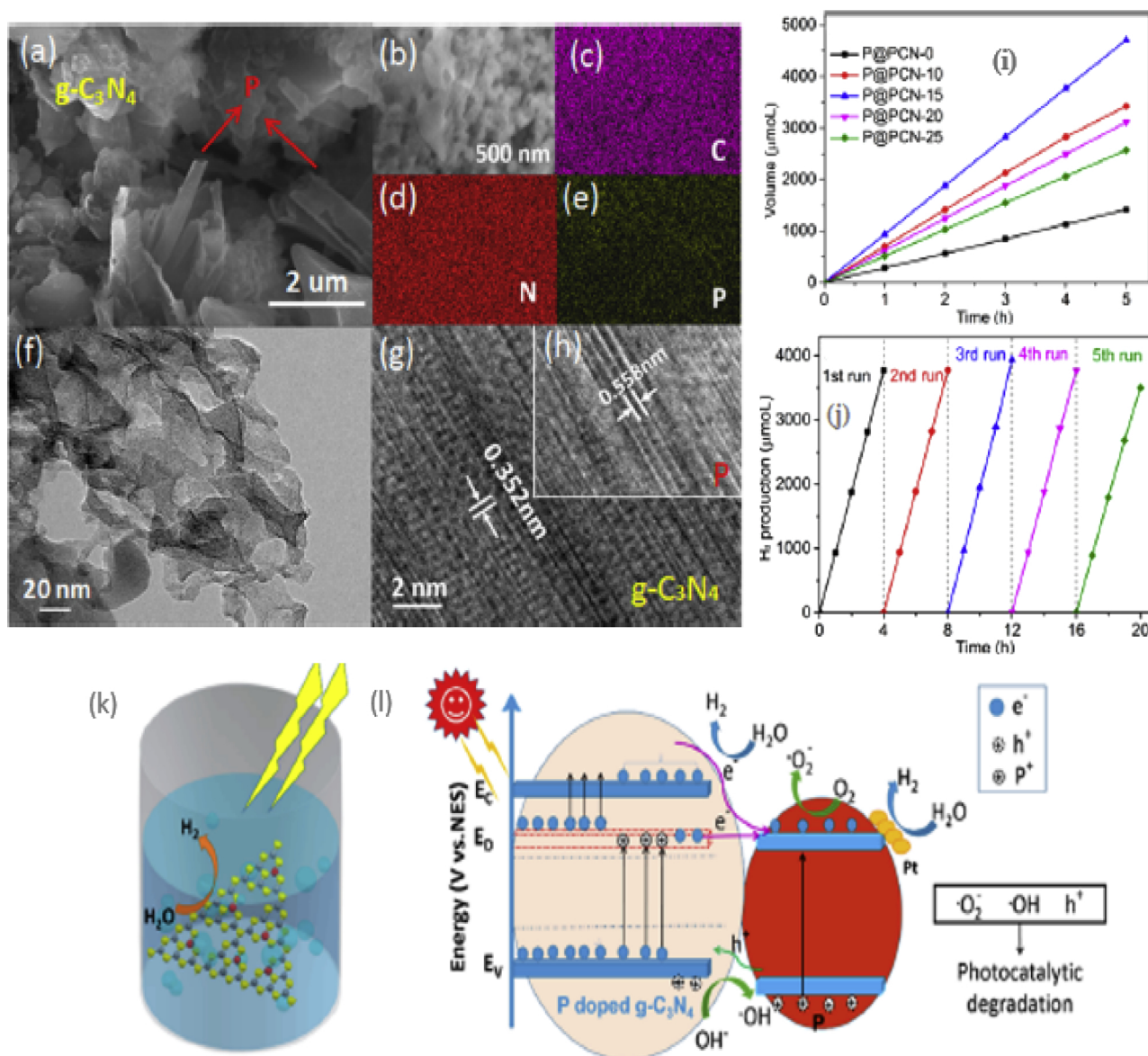Wang et al. demonstrated the preparation of Ag@AgBr and claimed

Fig. 19. (a) SEM and (b) FESEM images of P@PCN-15. The EDX mapping images of (c) C, (d) N, and (e) Pin P@PCN-15 sample. (f–h) The TEM and HRTEM images of P@PCN-15. Comparison of (i) H₂ evolution rate of the P@P-g-C₃N₄ composites. (j) Recycled H₂ evolution curves (k&l) H₂ evolution mechanism schematic illustration of the P@P-g-C₃N₄ catalysts. (Ec: conduction band; Ev: valence band; E_D: impurity level, $\Delta E_D = Ec-E_D$; $\Delta E_D \ll Eg$). Reproduced with permission. [494] Copyrights 2018 American Chemical Society.

that it is highly active plasmonic photocatalyst under visible light. [375] In another study Ag nanoparticles synthesized on monolayer g-C₃N₄ nanosheet which proved the role of SPR in the enhancement of photocatalytic activity. [376] A very recent study by Mo et al. employed Au/monolayer g-C₃N₄ in which Au plasmonic nanoparticles loaded on a monolayer of g-C₃N₄ by oil bath method. [377] The proposed composite displayed a better photocatalytic hydrogen evolution than monolayer g-C₃N₄ (Fig. 17).

The improvement in the activity of photocatalytic was due to the successful injection of Au nanoparticles that leads to an SPR effect. The proposed system presented in Fig. 17 that shows Au plasmonic nanoparticles and monolayer g-C₃N₄ were both excited to separate electron-hole pairs under visible light. Further, there are many other studies related to plasmonic photocatalysis have been done by different researchers, [378–391] and it offers a more mechanical aspect.

3.5. Perovskite-type oxides (ABO₃)

It is one of an effective photocatalyst due to its exclusive crystal structure and electronic properties used for water splitting. [392–399] It is an essential inorganic functional material having general formula ABO₃ where A contains 12 oxygen atoms, and B contains six oxygen atoms represents the alkaline earth metal and transition metal respectively. [400,401] The crystal structure of perovskite enhances the absorption of visible light and band edge potential by tuning the band gap. The separation of charge carriers is strongly influenced by lattice distortion in perovskite. There are five major groups in perovskite materials such as titanate perovskites [402–409], tantalite perovskites [400,410–413],vanadium-niobium based perovskites [412,414,415] and ferrite perovskites [410,416–418]. The perovskite band gap fully supports both UV & visible light and most important its band alignment concerning hydrogen and oxygen generation redox potentials allow water splitting. [393,394]. The water splitting efficiency of ABO₃ enhances by altering the chemical components A, B, and O. It can be done

by replacing ion doping or by additional doping of cocatalyst. [392,398].

Furthermore, this oxide is fabricated by heterojunction hybrid system with g-C_3N_4 for the better photocatalytic system. [422–424] In the recent study exfoliated g-C_3N_4 and $Ca_2Nb_2TaO_{10}$ nanosheets with a mass ratio of 80:20 was prepared as shown in Fig. 18. [419] The results exhibit that the hydrogen evolution is 2.8 times more than bare g-C_3N_4 bulk. The improvement of photocatalytic performance under visible light irradiation referenced to the interfacial connection between g-C_3N_4 and $Ca_2Nb_2TaO_{10}$ nanosheets which suppress the charge recombination.

Jiang et al. prepared a CN/KCTO 2D–2D nanosheet heterojunctions by two-step wet chemistry strategy having a strong interaction. [421] The heterojunctions showed the hydrogen evolution rate about 647.19 μmol g^{-1}, which is 2.07 times higher than that of CN. The construction of 2D-2D heterojunctions based on Dion Jacobson type perovskite oxide is an efficient way to enhance photocatalytic activity.

Moreover, the heterojunction hybrid system for charge separation of g-C_3N_4 is done by Z-scheme ternary hybrid. [16,303,424–428] There are some mix tantalum oxynitride perovskites of $ATaO_2N$ (A = Ca, Sr, Ba) are studied to enhance the hydrogen generation [420]. These materials manufactured by annealing amorphous $A_2Ta_2O_7$ under NH_3. The maximum hydrogen evolution rate from $BaTaO_2N$ was 50 μ mol/h, followed by $CaTaO_2N$ (24 μ mol/h) and $SrTaO_2N$ was 42 μ mol/h. In the past few years, there are frequent studies came into developed regarding photocatalytic hydrogen production by g-C_3N_4 nanomaterial. Table 1 summarizes and compared the recent advances in the hydrogen production according to reaction conditions and hydrogen rate.

4. Reduced band gap and charge recombination

4.1. Other doping materials

There are many doping materials that can be helpful to reduce band gap as well as reduce charge recombination. As the doping of phosphorus narrows the band gap and increase the charge separation efficiency. Zhou et al., the study reveals the result that P atoms were easily fitted in the carbon nitride lattice and change the electronic properties as well as reduce charge recombination's [228]. Moreover, they proposed that P atoms were located in the corner of carbon and bay carbon sites that is in converse to the finding of Hue et al. [220], Jing et al., prepared the red phosphorus modified g-C_3N_4, the results display that there is prominent hydrogen production of 6.2 times more than pure g-C_3N_4. [493]

Similarly very recently Feng et al., fabricated P doped g-C_3N_4 composite (P@P-g-C_3N_4) by solid reaction route. [494] TEM images in Fig. 19f show that sample morphology is smooth, flat and thin sheet while the SEM image Fig. 19a–b and the EDX elemental mapping indicates that there is a presence of C, N, and P on g-C_3N_4. By combining the SEM, HRSTEM and XRD pattern result, P has successfully doped into g-C_3N_4. The DFT calculation indicates that P doping in g-C_3N_4 at C_1/C_2 site holds the same band structure and P doping increase the light absorbance and improves the photocatalytic activity by introducing defective states in the forbidden band below covalent band edge. After altering the mass ratio of precursors, the P@PCN-15 sample shows the maximum hydrogen production about 941.80 μmol h^{-1} g^{-1}.

Hong et al. prepared S doped g-C_3N_4 with individual thiourea. It enhanced the light absorbance and reduced the charge recombination which results to produce 30 times more H_2 from the bare g-C_3N_4 [238]. Huang et al. studied O doping by treating melamine with H_2O_2 and concluded that oxygen doping happens on two sides of N position. It

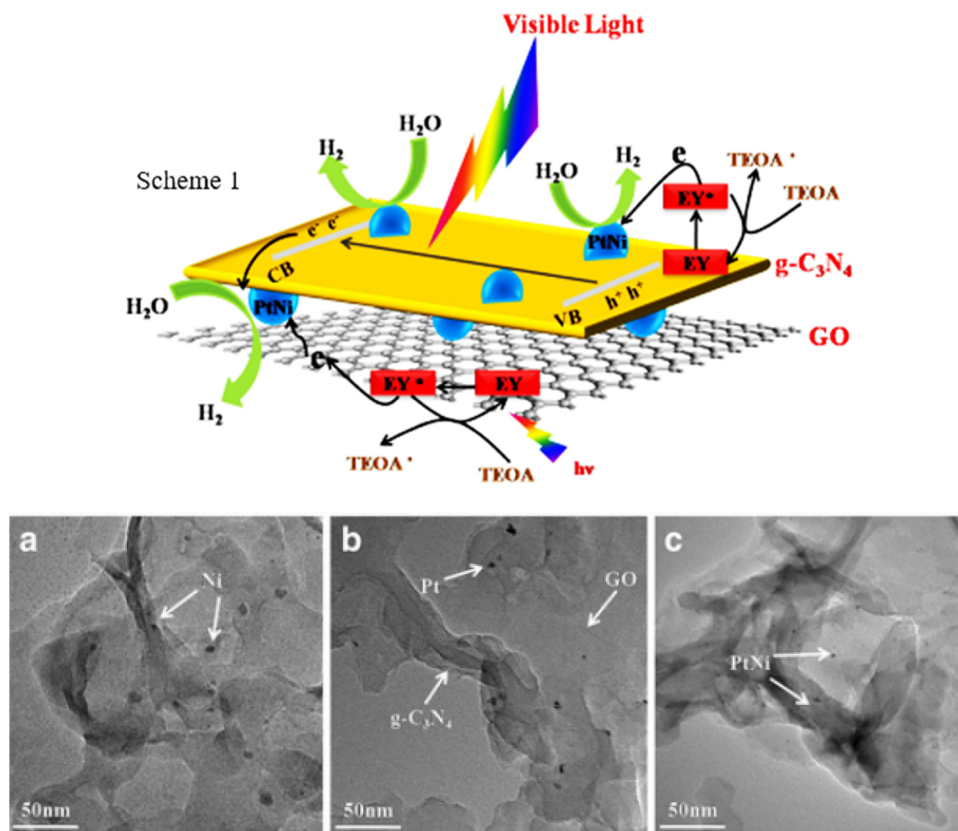**Fig. 20.** Schematic 1: A schematic diagram of H_2 evolution process for the Eosin Y-sensitized g-C_3N_4/PtNi/GO composite sample under visible light irradiation (a) TEM images of g-C_3N_4/Ni/GO-0.5%, (**b**) g-C_3N_4/Pt/GO-0.5%, (**c**), and g-C_3N_4/PtNi/GO-0.5%. Reproduced with permission. [508] Copyrights 2018 Springer.
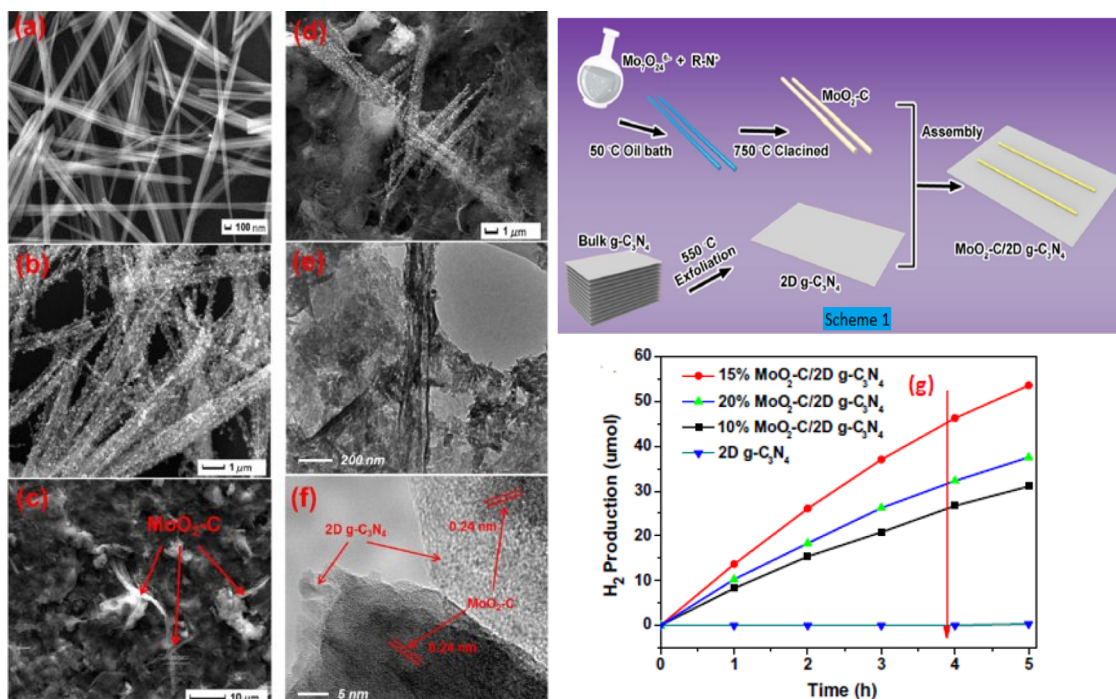
Fig. 21. Scheme 1. illustration of synthesizing 2D g-C$_3$N$_4$, MoO$_2$-C/2D g-C$_3$N$_4$. SEM images of Mo$_3$O$_{10}$ (C$_6$ H$_8$N).2H$_2$O organic intermediate (a), MoO$_2$-C (b), 15% MoO$_2$-C/2D g-C$_3$N$_4$ (c and d), (e) TEM image of 15% MoO$_2$-C/2D g-C$_3$N$_4$, (f) HR-TEM image of 15% MoO$_2$-C/2D g-C$_3$N$_4$ (g) Photocatalytic hydrogen evolution activity of 2D g-C$_3$N$_4$ and MoO$_2$-C/2D. (g) g-C$_3$N$_4$ composites loaded with the different amount of MoO$_2$-C. Reproduced with permission. [161]. Copyrights 2018 Elsevier.

promotes the light absorbance and charges separation which increases the hydrogen evolution. [202] Another halogen element bromine is also used to increase photocatalytic activity of g-C$_3$N$_4$. The Br-doped sample prepared by co-condensation of ammonia bromine and urea. [495] The results revealed that the rate of hydrogen generation is two times more than pure g-C$_3$N$_4$ and oxygen evolution is also enhanced.

Dong et al. described the self-doping of carbon in graphitic carbon nitride by replacing the N atoms bridging with C atoms, that can change the electronic and band structures. [181] According to DFT calculation results, the creation of delocalized π bond between carbon doped atoms and aromatic rings due to the replacement of carbon, there is an increase in the electrical conductivity of the material, and it supports the electron transfer. Further, carbon self-doping also narrows the bandgap up to 2.65 eV and help to get more visible light. In another study by Zhao et al. who prepared C self-doped g-C$_3$N$_4$ photocatalysts by using the poly porous carbon foam as a soft template for getting maximum photocatalytic activity toward purification of NO in the air. [226] They also claimed that C doped g-C$_3$N$_4$ increased the BET surface area and absorbed light near infrared range which enhanced electron holes separation. Zhang et al. prepared carbon-doped g-C$_3$N$_4$ nanosheet using a precursor of melamine and glucose which increased the light absorption and reduce band gap. [225]

Zhou et al. [496] studied the preparation of N-doped g-C$_3$N$_4$ using urea and citric acid for the thermal polymerization. It suggested that N doped graphitic carbon make a π-conjugated system which increases the visible light absorbance and enhances photocatalytic activity. In another study, N doped g-C$_3$N$_4$ symphonized by condensation of melamine and hydrazine hydrate. The results proved that N doping promotes the charge separation and photocatalytic hydrogen generation by visible light irradiation. [81]

4.2. Dye- sensitization of g-C$_3$N$_4$

A long time ago, dye-sensitized solar cells used for the effective consumption of solar energy. The photocatalytic activity efficiently increases by the electron injections from dye excitations and light absorption. [372] The dye with a low energy level between the HOMO-LUMO gap can use. The electron injected into the CB during the excitation of dye so that it can involve in the reduction reaction [497,498]. The transfer of an electron from the VB to semiconductor impedes by band alignment. Following this method, ZnO, TiO$_2$, Nb$_2$O$_5$, and other d$_0$ oxides sensitized to reduce water in visible light. [499,500] Similarly, the study of cadmium chalcogenide QDs (e.g., CdS, CdSe) or PbS QDs reported that these materials could use for sensitization and subsequent reduction of water on the wide bandgap oxides if they have higher CB edge than these oxides [498,501–503].

Wang et al. studied erythrosine B (ErB) dye on carbon nitride nanosheets. [504] After sensitization, it observed that maximum quantum efficiency was 33.4% while hydrogen evolution was 14.5 times higher than pure carbon nitride. This work reveals a simple method for stacking well isolated Pt nanoparticles on CN by using ErB photosensitizer for optimal improvement in photocatalytic activity under visible light. Xu et al. reported carbon nitride sensitized by eosin Y (EY) and found that maximum quantum yield in hydrogen evolution was 18.8%. [505]. They claimed that carbon nitride prepared at 600 °C have lowest defect but highest sensitization activity.

Zhang et al. [506] reported Erythrosine B dye used to sensitized into Cu-Cu$_2$O/g-C$_3$N$_4$ and the highest H$_2$ production rate was 5000 μmol g^{-1} h^{-1} observed. They proposed the possible photocatalytic method of Erythrosine B Cu-Cu$_2$O/g-C$_3$N$_4$ for the improvement of hydrogen generation. The transfer of electron from ErB dye is thermodynamically balance because CB edge of g-C$_3$N$_4$ is more negative than CB of Cu$_2$O vs NHE. The electron transfer from photoexcited dye to g-C$_3$N$_4$ and shift towards Cu$_2$O then to CuO for hydrogen production. Hence, the sensitization of ErB dye enhance the hydrogen evolution.

In another study, Wang et al. reported Eosin Y for sensitizing ternary g-C$_3$N$_4$/Pt/GO composite by using simple liquid-phase sonochemical approach. [507] The results show the highest hydrogen production rate of 3.82 mmol g^{-1} h^{-1} which is about 2.1 times and 7.7 times higher
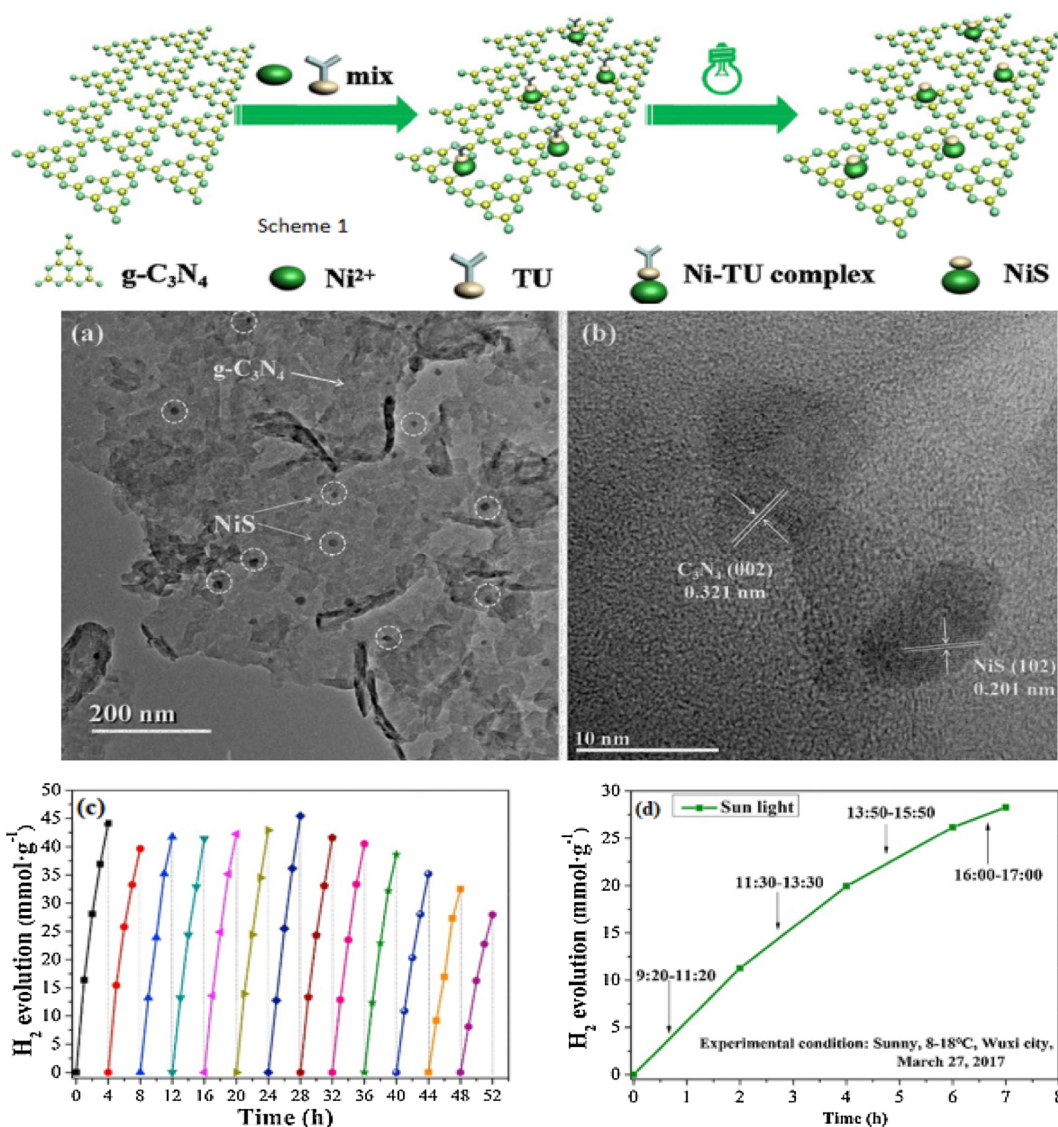
Fig. 22. Scheme 1. Proposed photochemical synthesis route of NiS/g-C$_3$N$_4$, (a) TEM image and (b) HRTEM image of NiS-20/g-C$_3$N$_4$., (c) Cycling runs for photo-catalytic hydrogen evolution in the presence of 5.0 mg NiS-20/g-C$_3$N$_4$ photocatalyst in a 10 vol% aqueous triethanolamine solution, using a 300 W Xe lamp with an AM 1.5 G cut filter as the light source. After every 4 h, the produced H$_2$ was evacuated and 1 mL sacrificial agent (TEOA) was renewed. (d) Photocatalytic hydrogen production during 7 h under sunlight irradiation in Wuxi city on March 27, 2017. Experimental condition: Outdoor temperature: 8–18 °C, Time: 9:20-17:00. The system contains 5.0 mg NiS-20/g-C$_3$N$_4$, 1 mL TEOA (98%) and 9 mL water. Reproduced with permission [526]. Copyrights 2018 Elsevier.

than the Eosin Y-sensitized binary g-C$_3$N$_4$/Pt and GO/Pt photocatalysts, respectively. according to the study, the large surface area is not only the factor to increase the photocatalytic effect as in this case hydrogen generation is enhanced by improving charge separating efficiency. A very recent wang et al. study the Eosin Y-sensitized g-C$_3$N$_4$/PtNi/GO-0.5% composite photocatalyst that yields about 1.54 and 1178 times higher hydrogen evolution rate than the Eosin Y-sensitized g-C$_3$N$_4$/Pt/GO-0.5% and g-C$_3$N$_4$/Ni/GO-0.5% samples, respectively. [508] According to the results, they also proposed a schematic illustration to understand the H$_2$ generation process for the Eosin Y-sensitized g-C$_3$N$_4$/PtNi/GO composite sample (Fig. 20 Scheme 1). The TEM images show three different samples having the same laminar structures. The result shows that the more hydrogen evolution site could be found by small size of PtNi alloy cocatalyst and electron transfer could enhance by their high dispersivity.

5. Enhanced surface kinetics

5.1. Bimetallic catalyst

In the photocatalytic process, the electrons and holes generation after light harvesting and transfer to surface redox reaction which accumulates at the surface of g-C$_3$N$_4$ and lowers the water splitting process. [62,113] This charge accumulation on the surface not only increase the recombination of charges but also affect the long-term stability of the material [113,509]. To accelerate the surface kinetics different types of cocatalyst used on the surface of the photocatalyst [64]. There are different cocatalyst that has been used in g-C$_3$N$_4$ to promote the photocatalytic effect such as, Pt [111], NiS [479,481], MoS$_2$, [467] Ni (OH)$_2$ act as hydrogen evolution catalyst (HEC) [473] and single site Co- based cocatalyst. [510] It cleared from the study that no hydrogen produced without cocatalyst over the bare C$_3$N$_4$ NTs. [511] General, Pt nanoparticles extensively used for photocatalytic hydrogen evolution [512–516]. Apart from Pt, Pd, Au, and Ag have also been loaded in g-C$_3$N$_4$ by various researchers. [373,374,472,517–521]
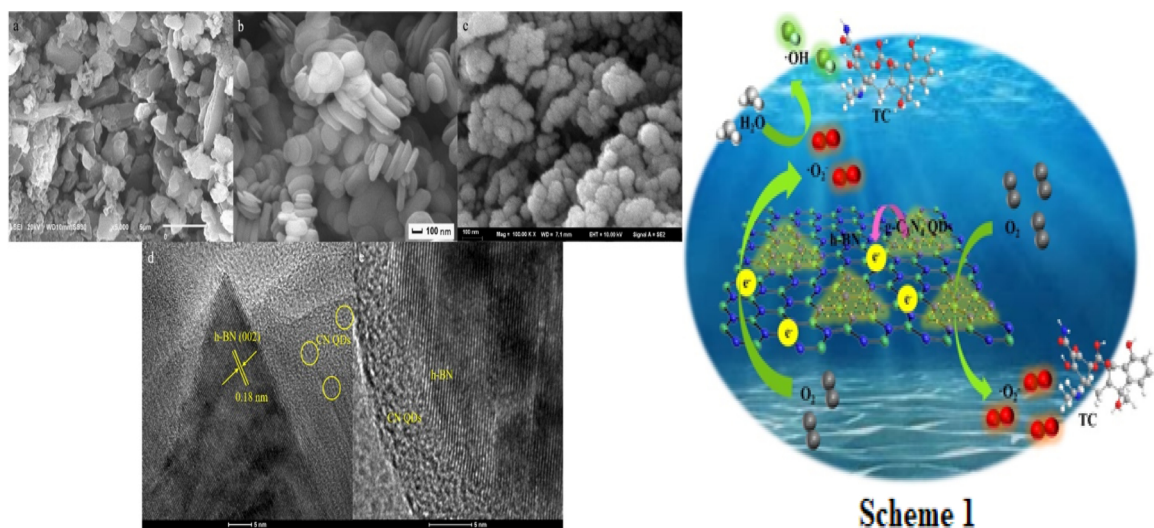
Fig. 23. SEM images of bulk CN (a), h-BN (b), and CNBN composites (c). HRTEM images of CNBN samples (d, e). Scheme 1: Proposal mechanism for photocatalytic performance over CNBN composites. Reproduced with permission [532] Copyrights 2018 Elsevier.
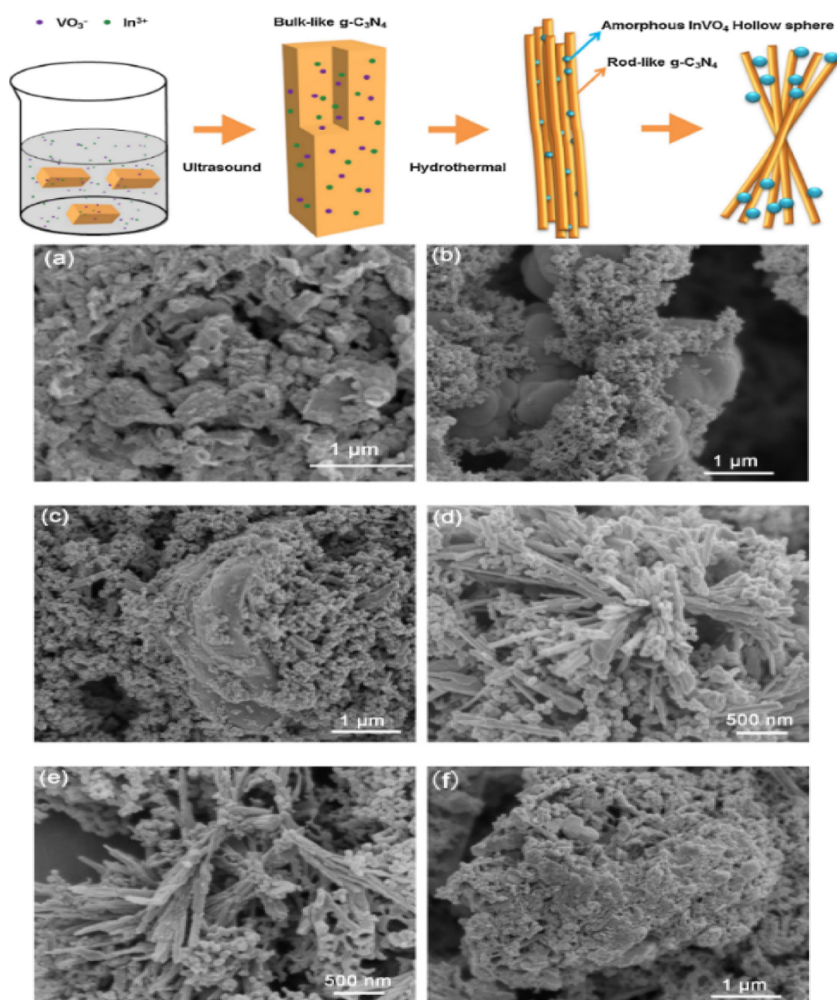
Fig. 24. Scheme 1. The schematic illustration of the formation of g-C$_3$N$_4$ nanorod/InVO$_4$ hollow sphere composites, SEM images of (a) CN, (b) RCN/SI-20, (c) RCN/SI-40, (d) RCN/SI-50 (e) RCN/SI-60 and (f) BCN/NI-50. Reproduced with permission [537]. Copyrights 2017 Elsevier.

Fig. 25. Scheme 1, Top-down process for the preparation of foam-like holey ultrathin g-C$_3$N$_4$ nanosheets. SEM images of A) CNB, B) CNS, and C) CNHS samples. TEM images of E) CNB, F) CNS, G) and H) CNHS samples, I) photographs of (1) CNB, (2) CNS, and (3) CNHS. Reproduced with permission [561]. Copyrights 2016 Wiley.

Due to the high cost and limited reserves of noble metals, there is a need to explore other inexpensive co-catalyst having high stability 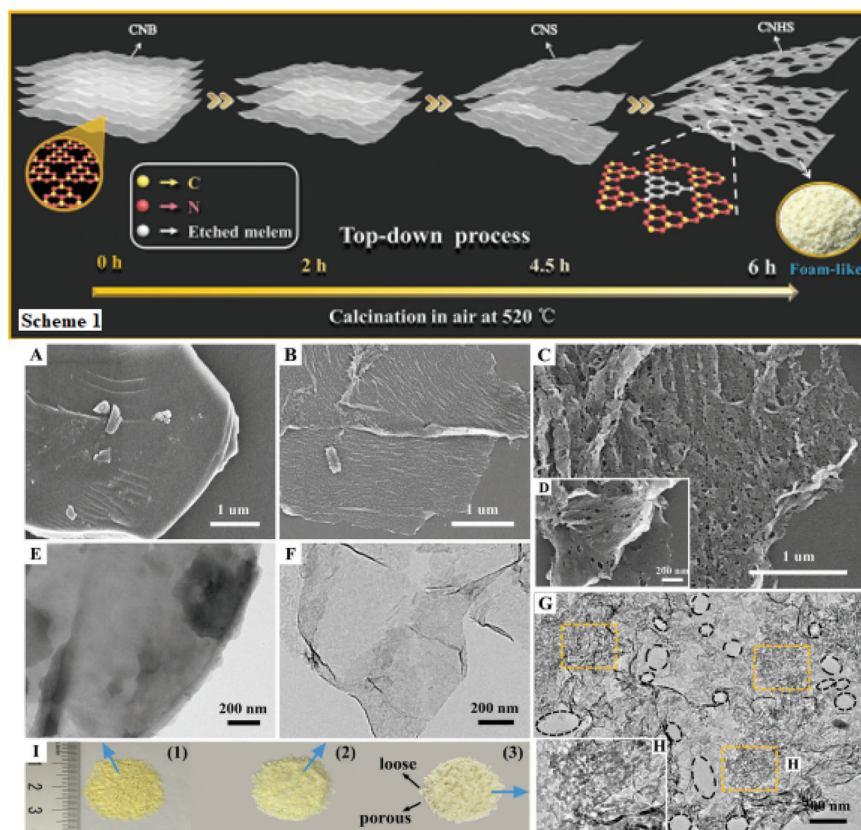like Ag and Cu [250,515,522]. MoS$_2$ is a potential candidate for replacing Pt cocatalyst for photocatalytic water splitting. A recent study by Chen et al. employed 1D MoO$_2$-C nanowire as a cocatalyst over 2D g-C$_3$N$_4$ for hydrogen evolution [161] (Fig. 21). The morphology of the material MoO$_2$-C studies by SEM and TEM images. The nanowire like material in Fig. 21a shows that it is 1D structure and after calcination, it maintains the 1D structure (Fig. 21b). MoO$_2$ cluster are fastened on the 2D g-C$_3$N$_4$ sheet as shown in SEM images Fig. 21c. The TEM images show that the carbon element is present in form of amorphous carbon. The results showed that the hydrogen evolution rate was about 1071.0 l mol g^{-1} h^{-1} that is 157.5 times higher than pure 2D g-C$_3$N$_4$. According to this study, MoO$_2$-C has good electrical conductivity, highly active sites are available and have great ability to extract photogenerated electrons that help for the photocatalytic hydrogen production.

In recent years, transition metal sulfides recognized as a promising candidate for hydrogen evolution. [523–525] Zhao et al. [526] reported the case of NiS/g-C$_3$N$_4$, photochemical synthesis way to distinctive transition metal sulfides as a cocatalyst for hydrogen evolution. NiS synthesized by a facile and rapid photochemical method (Scheme 1 Fig. 22). It is clear from the TEM images (Fig. 22b) that NiS particles of size 10 nm are deposited on the g-C$_3$N$_4$ sheet. Fig. 22c–d shows the hydrogen production as a function of irradiation time that indicated the good stability of NiS material over g-C$_3$N$_4$. The improved photocatalytic hydrogen evolution rate is straddling up to 16,400 μmol g^{-1} h^{-1} with 0.76 wt % NiS loading, which is about 2500 times higher than that of pure g-C$_3$N$_4$. Furthermore, the hydrogen evolution of the NiS/g-C$_3$N$_4$ composite photocatalyst reached 28.3 mmol g^{-1} during 7 h under natural sunlight. The loading of NiS has greatly controlled the charge transfer and separation in the composite which dominantly enhance the H$_2$ evolution.

5.2. Morphology tuning

The enhancement of photocatalytic hydrogen evolution performance of the material mainly depends on morphology, size and the structure of the photocatalyst. Moreover, different photocatalyst shows different optical, chemical and physical properties. [527,528] Therefore, we have classified to 0D quantum dots structure, 1D rod-like, 2D sheet-like, and 3D sphere-like nanostructures depends on their structures [62,529].

5.2.1. g-C$_3$N$_4$ quantum dots 0D structure

Due to an excellent optical behavior of graphitic carbon nitride quantum dots, it can convert NIR light to visible light and plays a crucial role in harvesting solar energy. [449] Li et al., modified single-crystalline TiO$_2$ nanotube by CN QDs and found enhancement in the photocatalytic hydrogen production. [85]. As quantum dots mostly adjust the position of conduction band more negative so it supports to directly transfer the electron from g-C$_3$N$_4$ to CB of TiO$_2$ then to Pt to produce hydrogen. In this work, both the single crystal enhanced the transfer of electron and efficiently inhibited the electron hole recombination with the development of highly efficient photocatalysis system. An et al., studied the similar work as CN QDs decorated TiO$_2$ nanowires and reported that photocatalytic performance significantly enhanced due to the sensitization effect of quantum dots. [530] In another study, GQDs@ZnO nanowires have designed by covalently bonding with amine groups. The GQDs@ZnO NWs photoelectrodes show enhanced performance for photochemical water splitting [531]. According to the study, the promising energy level of quantum dots and zinc oxide asssist the flow of charges and indorses the charge separation and retarded charge recombination. The smooth layer of QDs on ZnO wire also boost the charge movement and enhance the hydrogen production.

A very recent the metal-free material of CN QDs embedded in the h-BN and synthesized by using calcination. [532] The study proved that it does not only facilitate the redshift but also h-BN having OH group also act as an active site which enhances the photocatalytic performance (Fig. 23).

The SEM images of bulk CN indicates that it has a low surface area (Fig. 23a) and Fig. 23b shows that h-BN has a smooth round shape. The results of overall images show that CN quantum dots entirely entrenched on the h-BN surface, and it is helpful for electron transfer and its stability. Latest, Cai et al. prepared porous 0D/2D C_3N_4 nanocomposite (PCN) by the simple green one-pot method and modified with CN QDs. [533] The band alignment between CNQDs and nanosheets of C_3N_4 promote the charge separation carriers and give more active sites. Thus, the photocatalytic hydrogen generation rate of PCN is about 30 times more than that of the bulk g-C_3N_4.

5.2.2. 1D rod-like nanostructures

The 1D structures have a large area of surface and length/diameter ratio is high that can reduce the charge diffusion length and enhance the light harvesting. [534] It includes nanorods, nanowires, and nanotubes having exceptional properties. For example, the nanomaterials with a tubular structure can transfer the charge carriers along the 1D path and provide a high surface area for photocatalytic reaction. Hence, the modification of g-C_3N_4 with 1D structure can be helpful for future hydrogen generation. [535] Guo et al. reported phosphorus doped hexagonal tubular C_3N_4 (P-TCN) obtained from rod-like single crystal precursor and exhibit hydrogen evolution rate of $67 mmol h^{-1}$. [237]. The hexagonal structure pointedly increase the surface area which also enhance the density of active sites. The doping of phosphorus reduce the bandgap, increase the electrical conductivity and conquers the recombination of electron-hole pairs, as a result improve the efficiency of hydrogen evolution. In another study 1D g-C_3N_4 micro-rods showed 26 times higher photocatalytic hydrogen evolution performance than bulk g-C_3N_4. [534]. The nanopores have been generated on the 1D structure that persuaded the density of active sites and leads to the separation of electron hole transfer.

A recent study by Zeng et al. [536] employed preparation of g-C_3N_4 nanorods by calcination of hydrous melamine and oxygen atoms doped into a g-C_3N_4 matrix that broke the symmetry of pristine g-C_3N_4, resulting in more effective separation of electron-hole pairs. The photocatalytic hydrogen evolution rate was $96 \mu mol\, g^{-1} h^{-1}$.

A novel study on g-C_3N_4 nanorods/lnVO$_4$ hollow sphere composite was reported. [537] The InVO$_4$ hollow sphere uniformly added on the surface of the carbon nitride nanorod and forming a heterojunction. The bulk morphology of CN seen in Fig. 24a. The nanoparticles of lnVO$_4$ observed in Fig. 24b-c. The composite of g-C_3N_4/lnVO$_4$ seen in the SEM image Fig. 24f and g-C_3N_4 monolithic structures appears on it. The results showed that visible light photocatalytic activities had increased due to the synergetic effect of light harvesting, high transfer, and separation of charges.

5.2.3. 2D sheet-like nanostructures

To get a wide range of solar light and fast transfer of electron across heterojunctions, the large specific surface area of the catalyst is an important parameter. [452,538] In our understanding, two-dimensional (2D) structure have good conductivity, high chemical stability, high electron mobility, and good material [539,540]. Since now there are many designed have been discovered including graphene oxide, g-C_3N_4/CoO, Nb$_2$O$_5$ microspheres/ g-C_3N_4, g-C_3N_4/SiC, Co$_0$.5Cd$_0$.5S/g-C_3N_4, CuS/ g-C_3N_4, CdIn$_2$S$_4$/ g-C_3N_4, CdLa$_2$S$_4$/mesoporous g-C_3N_4, CdZnS quantum dots/2D g-C_3N_4, CdS/ g-C_3N_4/CuS, MoS$_2$/pyridine-modified g-C_3N_4, MoS$_2$/g-C_3N_4, CoTiO$_3$/g-C_3N_4, Mn$_0$.8Cd$_0$.2S/ g-C_3N_4, FeO$_x$/g-C_3N_4, and so on. [541–554] Among all these various semiconductors, metal sulfide has gained great attention in photocatalytic hydrogen evolution [555–559]. Jing et al. reported SnS$_2$/g-C_3N_4 composite and resulted exhibit a higher production of evolution

$6305.18 \mu mol\, h^{-1} g^{-1}$ which are 16 times higher than a SnS$_2$ nano-particle. [560]

The free standing 2 nm thickness g-C_3N_4 nanosheets synthesized using liquid exfoliation method. Its high surface area and C/N ratio not only provide the best environment to produce photocatalytic hydrogen but also indorsed charge separation and transfer. [562]

By using the same method, crystalline 2D g-C_3N_4 nanosheet of 1–2 nm was obtained. This sheet formed stable suspension under acidic and basic conditions and proved good material to enhance hydrogen production under visible light.

Li et al., employed the preparation of macroscopic foam like ultrathin g-C_3N_4 nanosheet by heating bulk g-C_3N_4 long time [561]. The holey 2D ultrathin structures and in-plane holes of nanosheets exhibit superior performance in the evolution of hydrogen. These features of g-C_3N_4 nanosheet exposed new edges and active sites, improved the charge transferability and enlarge the specific surface area (Fig. 25).

5.2.4. 3D sphere-like nanostructures

The study on ultrathin or monolayer g-C_3N_4 nanosheets reported that the processing steps are hazardous because they include some antagonistic acid treatment or chemical exfoliation. [457,563,564]. To overcome these shortcomings of 2D nanosheets, the preparation of three dimensional (3D) porous structure of g-C_3N_4 is a new approach that can enhance light absorption, more active sites for reaction, short diffusion paths and many available routes for diffusion and adsorption reactions. [565,566]. Many studies claimed the preparation of nanoporous g-C_3N_4 by using hard template approach (nanoporous silica scaffolds) or soft template approach (polymers). [565–568] There is a persistent need to expand a green and efficient strategy for the synthesis of g-C_3N_4 with a 3D porous structure, constructed from 2D ultrathin nanosheets linked via interpenetrating pores. Tian et al., first time introduced the idea of fabrication of g-C_3N_4 based photocatalyst by using precursor phase transformation. [191]. They reported that mild hydrothermal pretreatment of melamine in aqueous urea transform into melamine which yields a novel 3D porous N self-doped g-C_3N_4 nanosheet. The as-obtained ultrathin nanosheet was 3 nm thick and possess high specific area, a narrow band gap and have more charge transferability than pure g-C_3N_4.

The results showed the high hydrogen evolution with AQE 27.8% at 420 nm which is about 23-fold. To create a 3D sphere like nanostructure of g-C_3N_4 is also a significant approach to enhance the charge separation and improve photocatalytic activity. The preparation of hollow nanosphere sized g-C_3N_4 polymer reported by nanoparticles of silica as a template. Enhancing hydrogen generation by light harvesting (506) was helpful. In another study hollow g-C_3N_4 sphere improved by Pt NPs onto the interior and Co$_3$O$_4$ nanoparticles on the exterior surface to enhance the redox function for water splitting [569] (Fig. 26).

6. Conclusions and perspective

To satisfy the requirements of solar energy conversion efficiency the large band gap and charge recombination is remain the bottleneck for the researchers while graphitic carbon nitride (g-C_3N_4) has provoked a new wave of excitement in the future research generation because it has attractive electronic band structure, high chemical stability, earth-abundant and importantly easily fabricated. Despite all the exciting properties of g-C_3N_4, the practical application still hindered by several complications and inadequacies of pristine g-C_3N_4 like lacking solar light absorption, low surface area and the fast recombination of charges. In this work, we censoriously focus on the current progress and development of the different approaches by g-C_3N_4 for photocatalytic hydrogen generation. In this context, we discussed different categories like metal and non-metal doping, morphology tuning, a new design based on defects engineering, Z-scheme technology, plasmonic materials, dye-sensitization, perovskite oxides, carbon nitrides, carbon dots, metal organic framework, and a bimetallic cocatalyst.
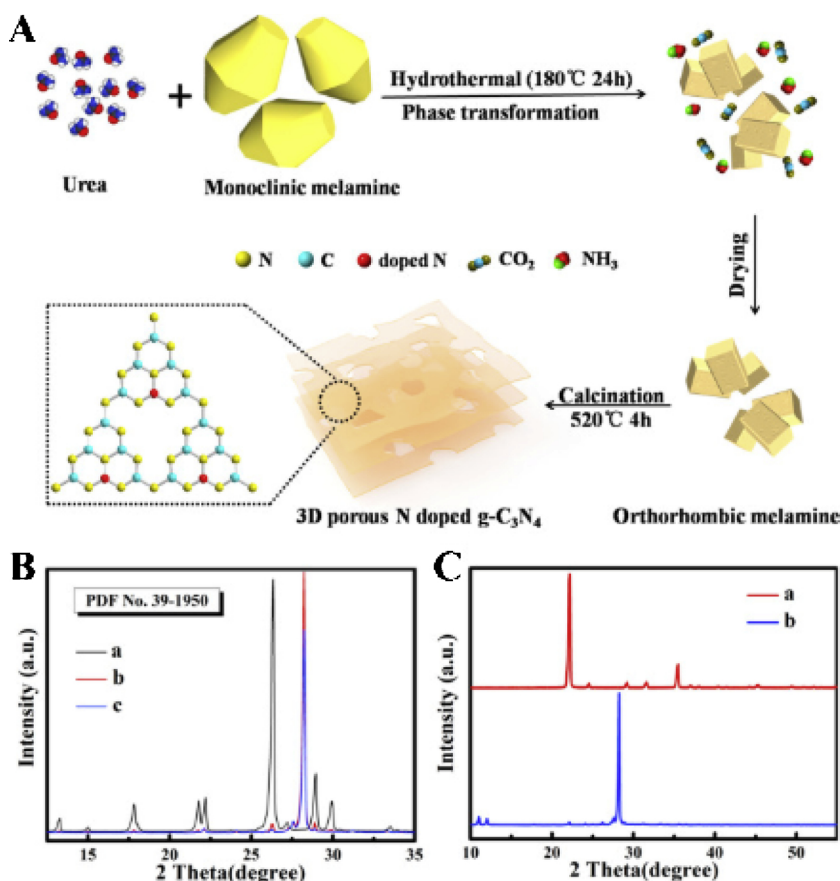
Fig. 26. A) Schematic illustration of the formation of 3D ultrathin porous N-doped g-C_3N_4. B) XRD patterns of (a) monoclinic-phase melamine (raw melamine), (b) orthorhombic-phase melamine (melamine pre-treated with a hydrothermal process), and (c) orthorhombic phase melamine (melamine pre-treated with a hydrothermal method in the presence of urea). C) XRD patterns of (a) raw urea and (b) melamine pre-treated with a hydrothermal method in the presence of urea. Reproduced with permission [191]. Copyrights 2017 Elsevier.

There are many promising results noted so far but still more studies are desired for detecting the intrinsic understanding of the photocatalytic enhancement of g-C_3N_4. There are many challenges that need to overcome for the better photocatalytic performance of g-C_3N_4. The surface area of g-C_3N_4 need to be improved by considering its structural stability. It is known that the catalytic activity has moderated by adopting different synthesis techniques especially the condensation route. Even though, the surface area has been increased by template method, but it could also devastate the structural morphology. Thus, there is dire need to explore the new synthesis method to increase the surface area with tunable pore size.

The surface activation of g-C_3N_4 is also crucial factor for the binding among functional groups that need to be studied. It also strengthens the growth of nanoparticles on the surface that can help to formulate the g-C_3N_4 composite for the photocatalytic hydrogen generation with better interfacial engineering. For instance, g-C_3N_4 has proved to be a good catalyst for various reactions but there is a conflict about its actual role. There should need to develop better correlation among the physico-chemical properties of g-C_3N_4 and their effect on catalytic activity.

Furthermore, the basic mechanism of g-C_3N_4 and the relation with active sites is complicated or somehow not so clear. There is need to explore the behavior of charge carriers and clarify the role of metal ions and heteroatoms. In this context, theoretical calculation by electronic/molecular level modeling is also significant future research direction. The bandgap engineering reduces the band gap and wider the light absorption but also reduces the redox potential that could influence the quantum efficiency. Therefore, the balance combination should be studied to improve the photocatalytic performance. The most important limitation for photocatalytic water splitting about the use of sacrificial agent to get hydrogen gas. There should need to overcome this limitation and find the way to do water splitting without using sacrificial agent. From the practical application point of view, it is expected that g-

C_3N_4 will get further research interest and will play a development role in the field of photocatalysis of water splitting. There are many applications that can get energy by solar but only there is a need of joint venture between the industrialist and academic researcher who can find the real practical application of g-C_3N_4.

Acknowledgments

References

[1] J. Liu, G. Cao, Z. Yang, D. Wang, D. Dubois, X. Zhou, G.L. Graff, L.R. Pederson, J.-G. Zhang, Oriented nanostructures for energy conversion and storage, ChemSusChem 1 (2008) 676–697.
[2] L. Dai, D.W. Chang, J.-B. Baek, W. Lu, Carbon nanomaterials for advanced energy conversion and storage, Small 8 (2012) 1130–1166.
[3] Y. Gong, J. Wang, Z. Wei, P. Zhang, H. Li, Y. Wang, Combination of carbon nitride and carbon nanotubes: synergistic catalysts for energy conversion, ChemSusChem 7 (2014) 2303–2309.
[4] S. Mekhilef, R. Saidur, A. Safari, A review on solar energy use in industries, Renew. Sustain. Energy Rev. 15 (2011) 1777–1790.
[5] I. Ayub, A. Munir, W. Amjad, A. Ghafoor, M.S. Nasir, Energy- and exergy-based thermal analyses of a solar bakery unit, J. Therm. Anal. Calorim. 133 (2018) 1001–1013.
[6] P. Kumar, R. Boukherroub, K. Shankar, Sunlight-driven water-splitting using two-dimensional carbon based semiconductors, J. Mater. Chem. A 6 (2018) 12876–12931.
[7] X. Zou, Y. Zhang, Noble metal-free hydrogen evolution catalysts for water splitting, Chem. Soc. Rev. 44 (2015) 5148–5180.
[8] T. da Silva Veras, T.S. Mozer, D. da Costa Rubim Messeder dos Santos, A. da Silva César, Hydrogen: trends, production and characterization of the main process worldwide, Int. J. Hydrogen Energy 42 (2017) 2018–2033.
[9] J. Yang, D. Wang, H. Han, C. Li, Roles of cocatalysts in photocatalysis and photoelectrocatalysis, Acc. Chem. Res. 46 (2013) 1900–1909.

[10] M.G. Walter, E.L. Warren, J.R. McKone, S.W. Boettcher, Q. Mi, E.A. Santori, N.S. Lewis, Solar water splitting cells, Chem. Rev. 110 (2010) 6446–6473.

[11] W. Fan, Q. Zhang, Y. Wang, Semiconductor-based nanocomposites for photo-catalytic H2 production and CO2 conversion, J. Chem. Soc. Faraday Trans. 15 (2013) 2632.

[12] Y. Lan, Y. Lu, Z. Ren, Mini review on photocatalysis of titanium dioxide nano-particles and their solar applications, Nano Energy 2 (2013) 1031–1045.

[13] W. Tu, Y. Zhou, Z. Zou, Versatile graphene-promoting photocatalytic performance of semiconductors: basic principles, synthesis, solar energy conversion, and en-vironmental applications, Adv. Funct. Mater. 23 (2013) 4996–5008.

[14] F. Fresno, R. Portela, S. Suárez, J.M. Coronado, Photocatalytic materials: recent achievements and near future trends, J. Mater. Chem. A 2 (2014) 2863–2884.

[15] M. Kapilashrami, Y. Zhang, Y.-S. Liu, A. Hagfeldt, J. Guo, Probing the optical property and electronic structure of TiO2 nanomaterials for renewable energy applications, Chem. Rev. 114 (2014) 9662–9707.

[16] H. Li, Y. Zhou, W. Tu, J. Ye, Z. Zou, State-of-the-art progress in diverse hetero-structured photocatalysts toward promoting photocatalytic performance, Adv. Funct. Mater. 25 (2015) 998–1013.

[17] L. Wondraczek, E. Tyystjärvi, J. Méndez-Ramos, F.A. Müller, Q. Zhang, Shifting the sun: solar spectral conversion and extrinsic sensitization in natural and arti-ficial photosynthesis, Adv. Sci. 2 (2015) 1500218.

[18] H. Zhang, G. Liu, L. Shi, H. Liu, T. Wang, J. Ye, Engineering coordination polymers for photocatalysis, Nano Energy 22 (2016) 149–168.

[19] M.L. Marin, L. Santos-Juanes, A. Arques, A.M. Amat, M.A. Miranda, Organic photocatalysts for the oxidation of pollutants and model compounds, Chem. Rev. 112 (2011) 1710–1750.

[20] A. Kubacka, M. Fernández-García, G. Colón, Advanced nanoarchitectures for solar photocatalytic applications, Chem. Rev. 112 (2011) 1555–1614.

[21] Y.-P. Yuan, L.-W. Ruan, J. Barber, S.C. Joachim Loo, C. Xue, Hetero-nanos-tructured suspended photocatalysts for solar-to-fuel conversion, Energy Environ. Sci. 7 (2014) 3934–3951.

[22] D.L. Ashford, M.K. Gish, A.K. Vannucci, M.K. Brennaman, J.L. Templeton, J.M. Papanikolas, T.J. Meyer, Molecular chromophore–catalyst assemblies for solar fuel applications, Chem. Rev. 115 (2015) 13006–13049.

[23] X. Li, J. Yu, J. Low, Y. Fang, J. Xiao, X. Chen, Engineering heterogeneous semi-conductors for solar water splitting, J. Mater. Chem. A 3 (2015) 2485–2534.

[24] Z. Li, J. Feng, S. Yan, Z. Zou, Solar fuel production: strategies and new opportu-nities with nanostructures, Nano Today 10 (2015) 468–486.

[25] S. Liu, Z.-R. Tang, Y. Sun, J.C. Colmenares, Y.-J. Xu, One-dimension-based spa-tially ordered architectures for solar energy conversion, Chem. Soc. Rev. 44 (2015) 5053–5075.

[26] R. Long, Y. Li, L. Song, Y. Xiong, Coupling solar energy into reactions: materials design for surface plasmon-mediated catalysis, Small 11 (2015) 3873–3889.

[27] Q. Xiang, B. Cheng, J. Yu, Graphene-based photocatalysts for solar-fuel genera-tion, Angew. Chem. Int. Ed. 54 (2015) 11350–11366.

[28] M.G. Kibria, Z. Mi, Artificial photosynthesis using metal/nonmetal-nitride semi-conductors: current status, prospects, and challenges, J. Mater. Chem. A 4 (2016) 2801–2820.

[29] S. Wang, H. Chen, G. Gao, T. Butburee, M. Lyu, S. Thaweesak, J.-H. Yun, A. Du, G. Liu, L. Wang, Synergistic crystal facet engineering and structural control of WO 3 films exhibiting unprecedented photoelectrochemical performance, Nano Energy 24 (2016) 94–102.

[30] F.-X. Xiao, M. Pagliaro, Y.-J. Xu, B. Liu, Layer-by-layer assembly of versatile na-noarchitectures with diverse dimensionality: a new perspective for rational con-struction of multilayer assemblies, Chem. Soc. Rev. 45 (2016) 3088–3121.

[31] S. Perathoner, G. Centi, D. Su, Turning perspective in photoelectrocatalytic cells for solar fuels, ChemSusChem 9 (2015) 345–357.

[32] X. Jia, Y. Zhao, G. Chen, L. Shang, R. Shi, X. Kang, G.I.N. Waterhouse, L.-Z. Wu, C.-H. Tung, T. Zhang, Water splitting: Ni3FeN nanoparticles derived from ultrathin NiFe-layered double hydroxide nanosheets: an efficient overall water splitting electrocatalyst (Adv. Energy Mater. 10/2016), Adv. Energy Mater. 6 (2016).

[33] Y. Miseki, S. Fujiyoshi, T. Gunji, K. Sayama, Photocatalytic water splitting under visible light utilizing I3−/I− and IO3−/I− redox mediators by Z-scheme system using surface treated PtOx/WO3 as O2 evolution photocatalyst, Catal. Sci. Technol. 3 (2013) 1750.

[34] B. Kiss, C. Didier, T. Johnson, T.D. Manning, M.S. Dyer, A.J. Cowan, J.B. Claridge, J.R. Darwent, M.J. Rosseinsky, Photocatalytic water oxidation by a pyrochlore oxide upon irradiation with visible light: rhodium substitution into yttrium tita-nate, Angew. Chem. Int. Ed. 53 (2014) 14480–14484.

[35] P. Zhang, J. Zhang, J. Gong, Tantalum-based semiconductors for solar water splitting, Chem. Soc. Rev. 43 (2014) 4395–4422.

[36] K. Meyer, M. Ranocchiari, J.A. van Bokhoven, Metal organic frameworks for photo-catalytic water splitting, Energy Environ. Sci. 8 (2015) 1923–1937.

[37] X. Yang, Z. Chen, J. Xu, H. Tang, K. Chen, Y. Jiang, Tuning the morphology of g-C3N4 for improvement of Z-scheme photocatalytic water oxidation, ACS Appl. Mater. Interfaces 7 (2015) 15285–15293.

[38] T. Arai, S. Sato, T. Kajino, T. Morikawa, Solar CO2 reduction using H2O by a semiconductor/metal-complex hybrid photocatalyst: enhanced efficiency and de-monstration of a wireless system using SrTiO3 photoanodes, Energy Environ. Sci. 6 (2013) 1274.

[39] D. Sun, Y. Fu, W. Liu, L. Ye, D. Wang, L. Yang, X. Fu, Z. Li, Studies on photo-catalytic CO2Reduction over NH2-Uio-66(Zr) and its derivatives: towards a better understanding of photocatalysis on metal-organic frameworks, Chem. Eur. J. 19 (2013) 14279–14285.

[40] M. Savage, S. Yang, M. Suyetin, E. Bichoutskaia, W. Lewis, A.J. Blake, S.A. Barnett, M. Schröder, A novel bismuth-based metal-organic framework for high volumetric

[41] W. Yu, D. Xu, T. Peng, Enhanced photocatalytic activity of g-C3N4 for selective CO2 reduction to CH3OH via facile coupling of ZnO: a direct Z-scheme me-chanism, J. Mater. Chem. A 3 (2015) 19936–19947.

[42] D.-H. Lan, H.-T. Wang, L. Chen, C.-T. Au, S.-F. Yin, Phosphorous-modified bulk graphitic carbon nitride: facile preparation and application as an acid-base bi-functional and efficient catalyst for CO 2 cycloaddition with epoxides, Carbon 100 (2016) 81–89.

[43] Y. Liu, X. Yuan, H. Wang, X. Chen, S. Gu, Q. Jiang, Z. Wu, L. Jiang, Y. Wu, G. Zeng, Novel visible light-induced g-C 3 N 4 –Sb 2 S 3 /Sb 4 O 5 Cl 2 composite photo-catalysts for efficient degradation of methyl orange, Catal. Commun. 70 (2015) 17–20.

[44] H. Wang, X. Yuan, Y. Wu, G. Zeng, X. Chen, L. Leng, H. Li, Synthesis and appli-cations of novel graphitic carbon nitride/metal-organic frameworks mesoporous photocatalyst for dyes removal, Appl. Catal. B 174-175 (2015) 445–454.

[45] H. Wang, X. Yuan, Y. Wu, G. Zeng, X. Chen, L. Leng, Z. Wu, L. Jiang, H. Li, Facile synthesis of amino-functionalized titanium metal-organic frameworks and their superior visible-light photocatalytic activity for Cr(VI) reduction, J. Hazard. Mater. 286 (2015) 187–194.

[46] L.-b. Jiang, X.-z. Yuan, J. Liang, J. Zhang, H. Wang, G.-m. Zeng, Nanostructured core-shell electrode materials for electrochemical capacitors, J. Power Sources 331 (2016) 408–425.

[47] Y. Li, X. Yuan, Z. Wu, H. Wang, Z. Xiao, Y. Wu, X. Chen, G. Zeng, Enhancing the sludge dewaterability by electrolysis/electrocoagulation combined with zero-va-lent iron activated persulfate process, Chem. Eng. J. 303 (2016) 636–645.

[48] Z. Wu, X. Yuan, J. Zhang, H. Wang, L. Jiang, G. Zeng, Photocatalytic deconta-mination of wastewater containing organic dyes by metal-organic frameworks and their derivatives, ChemCatChem 9 (2016) 41–64.

[49] H. Wang, X. Yuan, Y. Wu, G. Zeng, W. Tu, C. Sheng, Y. Deng, F. Chen, J.W. Chew, Plasmonic Bi nanoparticles and BiOCl sheets as cocatalyst deposited on perovskite-type ZnSn(OH) 6 microparticle with facet-oriented polyhedron for improved visible-light-driven photocatalysis, Appl. Catal. B 209 (2017) 543–553.

[50] Z. Wu, X. Yuan, H. Wang, Z. Wu, L. Jiang, H. Wang, L. Zhang, Z. Xiao, X. Chen, G. Zeng, Facile synthesis of a novel full-spectrum-responsive Co 2.67 S 4 nano-particles for UV-, vis- and NIR-driven photocatalysis, Appl. Catal. B 202 (2017) 104–111.

[51] J.-W. Xu, Z.-D. Gao, K. Han, Y. Liu, Y.-Y. Song, Synthesis of magnetically separable Ag3PO4/TiO2/Fe3O4 heterostructure with enhanced photocatalytic performance under visible light for photoinactivation of bacteria, ACS Appl. Mater. Interfaces 6 (2014) 15122–15131.

[52] D. Xia, Y. Li, G. Huang, C.C. Fong, T. An, G. Li, H.Y. Yip, H. Zhao, A. Lu, P.K. Wong, Visible-light-driven inactivation of Escherichia coli K-12 over thermal treated natural pyrrhotite, Appl. Catal. B 176-177 (2015) 749–756.

[53] W. Zhu, P. Liu, S. Xiao, W. Wang, D. Zhang, H. Li, Microwave-assisted synthesis of Ag-doped MOFs-like organotitanium polymer with high activity in visible-light driven photocatalytic NO oxidation, Appl. Catal. B 172-173 (2015) 46–51.

[54] G. Ding, W. Wang, T. Jiang, B. Han, H. Fan, G. Yang, Highly selective synthesis of phenol from benzene over a vanadium-doped graphitic carbon nitride catalyst, ChemCatChem 5 (2012) 192–200.

[55] H. Huang, H. Zhang, Z. Ma, Y. Liu, H. Ming, H. Li, Z. Kang, Tunable synthesis of metal–graphene complex nanostructures and their catalytic ability for solvent-free cyclohexene oxidation in air, Nanoscale 4 (2012) 4964.

[56] M. Xie, X. Dai, S. Meng, X. Fu, S. Chen, Selective oxidation of aromatic alcohols to corresponding aromatic aldehydes using In2S3 microsphere catalyst under visible light irradiation, Chem. Eng. J. 245 (2014) 107–116.

[57] D. Mosconi, D. Mazzier, S. Silvestrini, A. Privitera, C. Marega, L. Franco, A. Moretto, Synthesis and photochemical applications of processable polymers enclosing photoluminescent carbon quantum dots, ACS Nano 9 (2015) 4156–4164.

[58] K. Takanabe, Solar Water Splitting Using Semiconductor Photocatalyst Powders, Topics in Current Chemistry, Springer International Publishing, 2015, pp. 73–103.

[59] Q. Lu, Y. Yu, Q. Ma, B. Chen, H. Zhang, 2D transition-metal-dichalcogenide-na-nosheet-Based composites for photocatalytic and electrocatalytic hydrogen evo-lution reactions, Adv. Mater. 28 (2015) 1917–1933.

[60] M. Xiao, B. Luo, S. Wang, L. Wang, Solar energy conversion on g-C 3 N 4 photo-catalyst: light harvesting, charge separation, and surface kinetics, J. Energy Chem. 27 (2018) 1111–1123.

[61] S. Farsinezhad, H. Sharma, K. Shankar, Interfacial band alignment for photo-catalytic charge separation in TiO2 nanotube arrays coated with CuPt nano-particles, Phys. Chem. Chem. Phys. 17 (2015) 29723–29733.

[62] W.-J. Ong, L.-L. Tan, Y.H. Ng, S.-T. Yong, S.-P. Chai, Graphitic carbon nitride (g-C3N4)-based photocatalysts for artificial photosynthesis and environmental re-mediation: are we a step closer to achieving sustainability? Chem. Rev. 116 (2016) 7159–7329.

[63] P. Kuang, L. Zhang, B. Cheng, J. Yu, Enhanced charge transfer kinetics of Fe 2 O 3 /CdS composite nanorod arrays using cobalt-phosphate as cocatalyst, Appl. Catal. B 218 (2017) 570–580.

[64] K. Maeda, K. Domen, Development of novel photocatalyst and cocatalyst materials for water splitting under visible light, Bull. Chem. Soc. Jpn. 89 (2016) 627–648.

[65] S.U.M. Khan, Efficient photochemical water splitting by a chemically modified n-TiO2, Science 297 (2002) 2243–2245.

[66] H. Kato, K. Asakura, A. Kudo, Highly efficient water splitting into H2and O2over lanthanum-doped NaTaO3Photocatalysts with high crystallinity and surface na-nostructure, J. Am. Chem. Soc. 125 (2003) 3082–3089.

[67] K. Maeda, A. Xiong, T. Yoshinaga, T. Ikeda, N. Sakamoto, T. Hisatomi, M. Takashima, D. Lu, M. Kanehara, T. Setoyama, T. Teranishi, K. Domen,

Photocatalytic overall water splitting promoted by two different cocatalysts for hydrogen and oxygen evolution under visible light, Angew. Chem. Int. Ed. 49 (2010) 4096–4099.

[68] Z. Yi, J. Ye, N. Kikugawa, T. Kako, S. Ouyang, H. Stuart-Williams, H. Yang, J. Cao, W. Luo, Z. Li, Y. Liu, R.L. Withers, An orthophosphate semiconductor with photooxidation properties under visible-light irradiation, Nat. Mater. 9 (2010) 559–564.

[69] X. Chen, L. Liu, P.Y. Yu, S.S. Mao, Increasing solar absorption for photocatalysis with black hydrogenated titanium dioxide nanocrystals, Science 331 (2011) 746–750.

[70] F. Guzman, S.S.C. Chuang, C. Yang, Role of methanol sacrificing reagent in the photocatalytic evolution of hydrogen, Ind. Eng. Chem. Res. 52 (2013) 61–65.

[71] G. Zhang, Z.-A. Lan, L. Lin, S. Lin, X. Wang, Overall water splitting by Pt/g-C3N4 photocatalysts without using sacrificial agents, Chem. Sci. 7 (2016) 3062–3066.

[72] X. Wang, S. Blechert, M. Antonietti, Polymeric graphitic carbon nitride for heterogeneous photocatalysis, ACS Catal. 2 (2012) 1596–1606.

[73] C. Butchosa, P. Guiglion, M.A. Zwijnenburg, Carbon nitride photocatalysts for water splitting: a computational perspective, J. Phys. Chem. C 118 (2014) 24833–24842.

[74] S. Cao, J. Yu, G-C3N4-Based photocatalysts for hydrogen generation, J. Phys. Chem. Lett. 5 (2014) 2101–2107.

[75] J. Low, S. Cao, J. Yu, S. Wageh, Two-dimensional layered composite photocatalysts, Chem. Commun. 50 (2014) 10768.

[76] H. Zhang, X. Zuo, H. Tang, G. Li, Z. Zhou, Origin of photoactivity in graphitic carbon nitride and strategies for enhancement of photocatalytic efficiency: insights from first-principles computations, J. Chem. Soc. Faraday Trans. 17 (2015) 6280–6288.

[77] H. Gao, S. Yan, J. Wang, Y.A. Huang, P. Wang, Z. Li, Z. Zou, Towards efficient solar hydrogen production by intercalated carbon nitride photocatalyst, J. Chem. Soc. Faraday Trans. 15 (2013) 18077.

[78] A.B. Jorge, D.J. Martin, M.T.S. Dhanoa, A.S. Rahman, N. Makwana, J. Tang, A. Sella, F. Corà, S. Firth, J.A. Darr, P.F. McMillan, H2 and O2 evolution from water half-splitting reactions by graphitic carbon nitride materials, J. Phys. Chem. C 117 (2013) 7178–7185.

[79] J. Bian, Q. Li, C. Huang, J. Li, Y. Guo, M. Zaw, R.-Q. Zhang, Thermal vapor condensation of uniform graphitic carbon nitride films with remarkable photocurrent density for photoelectrochemical applications, Nano Energy 15 (2015) 353–361.

[80] G. Dong, W. Ho, Y. Li, L. Zhang, Facile synthesis of porous graphene-like carbon nitride (C6N9H3) with excellent photocatalytic activity for NO removal, Appl. Catal. B 174-175 (2015) 477–485.

[81] J. Fang, H. Fan, M. Li, C. Long, Nitrogen self-doped graphitic carbon nitride as efficient visible light photocatalyst for hydrogen evolution, J. Mater. Chem. A 3 (2015) 13819–13826.

[82] Q. Liang, Z.-H. Huang, F. Kang, Q.-H. Yang, Facile synthesis of crystalline polymeric carbon nitrides with an enhanced photocatalytic performance under visible light, ChemCatChem 7 (2015) 2897–2902.

[83] L. Shi, T. Wang, H. Zhang, K. Chang, J. Ye, Electrostatic self-assembly of nanosized carbon nitride nanosheet onto a zirconium metal-organic framework for enhanced photocatalytic CO2Reduction, Adv. Funct. Mater. 25 (2015) 5360–5367.

[84] M. Tahir, N. Mahmood, J. Zhu, A. Mahmood, F.K. Butt, S. Rizwan, I. Aslam, M. Tanveer, F. Idrees, I. Shakir, C. Cao, Y. Hou, One dimensional graphitic carbon nitrides as effective metal-free oxygen reduction catalysts, Sci. Rep. 5 (2015).

[85] G. Li, Z. Lian, W. Wang, D. Zhang, H. Li, Nanotube-confinement induced size-controllable g-C 3 N 4 quantum dots modified single-crystalline TiO 2 nanotube arrays for stable synergetic photoelectrocatalysis, Nano Energy 19 (2016) 446–454.

[86] K. Maeda, X. Wang, Y. Nishihara, D. Lu, M. Antonietti, K. Domen, Photocatalytic activities of graphitic carbon nitride powder for water reduction and oxidation under visible light, J. Phys. Chem. C 113 (2009) 4940–4947.

[87] J. Zhu, Y. Wei, W. Chen, Z. Zhao, A. Thomas, Graphitic carbon nitride as a metal-free catalyst for NO decomposition, Chem. Commun. 46 (2010) 6965.

[88] J. Liu, H. Wang, Z.P. Chen, H. Moehwald, S. Fiechter, R. van de Krol, L. Wen, L. Jiang, M. Antonietti, Microcontact-printing-Assisted access of graphitic carbon nitride films with favorable textures toward photoelectrochemical application, Adv. Mater. 27 (2014) 712–718.

[89] Y. Shiraishi, S. Kanazawa, Y. Sugano, D. Tsukamoto, H. Sakamoto, S. Ichikawa, T. Hirai, Highly selective production of hydrogen peroxide on graphitic carbon nitride (g-C3N4) photocatalyst activated by visible light, ACS Catal. 4 (2014) 774–780.

[90] Y. Shiraishi, Y. Kofuji, H. Sakamoto, S. Tanaka, S. Ichikawa, T. Hirai, Effects of surface defects on photocatalytic H2O2 production by mesoporous graphitic carbon nitride under visible light irradiation, ACS Catal. 5 (2015) 3058–3066.

[91] K. Schwinghammer, B. Tuffy, M.B. Mesch, E. Wirnhier, C. Martineau, F. Taulelle, W. Schnick, J. Senker, B.V. Lotsch, Triazine-based carbon nitrides for visible-light-driven hydrogen evolution, Angew. Chem. Int. Ed. 52 (2013) 2435–2439.

[92] G. Zhang, M. Zhang, X. Ye, X. Qiu, S. Lin, X. Wang, Iodine modified carbon nitride semiconductors as visible light photocatalysts for hydrogen evolution, Adv. Mater. 26 (2013) 805–809.

[93] T.Y. Ma, Y. Tang, S. Dai, S.Z. Qiao, Proton-functionalized two-dimensional graphitic carbon nitride nanosheet: an excellent metal-/label-Free biosensing platform, Small 10 (2014) 2382–2389.

[94] G. Liu, T. Wang, H. Zhang, X. Meng, D. Hao, K. Chang, P. Li, T. Kako, J. Ye, Nature-inspired environmental "Phosphorylation" boosts photocatalytic H2 production over carbon nitride nanosheets under visible-light irradiation, Angew. Chem. Int. Ed. 54 (2015) 13561–13565.

[95] J. Oh, R.J. Yoo, S.Y. Kim, Y.J. Lee, D.W. Kim, S. Park, Oxidized carbon nitrides:

[96] water-dispersible, atomically thin carbon nitride-based nanodots and their performances as bioimaging probes, Chem. Eur. J. 21 (2015) 6241–6246.

[96] D. Yang, T. Jiang, T. Wu, P. Zhang, H. Han, B. Han, Highly selective oxidation of cyclohexene to 2-cyclohexene-1-one in water using molecular oxygen over Fe–Co–g-C3N4, Catal. Sci. Technol. 6 (2016) 193–200.

[97] M. Zhang, W. Jiang, D. Liu, J. Wang, Y. Liu, Y. Zhu, Y. Zhu, Photodegradation of phenol via C 3 N 4 -agar hybrid hydrogel 3D photocatalysts with free separation, Appl. Catal. B 183 (2016) 263–268.

[98] Y. Wang, H. Li, J. Yao, X. Wang, M. Antonietti, Synthesis of boron doped polymeric carbon nitride solids and their use as metal-free catalysts for aliphatic C–H bond oxidation, Chem. Sci. 2 (2011) 446–450.

[99] G. Zhang, J. Zhang, M. Zhang, X. Wang, Polycondensation of thiourea into carbon nitride semiconductors as visible light photocatalysts, J. Mater. Chem. 22 (2012) 8083.

[100] J. Yu, K. Wang, W. Xiao, B. Cheng, Photocatalytic reduction of CO2 into hydrocarbon solar fuels over g-C3N4–Pt nanocomposite photocatalysts, J. Chem. Soc. Faraday Trans. 16 (2014) 11492.

[101] K. Wang, Q. Li, B. Liu, B. Cheng, W. Ho, J. Yu, Sulfur-doped g-C3N4 with enhanced photocatalytic CO2-reduction performance, Appl. Catal. B 176-177 (2015) 44–52.

[102] J. Xiao, Y. Xie, F. Nawaz, Y. Wang, P. Du, H. Cao, Dramatic coupling of visible light with ozone on honeycomb-like porous g-C 3 N 4 towards superior oxidation of water pollutants, Appl. Catal. B 183 (2016) 417–425.

[103] J. Liu, W. Li, L. Duan, X. Li, L. Ji, Z. Geng, K. Huang, L. Lu, L. Zhou, Z. Liu, W. Chen, L. Liu, S. Feng, Y. Zhang, A graphene-like oxygenated carbon nitride material for improved cycle-life lithium/sulfur batteries, Nano Lett. 15 (2015) 5137–5142.

[104] X. Song, Y. Hu, M. Zheng, C. Wei, Solvent-free in situ synthesis of g-C 3 N 4 /{0 0 1}TiO 2 composite with enhanced UV- and visible-light photocatalytic activity for NO oxidation, Appl. Catal. B 182 (2016) 587–597.

[105] D.H. Wang, J.N. Pan, H.H. Li, J.J. Liu, Y.B. Wang, L.T. Kang, J.N. Yao, A pure organic heterostructure of μ-oxo dimeric iron(iii) porphyrin and graphitic-C3N4 for solar H2 roduction from water, J. Mater. Chem. A 4 (2016) 290–296.

[106] Z. Zhang, D. Jiang, D. Li, M. He, M. Chen, Construction of SnNb 2 O 6 nanosheet/g-C 3 N 4 nanosheet two-dimensional heterostructures with improved photocatalytic activity: synergistic effect and mechanism insight, Appl. Catal. B 183 (2016) 113–123.

[107] Y. Cui, G. Zhang, Z. Lin, X. Wang, Condensed and low-defected graphitic carbon nitride with enhanced photocatalytic hydrogen evolution under visible light irradiation, Appl. Catal. B 181 (2016) 413–419.

[108] J. Liebig, Analyse der harnsäure, Ann. Der Pharm. 10 (1834) 47–48.

[109] H. Huang, S. Yang, R. Vajtai, X. Wang, P.M. Ajayan, Pt-decorated 3D architectures built from graphene and graphitic carbon nitride nanosheets as efficient methanol oxidation catalysts, Adv. Mater. 26 (2014) 5160–5165.

[110] F. Goettmann, A. Fischer, M. Antonietti, A. Thomas, Metal-free catalysis of sustainable Friedel–crafts reactions: direct activation of benzene by carbon nitrides to avoid the use of metal chlorides and halogenated compounds, Chem. Commun. (2006) 4530–4532.

[111] X. Wang, K. Maeda, A. Thomas, K. Takanabe, G. Xin, J.M. Carlsson, K. Domen, M. Antonietti, A metal-free polymeric photocatalyst for hydrogen production from water under visible light, Nat. Mater. 8 (2008) 76–80.

[112] D.M. Teter, R.J. Hemley, Low-compressibility carbon nitrides, Science 271 (1996) 53–55.

[113] Y. Zhao, J. Zhang, L. Qu, Graphitic carbon nitride/graphene hybrids as new active materials for energy conversion and storage, ChemNanoMat 1 (2015) 298–318.

[114] A. Zambon, J.M. Mouesca, C. Gheorghiu, P.A. Bayle, J. Pécaut, M. Claeys-Bruno, S. Gambarelli, L. Dubois, s-Heptazine oligomers: promising structural models for graphitic carbon nitride, Chem. Sci. 7 (2016) 945–950.

[115] Y. Zheng, L. Lin, B. Wang, X. Wang, Graphitic carbon nitride polymers toward sustainable photoredox catalysis, Angew. Chem. Int. Ed. 54 (2015) 12868–12884.

[116] B. Jürgens, E. Irran, J. Senker, P. Kroll, H. Müller, W. Schnick, Melem (2,5,8-Triamino-tri-s-triazine), an important intermediate during condensation of melamine rings to graphitic carbon nitride: synthesis, structure determination by X-ray powder diffractometry, solid-state NMR, and theoretical studies, J. Am. Chem. Soc. 125 (2003) 10288–10300.

[117] B.V. Lotsch, W. Schnick, From triazines to heptazines: novel nonmetal tricyanomelaminates as precursors for graphitic carbon nitride materials, Chem. Mater. 18 (2006) 1891–1900.

[118] M.J. Bojdys, J.-O. Müller, M. Antonietti, A. Thomas, Ionothermal synthesis of crystalline, condensed, graphitic carbon nitride, Chem. Eur. J. 14 (2008) 8177–8182.

[119] A. Sattler, S. Pagano, M. Zeuner, A. Zurawski, D. Gunzelmann, J. Senker, K. Müller-Buschbaum, W. Schnick, Melamine-melem adduct phases: investigating the thermal condensation of melamine, Chem. Eur. J. 15 (2009) 13161–13170.

[120] Y. Wang, Y. Di, M. Antonietti, H. Li, X. Chen, X. Wang, Excellent visible-light photocatalysis of fluorinated polymeric carbon nitride solids, Chem. Mater. 22 (2010) 5119–5121.

[121] F. Dong, Z. Zhao, T. Xiong, Z. Ni, W. Zhang, Y. Sun, W.-K. Ho, In situ construction of g-C3N4/g-C3N4 metal-free heterojunction for enhanced visible-light photocatalysis, ACS Appl. Mater. Interfaces 5 (2013) 11392–11401.

[122] J. Bai, W. Lv, Z. Ni, Z. Wang, G. Chen, H. Xu, H. Qin, Z. Zheng, X. Li, Integrating MoS2 on sulfur-doped porous g-C3N4 iostype heterojunction hybrids enhances visible-light photocatalytic performance, J. Alloys Compd. 768 (2018) 766–774.

[123] N. Tian, Y. Zhang, X. Li, K. Xiao, X. Du, F. Dong, G.I. Waterhouse, T. Zhang, H. Huang, Precursor-reforming protocol to 3D mesoporous g-C3N4 established by ultrathin self-doped nanosheets for superior hydrogen evolution, Nano Energy 38 (2017) 72–81.

[124] S. Cao, Q. Huang, B. Zhu, J. Yu, Trace-level phosphorus and sodium co-doping of g-C3N4 for enhanced photocatalytic H2 production, J. Power Sources 351 (2017) 151–159.

[125] E.S. Da Silva, N.M. Moura, A. Coutinho, G. Dražić, B.M. Teixeira, N.A. Sobolev, C.G. Silva, M.G.P. Neves, M. Prieto, J.L. Faria, B-cyclodextrin as a precursor to holey C-doped g-C3N4 nanosheets for photocatalytic hydrogen generation, ChemSusChem (2018).

[126] S. Guo, Y. Tang, Y. Xie, C. Tian, Q. Feng, W. Zhou, B. Jiang, P-doped tubular g-C3N4 with surface carbon defects: universal synthesis and enhanced visible-light photocatalytic hydrogen production, Appl. Catal. B 218 (2017) 664–671.

[127] D. Zeng, W. Xu, W.-J. Ong, J. Xu, H. Ren, Y. Chen, H. Zheng, D.-L. Peng, Toward noble-metal-free visible-light-driven photocatalytic hydrogen evolution: mono-disperse sub–15 nm Ni2P nanoparticles anchored on porous g-C3N4 nanosheets to engineer 0D-2D heterojunction interfaces, Appl. Catal. B 221 (2018) 47–55.

[128] Y. Zou, J. Shi, D. Ma, Z. Fan, L. Cheng, D. Sun, Z. Wang, C. Niu, CdS quantum dots decorated ultrathin WS2/g-C3N4 2D/2D heterojunction nanosheets for highly efficient photocatalytic hydrogen production under visible light, ChemSusChem (2018).

[129] F.-Y. Tian, D.-f. Hou, F. Tang, M. Deng, X. Qaio, T. Wu, D.-S. Li, Novel Zn0. 8Cd0. 2S@ g-C3N4 core-shell heterojuctions with twin structure for enhanced visible-light-driven photocatalytic hydrogen generation, J. Mater. Chem. A (2018).

[130] J. Wen, J. Xie, H. Zhang, A. Zhang, Y. Liu, X. Chen, X. Li, Constructing multi-functional metallic Ni interface layers in the g-C3N4 nanosheets/amorphous NiS heterojunctions for efficient photocatalytic H2 generation, ACS Appl. Mater. Interfaces 9 (2017) 14031–14042.

[131] W.-J. Ong, 2D/2D graphitic carbon nitride (g-C3N4) heterojunction nanocomposites for photocatalysis: why does face-to-face interface matter? Front. Mater. 4 (2017) 11.

[132] J. Wen, J. Xie, Z. Yang, R. Shen, H. Li, X. Luo, X. Chen, X. Li, Fabricating the robust g-C3N4 nanosheets/carbons/NiS multiple heterojunctions for enhanced photo-catalytic H2 generation: an insight into the trifunctional roles of nanocarbons, ACS Sustain. Chem. Eng. 5 (2017) 2224–2236.

[133] J. Fu, C. Bie, B. Cheng, C. Jiang, J. Yu, Hollow CoS x polyhedrons act as high-efficiency cocatalyst for enhancing the photocatalytic hydrogen generation of g-C3N4, ACS Sustain. Chem. Eng. 6 (2018) 2767–2779.

[134] M. Tahir, M. Rafique, M. Isa Khan, A. Majid, F. Nazar, M. Sagir, S. Gilani, M. Farooq, A. Ahmed, Enhanced photocatalytic hydrogen energy production of g-C3N4-WO3 composites under visible light irradiation, Int. J. Energy Res. (2018).

[135] F. Yang, D. Liu, Y. Li, L. Cheng, J. Ye, Salt-template-assisted construction of honeycomb-like structured g-C3N4 with tunable band structure for enhanced photocatalytic H2 production, Appl. Catal. B (2018).

[136] M. Liu, P. Xia, L. Zhang, B. Cheng, J. Yu, Enhanced photocatalytic H2-Production activity of g-C3N4 nanosheets via optimal photodeposition of Pt as cocatalyst, ACS Sustain. Chem. Eng. 6 (2018) 10472–10480.

[137] L. Yang, X. Wang, J. Wang, G. Cui, D. Liu, Graphite carbon nitride/boron-doped graphene hybrid for efficient hydrogen generation reaction, Nanotechnology 29 (2018) 345705.

[138] M.S. Ansari, A. Banik, M. Qureshi, Morphological tuning of photo-booster g-C3N4 with higher surface area and better charge transfers for enhanced power conversion efficiency of quantum dot sensitized solar cells, Carbon 121 (2017) 90–105.

[139] P. Xia, B. Zhu, B. Cheng, J. Yu, J. Xu, 2D/2D g-C3N4/MnO2 nanocomposite as a direct Z-Scheme photocatalyst for enhanced photocatalytic activity, ACS Sustain. Chem. Eng. 6 (2017) 965–973.

[140] S. Tonda, S. Kumar, Y. Gawli, M. Bhardwaj, S. Ogale, g-C3N4 (2D)/CdS (1D)/rGO (2D) dual-interface nano-composite for excellent and stable visible light photo-catalytic hydrogen generation, Int. J. Hydrogen Energy 42 (2017) 5971–5984.

[141] Y.-F. Xu, M.-Z. Yang, B.-X. Chen, X.-D. Wang, H.-Y. Chen, D.-B. Kuang, C.-Y. Su, A CsPbBr3 perovskite quantum dot/graphene oxide composite for photocatalytic CO2 reduction, JACS 139 (2017) 5660–5663.

[142] H.H. El-Maghrabi, A.A. Nada, K.R. Diab, A.M. Youssef, A. Hamdy, S. Roualdes, S.A. El-Wahab, Facile fabrication of NiTiO3/graphene nanocomposites for pho-tocatalytic hydrogen generation, J. Photochem. Photobiol. A: Chem. 365 (2018) 86–93.

[143] D. Saadetnejad, R. Yıldırım, Photocatalytic hydrogen production by water splitting over Au/Al-SrTiO3, Int. J. Hydrogen Energy 43 (2018) 1116–1122.

[144] S. Tonda, S. Kumar, Y. Gawli, M. Bhardwaj, S. Ogale, g-C 3 N 4 (2D)/CdS (1D)/ rGO (2D) dual-interface nano-composite for excellent and stable visible light photocatalytic hydrogen generation, Int. J. Hydrogen Energy 42 (2017) 5971–5984.

[145] K. Striegler, Modified Graphitic Carbon Nitrides for Photocatalytic Hydrogen Evolution From Water, Springer Fachmedien Wiesbaden, 2015.

[146] W. Huang, N. Liu, X. Zhang, M. Wu, L. Tang, Metal organic framework g-C 3 N 4 /MIL-53(Fe) heterojunctions with enhanced photocatalytic activity for Cr(VI) re-duction under visible light, Appl. Surf. Sci. 425 (2017) 107–116.

[147] P. Pachfule, A. Acharjya, J. Roeser, T. Langenhahn, M. Schwarze, R. Schomäcker, A. Thomas, J. Schmidt, Diacetylene functionalized covalent organic framework (COF) for photocatalytic hydrogen generation, JACS 140 (2018) 1423–1427.

[148] V.W.-h. Lau, V.W.-z. Yu, F. Ehrat, T. Botari, I. Moudrakovski, T. Simon, V. Duppel, E. Medina, J.K. Stolarczyk, J. Feldmann, V. Blum, B.V. Lotsch, Urea-modified carbon nitrides: enhancing photocatalytic hydrogen evolution by rational defect engineering, Adv. Energy Mater. 7 (2017) 1602251.

[149] L. Ma, H. Fan, K. Fu, S. Lei, Q. Hu, H. Huang, G. He, Protonation of graphitic carbon nitride (g-C3N4) for an electrostatically self-assembling Carbon@g-C3N4 core–shell nanostructure toward high hydrogen evolution, ACS Sustain. Chem. Eng. 5 (2017) 7093–7103.

[150] M. Zhang, Y. Duan, H. Jia, F. Wang, L. Wang, Z. Su, C. Wang, Defective graphitic carbon nitride synthesized by controllable co-polymerization with enhanced visible light photocatalytic hydrogen evolution, Catal. Sci. Technol. 7 (2017) 452–458.

[151] J. Wang, Z. Yang, W. Yao, X. Gao, D. Tao, Defects modified in the exfoliation of g-C3N4 nanosheets via a self-assembly process for improved hydrogen evolution performance, Appl. Catal. B 238 (2018) 629–637.

[152] K. He, J. Xie, X. Luo, J. Wen, S. Ma, X. Li, Y. Fang, X. Zhang, Enhanced visible light photocatalytic H 2 production over Z-scheme g-C 3 N 4 nansheets/WO 3 nanorods nanocomposites loaded with Ni(OH) x cocatalysts, Chin. J. Catal. 38 (2017) 240–252.

[153] L. Qian, Y. Hou, Z. Yu, M. Li, F. Li, L. Sun, W. Luo, G. Pan, Metal-induced Z-scheme CdS/Ag/g-C3N4 photocatalyst for enhanced hydrogen evolution under visible light: the synergy of MIP effect and electron mediator of Ag, Mol. Catal. 458 (2018) 43–51.

[154] Q. Xu, B. Zhu, C. Jiang, B. Cheng, J. Yu, Constructing 2D/2D Fe2 O3 /g-C3 N4 direct Z-Scheme photocatalysts with enhanced H2 generation performance, Sol. RRL 2 (2018) 1800006.

[155] Z. Zhu, M. Muruganantham, J. Gu, Y. Zhang, Fabrication of a Z-Scheme g-C3N4/ Fe-TiO2 photocatalytic composite with enhanced photocatalytic activity under visible light irradiation, Catalysts 8 (2018) 112.

[156] S. Hua, D. Qu, L. An, W. Jiang, Y. Wen, X. Wang, Z. Sun, Highly efficient p-type Cu3P/n-type g-C3N4 photocatalyst through Z-scheme charge transfer route, Appl. Catal. B 240 (2019) 253–261.

[157] Z. Yuan, R. Tang, Y. Zhang, L. Yin, Enhanced photovoltaic performance of dye-sensitized solar cells based on Co9S8 nanotube array counter electrode and TiO2/ g-C3N4 heterostructure nanosheet photoanode, J. Alloys Compd. 691 (2017) 983–991.

[158] P. Zhang, T. Wang, H. Zeng, Design of Cu-Cu2O/g-C3N4 nanocomponent photo-catalysts for hydrogen evolution under visible light irradiation using water-soluble Erythrosin B dye sensitization, Appl. Surf. Sci. 391 (2017) 404–414.

[159] Y. Xue, Y. Lei, X. Liu, Y. Li, W. Deng, F. Wang, S. Min, Highly active dye-sensitized photocatalytic H2 evolution catalyzed by a single-atom Pt cocatalyst anchored onto g-C3N4 nanosheets under long-wavelength visible light irradiation, New J. Chem. 42 (2018) 14083–14086.

[160] P. Wang, Z. Guan, Q. Li, J. Yang, Efficient visible-light-driven photocatalytic hy-drogen production from water by using Eosin Y-sensitized novel g-C3N4/Pt/GO composites, J. Mater. Sci. 53 (2018) 774–786.

[161] Z. Chen, K. Xia, X. She, Z. Mo, S. Zhao, J. Yi, Y. Xu, H. Chen, H. Xu, H. Li, 1D metallic MoO 2 -C as co-catalyst on 2D g-C 3 N 4 semiconductor to promote photocatlaytic hydrogen production, Appl. Surf. Sci. 447 (2018) 732–739.

[162] J. Fu, C. Bie, B. Cheng, C. Jiang, J. Yu, Hollow CoSx polyhedrons act as high-efficiency cocatalyst for enhancing the photocatalytic hydrogen generation of g-C3N4, ACS Sustain. Chem. Eng. 6 (2018) 2767–2779.

[163] K. He, J. Xie, M. Li, X. Li, In situ one-pot fabrication of g-C 3 N 4 nanosheets/NiS cocatalyst heterojunction with intimate interfaces for efficient visible light pho-tocatalytic H 2 generation, Appl. Surf. Sci. 430 (2018) 208–217.

[164] J. Liu, Q. Jia, J. Long, X. Wang, Z. Gao, Q. Gu, Amorphous NiO as co-catalyst for enhanced visible-light-driven hydrogen generation over g-C 3 N 4 photocatalyst, Appl. Catal. B 222 (2018) 35–43.

[165] W. Liu, J. Shen, Q. Liu, X. Yang, H. Tang, Porous MoP network structure as co-catalyst for H2 evolution over g-C3N4 nanosheets, Appl. Surf. Sci. 462 (2018) 822–830.

[166] G. Dong, Y. Zhang, Q. Pan, J. Qiu, A fantastic graphitic carbon nitride (g-C3N4) material: electronic structure, photocatalytic and photoelectronic properties, J. Photochem. Photobiol. C Photochem. Rev. 20 (2014) 33–50.

[167] L.-L. Feng, Y. Zou, C. Li, S. Gao, L.-J. Zhou, Q. Sun, M. Fan, H. Wang, D. Wang, G.-D. Li, X. Zou, Nanoporous sulfur-doped graphitic carbon nitride microrods: a durable catalyst for visible-light-driven H 2 evolution, Int. J. Hydrogen Energy 39 (2014) 15373–15379.

[168] S. Cao, J. Low, J. Yu, M. Jaroniec, Polymeric photocatalysts based on graphitic carbon nitride, Adv. Mater. 27 (2015) 2150–2176.

[169] S. Tonda, S. Kumar, S. Kandula, V. Shanker, Fe-doped and -mediated graphitic carbon nitride nanosheets for enhanced photocatalytic performance under natural sunlight, J. Mater. Chem. A 2 (2014) 6772.

[170] J. Xu, T.J.K. Brenner, Z. Chen, D. Neher, M. Antonietti, M. Shalom, Upconversion-agent induced improvement of g-C3N4 photocatalyst under visible light, ACS Appl. Mater. Interfaces 6 (2014) 16481–16486.

[171] T. Xiong, W. Cen, Y. Zhang, F. Dong, Bridging the g-C3N4 interlayers for enhanced photocatalysis, ACS Catal. 6 (2016) 2462–2472.

[172] Y. Oh, J.O. Hwang, E.-S. Lee, M. Yoon, V.-D. Le, Y.-H. Kim, D.H. Kim, S.O. Kim, Divalent Fe atom coordination in two-dimensional microporous graphitic carbon nitride, ACS Appl. Mater. Interfaces 8 (2016) 25438–25443.

[173] L. Jiang, X. Yuan, Y. Pan, J. Liang, G. Zeng, Z. Wu, H. Wang, Doping of graphitic carbon nitride for photocatalysis: a reveiw, Appl. Catal. B 217 (2017) 388–406.

[174] Y. Feng, C. Liao, L. Kong, D. Wu, Y. Liu, P.-H. Lee, K. Shih, Facile synthesis of highly reactive and stable Fe-doped g-C 3 N 4 composites for peroxymonosulfate activation: a novel nonradical oxidation process, J. Hazard. Mater. 354 (2018) 63–71.

[175] Y. Guo, Q. Liu, Z. Li, Z. Zhang, X. Fang, Enhanced photocatalytic hydrogen evo-lution performance of mesoporous graphitic carbon nitride co-doped with po-tassium and iodine, Appl. Catal. B 221 (2018) 362–370.

[176] Q. Han, C. Hu, F. Zhao, Z. Zhang, N. Chen, L. Qu, One-step preparation of iodine-doped graphitic carbon nitride nanosheets as efficient photocatalysts for visible light water splitting, J. Mater. Chem. A 3 (2015) 4612–4619.

[177] L. Ruan, G. Xu, L. Gu, C. Li, Y. Zhu, Y. Lu, The physical properties of Li-doped g-C3N4 monolayer sheet investigated by the first-principles, Mater. Res. Bull. 66

(2015) 156–162.

[178] S. Cao, Q. Huang, B. Zhu, J. Yu, Trace-level phosphorus and sodium co-doping of g-C 3 N 4 for enhanced photocatalytic H 2 production, J. Power Sources 351 (2017) 151–159.

[179] H.-L. Jiang, Y. Pan, D. Li, Sodium-doped C3N4/MOF heterojunction composites with tunable band structures for photocatalysis: interplay between light harvesting and electron transfer, Chem. Eur. J. (2018).

[180] L. Zhang, N. Ding, M. Hashimoto, K. Iwasaki, N. Chikamori, K. Nakata, Y. Xu, J. Shi, H. Wu, Y. Luo, D. Li, A. Fujishima, Q. Meng, Sodium-doped carbon nitride nanotubes for efficient visible light-driven hydrogen production, Nano Res. 11 (2018) 2295–2309.

[181] G. Dong, K. Zhao, L. Zhang, Carbon self-doping induced high electronic conductivity and photoreactivity of g-C3N4, Chem. Commun. 48 (2012) 6178.

[182] Q. Xu, B. Cheng, J. Yu, G. Liu, Making co-condensed amorphous carbon/g-C 3 N 4 composites with improved visible-light photocatalytic H 2 -production performance using Pt as cocatalyst, Carbon 118 (2017) 241–249.

[183] E.S. Da Silva, N.M.M. Moura, A. Coutinho, G. Dražić, B.M.S. Teixeira, N.A. Sobolev, C.G. Silva, M.G.P.M.S. Neves, M. Prieto, J.L. Faria, Cover feature: β-cyclodextrin as a precursor to Holey C-doped g-C3 N 4 nanosheets for photocatalytic hydrogen generation (ChemSusChem 16/2018), ChemSusChem 11 (2018) 2639.

[184] T.-F. Yeh, C.-Y. Teng, S.-J. Chen, H. Teng, Nitrogen-doped graphene oxide quantum dots as photocatalysts for overall water-splitting under visible light illumination, Adv. Mater. 26 (2014) 3297–3303.

[185] X. Wang, J. Chen, X. Guan, L. Guo, Enhanced efficiency and stability for visible light driven water splitting hydrogen production over Cd 0.5 Zn 0.5 S/g-C 3 N 4 composite photocatalyst, Int. J. Hydrogen Energy 40 (2015) 7546–7552.

[186] J. Li, B. Shen, Z. Hong, B. Lin, B. Gao, Y. Chen, A facile approach to synthesize novel oxygen-doped g-C3N4 with superior visible-light photoreactivity, Chem. Commun. 48 (2012) 12017.

[187] L. Xu, W.-Q. Huang, L.-L. Wang, Z.-A. Tian, W. Hu, Y. Ma, X. Wang, A. Pan, G.-F. Huang, Insights into enhanced visible-light photocatalytic hydrogen evolution of g-C3N4 and highly reduced graphene oxide composite: the role of oxygen, Chem. Mater. 27 (2015) 1612–1621.

[188] S. Guo, Y. Zhu, Y. Yan, Y. Min, J. Fan, Q. Xu, Holey structured graphitic carbon nitride thin sheets with edge oxygen doping via photo-Fenton reaction with enhanced photocatalytic activity, Appl. Catal. B 185 (2016) 315–321.

[189] Y. Zeng, X. Liu, C. Liu, L. Wang, Y. Xia, S. Zhang, S. Luo, Y. Pei, Scalable one-step production of porous oxygen-doped g-C3N4 nanorods with effective electron separation for excellent visible-light photocatalytic activity, Appl. Catal. B 224 (2018) 1–9.

[190] H. Yu, L. Shang, T. Bian, R. Shi, G.I.N. Waterhouse, Y. Zhao, C. Zhou, L.-Z. Wu, C.-H. Tung, T. Zhang, Carbon nanosheets: nitrogen-doped porous carbon nanosheets templated from g-C3 N4 as metal-free electrocatalysts for efficient oxygen reduction reaction (Adv. Mater. 25/2016), Adv. Mater. 28 (2016) 5140.

[191] N. Tian, Y. Zhang, X. Li, K. Xiao, X. Du, F. Dong, G.I.N. Waterhouse, T. Zhang, H. Huang, Precursor-reforming protocol to 3D mesoporous g-C 3 N 4 established by ultrathin self-doped nanosheets for superior hydrogen evolution, Nano Energy 38 (2017) 72–81.

[192] X. Ma, Y. Lv, J. Xu, Y. Liu, R. Zhang, Y. Zhu, A strategy of enhancing the photoactivity of g-C3N4 via doping of nonmetal elements: a first-principles study, J. Phys. Chem. C 116 (2012) 23485–23493.

[193] S. Stolbov, S. Zuluaga, Sulfur doping effects on the electronic and geometric structures of graphitic carbon nitride photocatalyst: insights from first principles, J. Phys. Condens. Matter 25 (2013) 085507.

[194] Y. Deng, L. Tang, C. Feng, G. Zeng, J. Wang, Y. Zhou, Y. Liu, B. Peng, H. Feng, Construction of plasmonic Ag modified phosphorous-doped ultrathin g-C3N4 nanosheets/BiVO4 photocatalyst with enhanced visible-near-infrared response ability for ciprofloxacin degradation, J. Hazard. Mater. 344 (2018) 758–769.

[195] H. Yang, Y. Zhou, Y. Wang, S. Hu, B. Wang, Q. Liao, H. Li, J. Bao, G. Ge, S. Jia, Three-dimensional flower-like phosphorus-doped g-C3N4 with a high surface area for visible-light photocatalytic hydrogen evolution, J. Mater. Chem. A 6 (2018) 16485–16494.

[196] H. Pan, H. Zhang, H. Liu, L. Chen, Interstitial boron doping effects on the electronic and magnetic properties of graphitic carbon nitride materials, Solid State Commun. 203 (2015) 35–40.

[197] F. Raziq, Y. Qu, X. Zhang, M. Humayun, J. Wu, A. Zada, H. Yu, X. Sun, L. Jing, Enhanced cocatalyst-free visible-light activities for photocatalytic fuel production of g-C3N4 by trapping holes and transferring electrons, J. Phys. Chem. C 120 (2015) 98–107.

[198] C. Lu, R. Chen, X. Wu, M. Fan, Y. Liu, Z. Le, S. Jiang, S. Song, Boron doped g-C3N4 with enhanced photocatalytic UO22+ reduction performance, Appl. Surf. Sci. 360 (2016) 1016–1022.

[199] G. Liu, P. Niu, C. Sun, S.C. Smith, Z. Chen, G.Q. Lu, H.-M. Cheng, Unique electronic structure induced high photoreactivity of sulfur-doped graphitic C3N4, J. Am. Chem. Soc. 132 (2010) 11642–11648.

[200] S.C. Yan, Z.S. Li, Z.G. Zou, Photodegradation of Rhodamine B and methyl orange over boron-doped g-C3N4under visible light irradiation, Langmuir 26 (2010) 3894–3901.

[201] B. Yue, Q. Li, H. Iwai, T. Kako, J. Ye, Hydrogen production using zinc-doped carbon nitride catalyst irradiated with visible light, Sci. Technol. Adv. Mater. 12 (2011) 034401.

[202] Z.-F. Huang, J. Song, L. Pan, Z. Wang, X. Zhang, J.-J. Zou, W. Mi, X. Zhang, L. Wang, Carbon nitride with simultaneous porous network and O-doping for efficient solar-energy-driven hydrogen evolution, Nano Energy 12 (2015) 646–656.

[203] J. Ran, T.Y. Ma, G. Gao, X.-W. Du, S.Z. Qiao, Porous P-doped graphitic carbon

[204] Y. Wang, Y. Li, X. Bai, Q. Cai, C. Liu, Y. Zuo, S. Kang, L. Cui, Facile synthesis of Y-doped graphitic carbon nitride with enhanced photocatalytic performance, Catal. Commun. 84 (2016) 179–182.

[205] S.W. Hu, L.W. Yang, Y. Tian, X.L. Wei, J.W. Ding, J.X. Zhong, P.K. Chu, Simultaneous nanostructure and heterojunction engineering of graphitic carbon nitride via in situ Ag doping for enhanced photoelectrochemical activity, Appl. Catal. B 163 (2015) 611–622.

[206] Z. Ding, X. Chen, M. Antonietti, X. Wang, Synthesis of transition metal-modified carbon nitride polymers for selective hydrocarbon oxidation, ChemSusChem (2010) n/a-n/a.

[207] L.-F. Gao, T. Wen, J.-Y. Xu, X.-P. Zhai, M. Zhao, G.-W. Hu, P. Chen, Q. Wang, H.-L. Zhang, Iron-doped carbon nitride-type polymers as homogeneous organocatalysts for visible light-driven hydrogen evolution, ACS Appl. Mater. Interfaces 8 (2015) 617–624.

[208] J. Gao, Y. Wang, S. Zhou, W. Lin, Y. Kong, A facile one-step synthesis of Fe-Doped g-C3 N 4 nanosheets and their improved visible-light photocatalytic performance, ChemCatChem 9 (2017) 1708–1715.

[209] G. Zhang, C. Huang, X. Wang, Dispersing molecular cobalt in graphitic carbon nitride frameworks for photocatalytic water oxidation, Small 11 (2014) 1215–1221.

[210] Y. Shang, Y. Ma, X. Chen, X. Xiong, J. Pan, Effect of sodium doping on the structure and enhanced photocatalytic hydrogen evolution performance of graphitic carbon nitride, Mol. Catal. 433 (2017) 128–135.

[211] J. Ding, L. Wang, Q. Liu, Y. Chai, X. Liu, W.-L. Dai, Remarkable enhancement in visible-light absorption and electron transfer of carbon nitride nanosheets with 1% tungstate dopant, Appl. Catal. B 176-177 (2015) 91–98.

[212] Y. Wang, Y. Wang, Y. Li, H. Shi, Y. Xu, H. Qin, X. Li, Y. Zuo, S. Kang, L. Cui, Simple synthesis of Zr-doped graphitic carbon nitride towards enhanced photocatalytic performance under simulated solar light irradiation, Catal. Commun. 72 (2015) 24–28.

[213] X. Rong, F. Qiu, J. Rong, X. Zhu, J. Yan, D. Yang, Enhanced visible light photocatalytic activity of W-doped porous g-C 3 N 4 and effect of H 2 O 2, Mater. Lett. 164 (2016) 127–131.

[214] L. Zhou, H. Zhang, H. Sun, S. Liu, M.O. Tade, S. Wang, W. Jin, Recent advances in non-metal modification of graphitic carbon nitride for photocatalysis: a historic review, Catal. Sci. Technol. 6 (2016) 7002–7023.

[215] P. Kanhere, J. Zheng, Z. Chen, Visible light driven photocatalytic hydrogen evolution and photophysical properties of Bi3+ doped NaTaO3, Int. J. Hydrogen Energy 37 (2012) 4889–4896.

[216] S. Mansingh, D.K. Padhi, K.M. Parida, Enhanced photocatalytic activity of nanostructured Fe doped CeO2 for hydrogen production under visible light irradiation, Int. J. Hydrogen Energy 41 (2016) 14133–14146.

[217] H. Pan, Y.-W. Zhang, V.B. Shenoy, H. Gao, Ab initio study on a novel photocatalyst: functionalized graphitic carbon nitride nanotube, ACS Catal. 1 (2011) 99–104.

[218] H. Sun, S. Wang, H.M. Ang, M.O. Tadé, Q. Li, Halogen element modified titanium dioxide for visible light photocatalysis, Chem. Eng. J. 162 (2010) 437–447.

[219] H. Sun, R. Ullah, S. Chong, H.M. Ang, M.O. Tadé, S. Wang, Room-light-induced indoor air purification using an efficient Pt/N-TiO2 photocatalyst, Appl. Catal. B 108-109 (2011) 127–133.

[220] S. Hu, L. Ma, J. You, F. Li, Z. Fan, F. Wang, D. Liu, J. Gui, A simple and efficient method to prepare a phosphorus modified g-C3N4 visible light photocatalyst, RSC Adv. 4 (2014) 21657–21663.

[221] Q. Fan, J. Liu, Y. Yu, S. Zuo, B. Li, A simple fabrication for sulfur doped graphitic carbon nitride porous rods with excellent photocatalytic activity degrading RhB dye, Appl. Surf. Sci. 391 (2017) 360–368.

[222] F. He, G. Chen, Y. Yu, Y. Zhou, Y. Zheng, S. Hao, The sulfur-bubble template-mediated synthesis of uniform porous g-C3N4 with superior photocatalytic performance, Chem. Commun. 51 (2015) 425–427.

[223] S. Lin, X. Ye, X. Gao, J. Huang, Mechanistic insight into the water photooxidation on pure and sulfur-doped g-C3N4 photocatalysts from DFT calculations with dispersion corrections, J. Mol. Catal. A Chem. 406 (2015) 137–144.

[224] C. Lu, P. Zhang, S. Jiang, X. Wu, S. Song, M. Zhu, Z. Lou, Z. Li, F. Liu, Y. Liu, Y. Wang, Z. Le, Photocatalytic reduction elimination of UO 2 2 + pollutant under visible light with metal-free sulfur doped g-C 3 N 4 photocatalyst, Appl. Catal. B 200 (2017) 378–385.

[225] P. Zhang, X. Li, C. Shao, Y. Liu, Hydrothermal synthesis of carbon-rich graphitic carbon nitride nanosheets for photoredox catalysis, J. Mater. Chem. A 3 (2015) 3281–3284.

[226] Z. Zhao, Y. Sun, F. Dong, Y. Zhang, H. Zhao, Template synthesis of carbon self-doped g-C3N4 with enhanced visible to near-infrared absorption and photocatalytic performance, RSC Adv. 5 (2015) 39549–39556.

[227] L. Zhang, X. Chen, J. Guan, Y. Jiang, T. Hou, X. Mu, Facile synthesis of phosphorus doped graphitic carbon nitride polymers with enhanced visible-light photocatalytic activity, Mater. Res. Bull. 48 (2013) 3485–3491.

[228] Y. Zhou, L. Zhang, J. Liu, X. Fan, B. Wang, M. Wang, W. Ren, J. Wang, M. Li, J. Shi, Brand new P-doped g-C3N4: enhanced photocatalytic activity for H2 evolution and Rhodamine B degradation under visible light, J. Mater. Chem. A 3 (2015) 3862–3867.

[229] S. Hu, L. Ma, Y. Xie, F. Li, Z. Fan, F. Wang, Q. Wang, Y. Wang, X. Kang, G. Wu, Hydrothermal synthesis of oxygen functionalized S–P codoped g-C3N4 nanorods with outstanding visible light activity under anoxic conditions, J. Chem. Soc. Dalton Trans. 44 (2015) 20889–20897.

[230] N. Sagara, S. Kamimura, T. Tsubota, T. Ohno, Photoelectrochemical CO 2

nitride nanosheets for synergistically enhanced visible-light photocatalytic H2 production, Energy Environ. Sci. 8 (2015) 3708–3717.

reduction by a p-type boron-doped g-C 3 N 4 electrode under visible light, Appl. Catal. B 192 (2016) 193–198.

[231] Y. Bu, Z. Chen, Effect of oxygen-doped C3N4 on the separation capability of the photoinduced electron-hole pairs generated by O-C3N4@TiO2 with quasi-shell-core nanostructure, Electrochim. Acta 144 (2014) 42–49.

[232] G. Dong, Z. Ai, L. Zhang, Efficient anoxic pollutant removal with oxygen functionalized graphitic carbon nitride under visible light, RSC Adv. 4 (2014) 5553.

[233] X. She, L. Liu, H. Ji, Z. Mo, Y. Li, L. Huang, D. Du, H. Xu, H. Li, Template-free synthesis of 2D porous ultrathin nonmetal-doped g-C 3 N 4 nanosheets with highly efficient photocatalytic H 2 evolution from water under visible light, Appl. Catal. B 187 (2016) 144–153.

[234] B. Zhu, J. Zhang, C. Jiang, B. Cheng, J. Yu, First principle investigation of halogen-doped monolayer g-C 3 N 4 photocatalyst, Appl. Catal. B 207 (2017) 27–34.

[235] Y. Zhang, T. Mori, J. Ye, M. Antonietti, Phosphorus-doped carbon nitride solid: enhanced electrical conductivity and photocurrent generation, J. Am. Chem. Soc. 132 (2010) 6294–6295.

[236] Y.-P. Zhu, T.-Z. Ren, Z.-Y. Yuan, Mesoporous phosphorus-doped g-C3N4 nanostructured flowers with superior photocatalytic hydrogen evolution performance, ACS Appl. Mater. Interfaces 7 (2015) 16850–16856.

[237] S. Guo, Z. Deng, M. Li, B. Jiang, C. Tian, Q. Pan, H. Fu, Phosphorus-doped carbon nitride tubes with a layered micro-nanostructure for enhanced visible-light photocatalytic hydrogen evolution, Angew. Chem. Int. Ed. 55 (2015) 1830–1834.

[238] J. Hong, X. Xia, Y. Wang, R. Xu, Mesoporous carbon nitride with in situ sulfur doping for enhanced photocatalytic hydrogen evolution from water under visible light, J. Mater. Chem. 22 (2012) 15006.

[239] Y. Zhang, T. Mori, L. Niu, J. Ye, Non-covalent doping of graphitic carbon nitride polymer with graphene: controlled electronic structure and enhanced optoelectronic conversion, Energy Environ. Sci. 4 (2011) 4517.

[240] L.J. Fang, X.L. Wang, J.J. Zhao, Y.H. Li, Y.L. Wang, X.L. Du, Z.F. He, H.D. Zeng, H.G. Yang, One-step fabrication of porous oxygen-doped g-C3N4 with feeble nitrogen vacancies for enhanced photocatalytic performance, Chem. Commun. 52 (2016) 14408–14411.

[241] Z. Lin, X. Wang, Nanostructure engineering and doping of conjugated carbon nitride semiconductors for hydrogen photosynthesis, Angew. Chem. Int. Ed. 52 (2013) 1735–1738.

[242] S. Hu, J. Zhu, L. Wu, X. Wang, P. Liu, Y. Zhang, Z. Li, Effect of fluorination on photocatalytic degradation of Rhodamine B over In(OH)ySz: promotion or suppression? J. Phys. Chem. C 115 (2010) 460–467.

[243] J. Zhang, Y. Wu, M. Xing, S.A.K. Leghari, S. Sajjad, Development of modified N doped TiO2 photocatalyst with metals, nonmetals and metal oxides, Energy Environ. Sci. 3 (2010) 715.

[244] P. Niu, L.-C. Yin, Y.-Q. Yang, G. Liu, H.-M. Cheng, Increasing the visible light absorption of graphitic carbon nitride (Melon) photocatalysts by homogeneous self-modification with nitrogen vacancies, Adv. Mater. 26 (2014) 8046–8052.

[245] Q. Liang, Z. Li, Z.-H. Huang, F. Kang, Q.-H. Yang, Hydrogen evolution: holey graphitic carbon nitride nanosheets with carbon vacancies for highly improved photocatalytic hydrogen production (Adv. Funct. Mater. 44/2015), Adv. Funct. Mater. 25 (2015) 6952.

[246] H. Yu, R. Shi, Y. Zhao, T. Bian, Y. Zhao, C. Zhou, G.I.N. Waterhouse, L.-Z. Wu, C.-H. Tung, T. Zhang, Photocatalysis: alkali-assisted synthesis of nitrogen deficient graphitic carbon nitride with tunable band structures for efficient visible-light-driven hydrogen evolution (Adv. Mater. 16/2017, Adv. Mater. 29 (2017).

[247] W. Wu, J. Zhang, W. Fan, Z. Li, L. Wang, X. Li, Y. Wang, R. Wang, J. Zheng, M. Wu, H. Zeng, Remedying defects in carbon nitride to improve both photooxidation and H2 generation efficiencies, ACS Catal. 6 (2016) 3365–3371.

[248] Q. Tay, P. Kanhere, C.F. Ng, S. Chen, S. Chakraborty, A.C.H. Huan, T.C. Sum, R. Ahuja, Z. Chen, Defect engineered g-C3N4 for efficient visible light photocatalytic hydrogen production, Chem. Mater. 27 (2015) 4930–4933.

[249] V.W.-h. Lau, I. Moudrakovski, T. Botari, S. Weinberger, M.B. Mesch, V. Duppel, J. Senker, V. Blum, B.V. Lotsch, Rational design of carbon nitride photocatalysts by identification of cyanamide defects as catalytically relevant sites, Nat. Commun. 7 (2016) 12165.

[250] J. Qin, J. Huo, P. Zhang, J. Zeng, T. Wang, H. Zeng, Improving the photocatalytic hydrogen production of Ag/g-C3N4 nanocomposites by dye-sensitization under visible light irradiation, Nanoscale 8 (2016) 2249–2259.

[251] L. Shi, K. Chang, H. Zhang, X. Hai, L. Yang, T. Wang, J. Ye, Drastic enhancement of photocatalytic activities over phosphoric acid protonated porous g-C3N4Nanosheets under visible light, Small 12 (2016) 4431–4439.

[252] X. She, J. Wu, J. Zhong, H. Xu, Y. Yang, R. Vajtai, J. Lou, Y. Liu, D. Du, H. Li, P.M. Ajayan, Oxygenated monolayer carbon nitride for excellent photocatalytic hydrogen evolution and external quantum efficiency, Nano Energy 27 (2016) 138–146.

[253] Y. Li, H. Xu, S. Ouyang, D. Lu, X. Wang, D. Wang, J. Ye, In situ surface alkalinized g-C3N4 toward enhancement of photocatalytic H2 evolution under visible-light irradiation, J. Mater. Chem. A 4 (2016) 2943–2950.

[254] Y. Kang, Y. Yang, L.-C. Yin, X. Kang, G. Liu, H.-M. Cheng, An amorphous carbon nitride photocatalyst with greatly extended visible-light-responsive range for photocatalytic hydrogen generation, Adv. Mater. 27 (2015) 4572–4577.

[255] Y. Cao, Z. Zhang, J. Long, J. Liang, H. Lin, H. Lin, X. Wang, Vacuum heat-treatment of carbon nitride for enhancing photocatalytic hydrogen evolution, J. Mater. Chem. A 2 (2014) 17797–17807.

[256] Y. Kang, Y. Yang, L.-C. Yin, X. Kang, L. Wang, G. Liu, H.-M. Cheng, Selective breaking of hydrogen bonds of layered carbon nitride for visible light photocatalysis, Adv. Mater. 28 (2016) 6471–6477.

[257] Y. Yang, S. Wang, Y. Li, J. Wang, L. Wang, Strategies for efficient solar water splitting using carbon nitride, Chem.—Asian J. 12 (2017) 1421–1434.

[258] X. Pan, M.-Q. Yang, X. Fu, N. Zhang, Y.-J. Xu, Defective TiO2 with oxygen vacancies: synthesis, properties and photocatalytic applications, Nanoscale 5 (2013) 3601.

[259] L. Triggiani, A. Brunetti, A. Aloi, R. Comparelli, M.L. Curri, A. Agostiano, M. Striccoli, R. Tommasi, Excitation-dependent ultrafast carrier dynamics of colloidal TiO2 nanorods in organic solvent, J. Phys. Chem. C 118 (2014) 25215–25222.

[260] S. Li, G. Dong, R. Hailili, L. Yang, Y. Li, F. Wang, Y. Zeng, C. Wang, Effective photocatalytic H 2 O 2 production under visible light irradiation at g-C 3 N 4 modulated by carbon vacancies, Appl. Catal. B 190 (2016) 26–35.

[261] J. Liu, W. Fang, Z. Wei, Z. Qin, Z. Jiang, W. Shangguan, Efficient photocatalytic hydrogen evolution on N-deficient g-C3N4 achieved by a molten salt post-treatment approach, Appl. Catal. B 238 (2018) 465–470.

[262] Q. Han, Z. Cheng, B. Wang, H. Zhang, L. Qu, Significant enhancement of visible-light-Driven hydrogen evolution by structure regulation of carbon nitrides, ACS Nano (2018).

[263] D. Wang, R. Huang, W. Liu, D. Sun, Z. Li, Fe-based MOFs for photocatalytic CO2 reduction: role of coordination unsaturated sites and dual excitation pathways, ACS Catal. 4 (2014) 4254–4260.

[264] M. Peplow, Materials science: the hole story, Nature 520 (2015) 148–150.

[265] W. Xia, A. Mahmood, R. Zou, Q. Xu, Metal–organic frameworks and their derived nanostructures for electrochemical energy storage and conversion, Energy Environ. Sci. 8 (2015) 1837–1866.

[266] H.-Q. Xu, J. Hu, D. Wang, Z. Li, Q. Zhang, Y. Luo, S.-H. Yu, H.-L. Jiang, Visible-light photoreduction of CO2 in a metal–organic framework: boosting electron--hole separation via Electron trap states, J. Am. Chem. Soc. 137 (2015) 13440–13443.

[267] H. Zhang, J. Wei, J. Dong, G. Liu, L. Shi, P. An, G. Zhao, J. Kong, X. Wang, X. Meng, J. Zhang, J. Ye, Efficient visible-light-driven carbon dioxide reduction by a single-atom implanted metal-organic framework, Angew. Chem. Int. Ed. 55 (2016) 14310–14314.

[268] C. Breyer, D. Bogdanov, A. Gulagi, A. Aghahosseini, L.S.N.S. Barbosa, O. Koskinen, M. Barasa, U. Caldera, S. Afanasyeva, M. Child, J. Farfan, P. Vainikka, On the role of solar photovoltaics in global energy transition scenarios, Prog. Photovolt. Res. Appl. 25 (2017) 727–745.

[269] S. Dang, Q.-L. Zhu, Q. Xu, Nanomaterials derived from metal–organic frameworks, Nat. Rev. Mater. 3 (2017) 17075.

[270] J.-L. Wang, C. Wang, W. Lin, Metal–Organic frameworks for light harvesting and photocatalysis, ACS Catal. 2 (2012) 2630–2640.

[271] Y. Horiuchi, T. Toyao, M. Takeuchi, M. Matsuoka, M. Anpo, Recent advances in visible-light-responsive photocatalysts for hydrogen production and solar energy conversion – from semiconductor TiO2 to MOF/PCP photocatalysts, J. Chem. Soc. Faraday Trans. 15 (2013) 13243.

[272] S.-L. Li, Q. Xu, Metal–organic frameworks as platforms for clean energy, Energy Environ. Sci. 6 (2013) 1656.

[273] C.-C. Wang, J.-R. Li, X.-L. Lv, Y.-Q. Zhang, G. Guo, Photocatalytic organic pollutants degradation in metal–organic frameworks, Energy Environ. Sci. 7 (2014) 2831–2867.

[274] E.M. Dias, C. Petit, Towards the use of metal–organic frameworks for water reuse: a review of the recent advances in the field of organic pollutants removal and degradation and the next steps in the field, J. Mater. Chem. A 3 (2015) 22484–22506.

[275] L. Shen, R. Liang, L. Wu, Strategies for engineering metal-organic frameworks as efficient photocatalysts, Chin. J. Catal. 36 (2015) 2071–2088.

[276] S. Wang, X. Wang, Multifunctional metal-organic frameworks for photocatalysis, Small 11 (2015) 3097–3112.

[277] L. Zeng, X. Guo, C. He, C. Duan, Metal–organic frameworks: versatile materials for heterogeneous photocatalysis, ACS Catal. 6 (2016) 7935–7947.

[278] Y. Chen, D. Wang, X. Deng, Z. Li, Metal–organic frameworks (MOFs) for photocatalytic CO2 reduction, Catal. Sci. Technol. 7 (2017) 4893–4904.

[279] X. Deng, Z. Li, H. García, Visible light induced organic transformations using metal-organic-frameworks (MOFs), Chem. Eur. J. 23 (2017) 11189–11209.

[280] D. Sun, Z. Li, Robust Ti- and Zr-based metal-organic frameworks for photocatalysis, Chinese J. Chem. 35 (2017) 135–147.

[281] X. Yu, L. Wang, S.M. Cohen, Photocatalytic metal–organic frameworks for organic transformations, CrystEngComm 19 (2017) 4126–4136.

[282] Z. Wang, Z. Jin, G. Wang, B. Ma, Efficient hydrogen production over MOFs (ZIF-67) and g-C 3 N 4 boosted with MoS 2 nanoparticles, Int. J. Hydrogen Energy 43 (2018) 13039–13050.

[283] F. Chen, H. Yang, X. Wang, H. Yu, Facile synthesis and enhanced photocatalytic H 2 -evolution performance of NiS 2 -modified g-C 3 N 4 photocatalysts, Chin. J. Catal. 38 (2017) 296–304.

[284] P.C. Banerjee, D.E. Lobo, R. Middag, W.K. Ng, M.E. Shaibani, M. Majumder, Electrochemical capacitance of Ni-Doped metal organic framework and reduced graphene oxide composites: more than the sum of its parts, ACS Appl. Mater. Interfaces 7 (2015) 3655–3664.

[285] L. Tian, X. Yang, Q. Liu, F. Qu, H. Tang, Anchoring metal-organic framework nanoparticles on graphitic carbon nitrides for solar-driven photocatalytic hydrogen evolution, Appl. Surf. Sci. 455 (2018) 403–409.

[286] M. Mohamedali, H. Ibrahim, A. Henni, Incorporation of acetate-based ionic liquids into a zeolitic imidazolate framework (ZIF-8) as efficient sorbents for carbon dioxide capture, Chem. Eng. J. 334 (2018) 817–828.

[287] R. Chandra, S. Mukhopadhyay, M. Nath, TiO 2 @ZIF-8: a novel approach of modifying micro-environment for enhanced photo-catalytic dye degradation and high usability of TiO 2 nanoparticles, Mater. Lett. 164 (2016) 571–574.

[288] Y. Guan, J. Shi, M. Xia, J. Zhang, Z. Pang, A. Marchetti, X. Wang, J. Cai, X. Kong,

Monodispersed ZIF-8 particles with enhanced performance for CO2 adsorption and heterogeneous catalysis, Appl. Surf. Sci. 423 (2017) 349–353.

[289] S.K. Movahed, Z. Piramanai, M. Dabiri, A nitrogen-doped porous carbon derived from copper phthalocyanines on/in ZIF-8 as an efficient photocatalyst for the degradation of dyes and the C H activation of formamides, J. Photochem. Photobiol. A: Chem. 351 (2018) 208–224.

[290] Y. Zhang, Z. Jin, A. luan, G. Wang, Charge transfer behaviors over MOF-5@g-C 3 N 4 with Ni x Mo 1 − x S 2 modification, Int. J. Hydrogen Energy 43 (2018) 9914–9923.

[291] H. Wang, X. Yuan, H. Wang, X. Chen, Z. Wu, L. Jiang, W. Xiong, G. Zeng, Facile synthesis of Sb2S3/ultrathin g-C3N4 sheets heterostructures embedded with g-C3N4 quantum dots with enhanced NIR-light photocatalytic performance, Appl. Catal. B 193 (2016) 36–46.

[292] F. Chen, Q. Yang, X. Li, G. Zeng, D. Wang, C. Niu, J. Zhao, H. An, T. Xie, Y. Deng, Hierarchical assembly of graphene-bridged Ag 3 PO 4 /Ag/BiVO 4 (040) Z-scheme photocatalyst: an efficient, sustainable and heterogeneous catalyst with enhanced visible-light photoactivity towards tetracycline degradation under visible light irradiation, Appl. Catal. B 200 (2017) 330–342.

[293] L. Ye, D. Wang, S. Chen, Fabrication and enhanced photoelectrochemical performance of MoS2/S-Doped g-C3N4 heterojunction film, ACS Appl. Mater. Interfaces 8 (2016) 5280–5289.

[294] F. Chen, Q. Yang, Y. Wang, J. Zhao, D. Wang, X. Li, Z. Guo, H. Wang, Y. Deng, C. Niu, G. Zeng, Novel ternary heterojunction photocatalyst of Ag nanoparticles and g-C 3 N 4 nanosheets co-modified BiVO 4 for wider spectrum visible-light photocatalytic degradation of refractory pollutant, Appl. Catal. B 205 (2017) 133–147.

[295] L. Jiang, X. Yuan, G. Zeng, X. Chen, Z. Wu, J. Liang, J. Zhang, H. Wang, H. Wang, Phosphorus- and sulfur-Codoped g-C3N4: facile preparation, mechanism insight, and application as efficient photocatalyst for tetracycline and methyl orange degradation under visible light irradiation, ACS Sustain. Chem. Eng. 5 (2017) 5831–5841.

[296] L. Jiang, X. Yuan, G. Zeng, Z. Wu, J. Liang, X. Chen, L. Leng, H. Wang, H. Wang, Metal-free efficient photocatalyst for stable visible-light photocatalytic degradation of refractory pollutant, Appl. Catal. B 221 (2018) 715–725.

[297] Z. Xing, Z. Chen, X. Zong, L. Wang, A new type of carbon nitride-based polymer composite for enhanced photocatalytic hydrogen production, Chem. Commun. 50 (2014) 6762–6764.

[298] H. Cheng, J. Hou, O. Takeda, X.-M. Guo, H. Zhu, A unique Z-scheme 2D/2D nanosheet heterojunction design to harness charge transfer for photocatalysis, J. Mater. Chem. A 3 (2015) 11006–11013.

[299] Y. Hong, Y. Jiang, C. Li, W. Fan, X. Yan, M. Yan, W. Shi, In-situ synthesis of direct solid-state Z-scheme V 2 O 5 /g-C 3 N 4 heterojunctions with enhanced visible light efficiency in photocatalytic degradation of pollutants, Appl. Catal. B 180 (2016) 663–673.

[300] K. Song, F. Xiao, L. Zhang, F. Yue, X. Liang, J. Wang, X. Su, W 18 O 49 nanowires grown on g-C 3 N 4 sheets with enhanced photocatalytic hydrogen evolution activity under visible light, J. Mol. Catal. A Chem. 418-419 (2016) 95–102.

[301] Z. Jin, N. Murakami, T. Tsubota, T. Ohno, Complete oxidation of acetaldehyde over a composite photocatalyst of graphitic carbon nitride and tungsten(VI) oxide under visible-light irradiation, Appl. Catal. B 150-151 (2014) 479–485.

[302] H. Katsumata, T. Sakai, T. Suzuki, S. Kaneco, Highly efficient photocatalytic activity of g-C3N4/Ag3PO4 hybrid photocatalysts through Z-Scheme photocatalytic mechanism under visible light, Ind. Eng. Chem. Res. 53 (2014) 8018–8025.

[303] Y. He, L. Zhang, X. Wang, Y. Wu, H. Lin, L. Zhao, W. Weng, H. Wang, M. Fan, Enhanced photodegradation activity of methyl orange over Z-scheme type MoO3–g-C3N4 composite under visible light irradiation, RSC Adv. 4 (2014) 13610–13619.

[304] N. Tian, H. Huang, Y. He, Y. Guo, T. Zhang, Y. Zhang, Mediator-free direct Z-scheme photocatalytic system: BiVO4/g-C3N4 organic–inorganic hybrid photocatalyst with highly efficient visible-light-induced photocatalytic activity, J. Chem. Soc. Dalton Trans. 44 (2015) 4297–4307.

[305] J. Yu, S. Wang, J. Low, W. Xiao, Enhanced photocatalytic performance of direct Z-scheme g-C3N4–TiO2 photocatalysts for the decomposition of formaldehyde in air, J. Chem. Soc. Faraday Trans. 15 (2013) 16883.

[306] J.-C. Wang, H.-C. Yao, Z.-Y. Fan, L. Zhang, J.-S. Wang, S.-Q. Zang, Z.-J. Li, Indirect Z-Scheme BiOI/g-C3N4 photocatalysts with enhanced photoreduction CO2 activity under visible light irradiation, ACS Appl. Mater. Interfaces 8 (2016) 3765–3775.

[307] Y. Bai, P.-Q. Wang, J.-Y. Liu, X.-J. Liu, Enhanced photocatalytic performance of direct Z-scheme BiOCl–g-C3N4 photocatalysts, RSC Adv. 4 (2014) 19456.

[308] Y. Feng, J. Shen, Q. Cai, H. Yang, Q. Shen, The preparation and properties of a g-C3N4/AgBr nanocomposite photocatalyst based on protonation pretreatment, New J. Chem. 39 (2015) 1132–1138.

[309] S. Meng, X. Ning, T. Zhang, S.-F. Chen, X. Fu, What is the transfer mechanism of photogenerated carriers for the nanocomposite photocatalyst Ag3PO4/g-C3N4, band–band transfer or a direct Z-scheme? J. Chem. Soc. Faraday Trans. 17 (2015) 11577–11585.

[310] J. Chen, J. Zhong, J. Li, S. Huang, W. Hu, M. Li, Q. Du, Synthesis and characterization of novel Ag 2 CO 3 /g-C 3 N 4 composite photocatalysts with excellent solar photocatalytic activity and mechanism insight, Mol. Catal. 435 (2017) 91–98.

[311] D. Tang, G. Zhang, Fabrication of AgFeO 2 /g-C 3 N 4 nanocatalyst with enhanced and stable photocatalytic performance, Appl. Surf. Sci. 391 (2017) 415–422.

[312] B. Zhu, P. Xia, Y. Li, W. Ho, J. Yu, Fabrication and photocatalytic activity enhanced mechanism of direct Z-scheme g-C 3 N 4 /Ag 2 WO 4 photocatalyst, Appl. Surf. Sci. 391 (2017) 175–183.

[313] X. Xiao, J. Wei, Y. Yang, R. Xiong, C. Pan, J. Shi, Photoreactivity and mechanism of g-C3N4 and Ag Co-modified Bi2WO6 microsphere under visible light irradiation, ACS Sustain. Chem. Eng. 4 (2016) 3017–3023.

[314] X. She, J. Wu, H. Xu, J. Zhong, Y. Wang, Y. Song, K. Nie, Y. Liu, Y. Yang, M.-T.F. Rodrigues, R. Vajtai, J. Lou, D. Du, H. Li, P.M. Ajayan, High efficiency photocatalytic water splitting using 2D α-Fe2 O 3 /g-C3 N 4 Z-Scheme catalysts, Adv. Energy Mater. 7 (2017) 1700025.

[315] M. Han, L. Hu, Y. Zhou, S. Zhao, L. Bai, Y. Sun, H. Huang, Y. Liu, Z. Kang, Z-Scheme in a Co3(PO4)2/α-Fe2O3 photocatalysis system for overall water splitting under visible light, Catal. Sci. Technol. 8 (2018) 840–846.

[316] Y. Zou, J.-W. Shi, D. Ma, Z. Fan, C. Niu, L. Wang, Fabrication of g-C3 N 4 /Au/C-TiO2 hollow structures as visible-light-driven Z-scheme photocatalysts with enhanced photocatalytic H2 evolution, ChemCatChem 9 (2017) 3752–3761.

[317] D. Lu, H. Wang, X. Zhao, K.K. Kondamareddy, J. Ding, C. Li, P. Fang, Highly efficient visible-light-Induced photoactivity of Z-Scheme g-C3N4/Ag/MoS2 ternary photocatalysts for organic pollutant degradation and production of hydrogen, ACS Sustain. Chem. Eng. 5 (2017) 1436–1445.

[318] M. Kaneko, N. Katakura, C. Harada, Y. Takei, M. Hoshino, Visible light decomposition of ammonia to dinitrogen by a new visible light photocatalytic system composed of sensitizer (Ru(bpy)32 +), electron mediator (methylviologen) and electron acceptor (dioxygen), Chem. Commun. (Camb.) (2005) 3436.

[319] J. Liang, Y. Zheng, J. Chen, J. Liu, D. Hulicova-Jurcakova, M. Jaroniec, S.Z. Qiao, Facile oxygen reduction on a three-dimensionally ordered macroporous graphitic C3N4/Carbon composite electrocatalyst, Angew. Chem. Int. Ed. 51 (2012) 3892–3896.

[320] D. Jiang, Y. Zhang, H. Chu, J. Liu, J. Wan, M. Chen, N-doped graphene quantum dots as an effective photocatalyst for the photochemical synthesis of silver deposited porous graphitic C3N4 nanocomposites for nonenzymatic electrochemical H2O2 sensing, RSC Adv. 4 (2014) 16163–16171.

[321] H. Sun, G. Zhou, Y. Wang, A. Suvorova, S. Wang, A new metal-free carbon hybrid for enhanced photocatalysis, ACS Appl. Mater. Interfaces 6 (2014) 16745–16754.

[322] H. Sun, Y. Cao, L. Feng, Y. Chen, Immobilizing photogenerated electrons from graphitic carbon nitride for an improved visible-light photocatalytic activity, Sci. Rep. 6 (2016).

[323] J.-P. Zou, L.-C. Wang, J. Luo, Y.-C. Nie, Q.-J. Xing, X.-B. Luo, H.-M. Du, S.-L. Luo, S.L. Suib, Synthesis and efficient visible light photocatalytic H 2 evolution of a metal-free g-C 3 N 4 /graphene quantum dots hybrid photocatalyst, Appl. Catal. B 193 (2016) 103–109.

[324] Y. Guo, P. Yao, D. Zhu, C. Gu, A novel method for the development of a carbon quantum dot/carbon nitride hybrid photocatalyst that responds to infrared light irradiation, J. Mater. Chem. A 3 (2015) 13189–13192.

[325] J.-B. Baek, L. Dai, Metal-free and Oxygen-free Graphene As Oxygen Reduction Catalysts for Highly Efficient Fuel Cells, Defense Technical Information Center, 2013.

[326] X.-K. Kong, C.-L. Chen, Q.-W. Chen, Doped graphene for metal-free catalysis, Chem. Soc. Rev. 43 (2014) 2841–2857.

[327] G. Gao, Y. Jiao, F. Ma, Y. Jiao, E. Waclawik, A. Du, Carbon nanodot decorated graphitic carbon nitride: new insights into the enhanced photocatalytic water splitting from ab initio studies, J. Chem. Soc. Faraday Trans. 17 (2015) 31140–31144.

[328] S. Fang, Y. Xia, K. Lv, Q. Li, J. Sun, M. Li, Effect of carbon-dots modification on the structure and photocatalytic activity of g-C 3 N 4, Appl. Catal. B 185 (2016) 225–232.

[329] X. Jian, X. Liu, H.-m. Yang, J.-g. Li, X.-l. Song, H.-y. Dai, Z.-h. Liang, Construction of carbon quantum dots/proton-functionalized graphitic carbon nitride nanocomposite via electrostatic self-assembly strategy and its application, Appl. Surf. Sci. 370 (2016) 514–521.

[330] H. Zhang, L. Zhao, F. Geng, L.-H. Guo, B. Wan, Y. Yang, Carbon dots decorated graphitic carbon nitride as an efficient metal-free photocatalyst for phenol degradation, Appl. Catal. B 180 (2016) 656–662.

[331] G. Gogoi, S. Keene, A.S. Patra, T.K. Sahu, S. Ardo, M. Qureshi, Hybrid of g-C3N4 and MoS2 integrated onto Cd0.5Zn0.5S: rational design with efficient charge transfer for enhanced photocatalytic activity, ACS Sustain. Chem. Eng. 6 (2018) 6718–6729.

[332] K. Li, F.-Y. Su, W.-D. Zhang, Modification of g-C 3 N 4 nanosheets by carbon quantum dots for highly efficient photocatalytic generation of hydrogen, Appl. Surf. Sci. 375 (2016) 110–117.

[333] M.J. Allen, V.C. Tung, R.B. Kaner, Honeycomb carbon: a review of graphene, Chem. Rev. 110 (2010) 132–145.

[334] J. Coraux, L. Marty, N. Bendiab, V. Bouchiat, Functional hybrid systems based on large-area high-quality graphene, Acc. Chem. Res. 46 (2012) 2193–2201.

[335] S. Fujii, T. Enoki, Nanographene and Graphene Edges: Electronic Structure and Nanofabrication, Acc. Chem. Res. 46 (2012) 2202–2210.

[336] C. Berger, Electronic Confinement and Coherence in Patterned Epitaxial Graphene, Science 312 (2006) 1191–1196.

[337] K.S. Kim, Y. Zhao, H. Jang, S.Y. Lee, J.M. Kim, K.S. Kim, J.-H. Ahn, P. Kim, J.-Y. Choi, B.H. Hong, Large-scale pattern growth of graphene films for stretchable transparent electrodes, Nature 457 (2009) 706–710.

[338] O.C. Compton, S.T. Nguyen, Graphene oxide, highly reduced graphene oxide, and graphene: versatile building blocks for carbon-based materials, Small 6 (2010) 711–723.

[339] X.-Y. Peng, X.-X. Liu, D. Diamond, K.T. Lau, Synthesis of electrochemically-reduced graphene oxide film with controllable size and thickness and its use in supercapacitor, Carbon 49 (2011) 3488–3496.

[340] X. Wang, X. Zhou, K. Yao, J. Zhang, Z. Liu, A SnO2/graphene composite as a high stability electrode for lithium ion batteries, Carbon 49 (2011) 133–139.

[341] S. Pei, H.-M. Cheng, The reduction of graphene oxide, Carbon 50 (2012) 3210–3228.

[342] H.J. Qiu, Y. Ito, W. Cong, Y. Tan, P. Liu, A. Hirata, T. Fujita, Z. Tang, M. Chen, Nanoporous graphene with single-atom nickel dopants: an efficient and stable catalyst for electrochemical hydrogen production, Angew. Chem. Int. Ed. 54 (2015) 14031–14035.

[343] M. Yan, Y. Hua, F. Zhu, L. Sun, W. Gu, W. Shi, Constructing nitrogen doped graphene quantum dots-ZnNb 2 O 6 /g-C 3 N 4 catalysts for hydrogen production under visible light, Appl. Catal. B 206 (2017) 531–537.

[344] R.C. Pawar, S. Kang, S.H. Ahn, C.S. Lee, Gold nanoparticle modified graphitic carbon nitride/multi-walled carbon nanotube (g-C3N4/CNTs/Au) hybrid photocatalysts for effective water splitting and degradation, RSC Adv. 5 (2015) 24281–24292.

[345] Y. Chen, J. Li, Z. Hong, B. Shen, B. Lin, B. Gao, Origin of the enhanced visible-light photocatalytic activity of CNT modified g-C3N4 for H2 production, J. Chem. Soc. Faraday Trans. 16 (2014) 8106.

[346] L. Ge, C. Han, Synthesis of MWNTs/g-C3N4 composite photocatalysts with efficient visible light photocatalytic hydrogen evolution activity, Appl. Catal. B 117-118 (2012) 268–274.

[347] K.C. Christoforidis, Z. Syrgiannis, V. La Parola, T. Montini, C. Petit, E. Stathatos, R. Godin, J.R. Durrant, M. Prato, P. Fornasiero, Metal-free dual-phase full organic carbon nanotubes/g-C 3 N 4 heteroarchitectures for photocatalytic hydrogen production, Nano Energy 50 (2018) 468–478.

[348] L.M. Liz-Marzán, Tailoring surface plasmons through the morphology and assembly of metal nanoparticles, Langmuir 22 (2006) 32–41.

[349] S. Linic, P. Christopher, D.B. Ingram, Plasmonic-metal nanostructures for efficient conversion of solar to chemical energy, Nat. Mater. 10 (2011) 911–921.

[350] L. Polavarapu, S. Mourdikoudis, I. Pastoriza-Santos, J. Pérez-Juste, Nanocrystal engineering of noble metals and metal chalcogenides: controlling the morphology, composition and crystallinity, CrystEngComm 17 (2015) 3727–3762.

[351] U. Bhattacharjee, L. Men, B.A. Rosales, S.R. Alvarado, J. Vela, J.W. Petrich, Using ATTO dyes to probe the photocatalytic activity of Au–CdS nanoparticles, J. Phys. Chem. C 121 (2016) 676–683.

[352] Y. Li, K. Lv, W. Ho, Z. Zhao, Y. Huang, Enhanced visible-light photo-oxidation of nitric oxide using bismuth-coupled graphitic carbon nitride composite heterostructures, Chin. J. Catal. 38 (2017) 321–329.

[353] S. Tan, L. Liu, Y. Dai, J. Ren, J. Zhao, H. Petek, Ultrafast plasmon-enhanced hot electron generation at Ag nanocluster/graphite heterojunctions, J. Am. Chem. Soc. 139 (2017) 6160–6168.

[354] T.T. Wang, P. Raghunath, Y.G. Lin, M.C. Lin, Synergistic effect of hydrogenation and thiocyanate treatments on Ag-Loaded TiO2 nanoparticles for solar-to-Hydrogen conversion, J. Phys. Chem. C 121 (2017) 9681–9690.

[355] S. Bai, X. Li, Q. Kong, R. Long, C. Wang, J. Jiang, Y. Xiong, Toward enhanced photocatalytic oxygen evolution: synergetic utilization of plasmonic effect and schottky junction via interfacing facet selection, Adv. Mater. 27 (2015) 3444–3452.

[356] S.K. Cushing, N. Wu, Progress and perspectives of plasmon-enhanced solar energy conversion, J. Phys. Chem. Lett. 7 (2016) 666–675.

[357] J.W. Hong, D.H. Wi, S.-U. Lee, S.W. Han, Metal–Semiconductor heteronanocrystals with desired configurations for plasmonic photocatalysis, J. Am. Chem. Soc. 138 (2016) 15766–15773.

[358] X. Meng, L. Liu, S. Ouyang, H. Xu, D. Wang, N. Zhao, J. Ye, Nanometals for solar-to-Chemical energy conversion: from semiconductor-based photocatalysis to plasmon-mediated photocatalysis and photo-thermocatalysis, Adv. Mater. 28 (2016) 6781–6803.

[359] M. Valenti, M.P. Jonsson, G. Biskos, A. Schmidt-Ott, W.A. Smith, Plasmonic nanoparticle-semiconductor composites for efficient solar water splitting, J. Mater. Chem. A 4 (2016) 17891–17912.

[360] L. Yan, F. Wang, S. Meng, Quantum mode selectivity of plasmon-induced water splitting on gold nanoparticles, ACS Nano 10 (2016) 5452–5458.

[361] J. Zhang, X. Jin, P.I. Morales-Guzman, X. Yu, H. Liu, H. Zhang, L. Razzari, J.P. Claverie, Engineering the absorption and field enhancement properties of Au–TiO2 nanohybrids via whispering gallery mode resonances for photocatalytic water splitting, ACS Nano 10 (2016) 4496–4503.

[362] A.A. Golubev, B.N. Khlebtsov, R.D. Rodriguez, Y. Chen, D.R.T. Zahn, Plasmonic heating plays a dominant role in the plasmon-induced photocatalytic reduction of 4-Nitrobenzenethiol, J. Phys. Chem. C 122 (2018) 5657–5663.

[363] Y. Yu, V. Sundaresan, K.A. Willets, Hot carriers versus thermal effects: resolving the enhancement mechanisms for plasmon-mediated photoelectrochemical reactions, J. Phys. Chem. C 122 (2018) 5040–5048.

[364] N. Zhou, V. López-Puente, Q. Wang, L. Polavarapu, I. Pastoriza-Santos, Q.-H. Xu, Plasmon-enhanced light harvesting: applications in enhanced photocatalysis, photodynamic therapy and photovoltaics, RSC Adv. 5 (2015) 29076–29097.

[365] K. Ueno, T. Oshikiri, H. Misawa, Plasmon-induced water splitting using metallic-nanoparticle-loaded photocatalysts and photoelectrodes, ChemPhysChem 17 (2016) 194.

[366] M. Wang, M. Ye, J. Iocozzia, C. Lin, Z. Lin, Plasmon-mediated solar energy conversion via Photocatalysis in noble metal/semiconductor composites, Adv. Sci. 3 (2016) 1600024.

[367] N. Zhou, L. Polavarapu, N. Gao, Y. Pan, P. Yuan, Q. Wang, Q.-H. Xu, TiO2 coated Au/Ag nanorods with enhanced photocatalytic activity under visible light irradiation, Nanoscale 5 (2013) 4236.

[368] C.N. Van, W.S. Chang, J.-W. Chen, K.-A. Tsai, W.-Y. Tzeng, Y.-C. Lin, H.-H. Kuo, H.-J. Liu, K.-D. Chang, W.-C. Chou, C.-L. Wu, Y.-C. Chen, C.-W. Luo, Y.-J. Hsu, Y.-H. Chu, Heteroepitaxial approach to explore charge dynamics across Au/BiVO 4 interface for photoactivity enhancement, Nano Energy 15 (2015) 625–633.

[369] Z. Lou, M. Fujitsuka, T. Majima, Pt–Au triangular nanoprisms with strong dipole plasmon resonance for hydrogen generation studied by single-particle spectroscopy, ACS Nano 10 (2016) 6299–6305.

[370] B. Wu, D. Liu, S. Mubeen, T.T. Chuong, M. Moskovits, G.D. Stucky, Anisotropic growth of TiO2 onto gold nanorods for plasmon-enhanced hydrogen production from water reduction, J. Am. Chem. Soc. 138 (2016) 1114–1117.

[371] H. Sun, S. Zeng, Q. He, P. She, K. Xu, Z. Liu, Spiky TiO2/Au nanorod plasmonic photocatalysts with enhanced visible-light photocatalytic activity, J. Chem. Soc. Dalton Trans. 46 (2017) 3887–3894.

[372] J.K. Stolarczyk, S. Bhattacharyya, L. Polavarapu, J. Feldmann, Challenges and prospects in solar water splitting and CO2 reduction with inorganic and hybrid nanostructures, ACS Catal. 8 (2018) 3602–3635.

[373] N. Cheng, J. Tian, Q. Liu, C. Ge, A.H. Qusti, A.M. Asiri, A.O. Al-Youbi, X. Sun, Au-nanoparticle-loaded graphitic carbon nitride nanosheets: green photocatalytic synthesis and application toward the degradation of organic pollutants, ACS Appl. Mater. Interfaces 5 (2013) 6815–6819.

[374] S. Tonda, S. Kumar, V. Shanker, Surface plasmon resonance-induced photocatalysis by Au nanoparticles decorated mesoporous g-C 3 N 4 nanosheets under direct sunlight irradiation, Mater. Res. Bull. 75 (2016) 51–58.

[375] P. Wang, B. Huang, X. Zhang, X. Qin, H. Jin, Y. Dai, Z. Wang, J. Wei, J. Zhan, S. Wang, J. Wang, M.-H. Whangbo, Highly efficient visible-light plasmonic photocatalyst Ag@AgBr, Chem. Eur. J. 15 (2009) 1821–1824.

[376] J. Yi, X. She, Y. Song, H. Xu, P. Zhang, Z. Mo, L. Liu, D. Du, H. Li, A silver on 2D white-C3N4 support photocatalyst for mechanistic insights: synergetic utilization of plasmonic effect for solar hydrogen evolution, RSC Adv. 6 (2016) 112420–112428.

[377] Z. Mo, H. Xu, Z. Chen, X. She, Y. Song, P. Yan, Y. Xu, Y. Lei, S. Yuan, H. Li, Gold/monolayer graphitic carbon nitride plasmonic photocatalyst for ultrafast electron transfer in solar-to-hydrogen energy conversion, Chin. J. Catal. 39 (2018) 760–770.

[378] Z. Liu, W. Hou, P. Pavaskar, M. Aykol, S.B. Cronin, Plasmon resonant enhancement of photocatalytic water splitting under visible illumination, Nano Lett. 11 (2011) 1111–1116.

[379] J. Cui, Y. Li, L. Liu, L. Chen, J. Xu, J. Ma, G. Fang, E. Zhu, H. Wu, L. Zhao, L. Wang, Y. Huang, Near-infrared plasmonic-enhanced solar energy harvest for highly efficient photocatalytic reactions, Nano Lett. 15 (2015) 6295–6301.

[380] J. Chen, H. Che, K. Huang, C. Liu, W. Shi, Fabrication of a ternary plasmonic photocatalyst CQDs/Ag/Ag 2 O to harness charge flow for photocatalytic elimination of pollutants, Appl. Catal. B 192 (2016) 134–144.

[381] X.-Q. Deng, B. Zhu, X.-S. Li, J.-L. Liu, X. Zhu, A.-M. Zhu, Visible-light photocatalytic oxidation of CO over plasmonic Au/TiO 2: unusual features of oxygen plasma activation, Appl. Catal. B 188 (2016) 48–55.

[382] W. Guo, Q. Qin, L. Geng, D. Wang, Y. Guo, Y. Yang, Morphology-controlled preparation and plasmon-enhanced photocatalytic activity of Pt–BiOBr heterostructures, J. Hazard. Mater. 308 (2016) 374–385.

[383] W. Jiang, S. Bai, L. Wang, X. Wang, L. Yang, Y. Li, D. Liu, X. Wang, Z. Li, J. Jiang, Y. Xiong, Integration of multiple plasmonic and Co-catalyst nanostructures on TiO2 nanosheets for visible-near-Infrared photocatalytic hydrogen evolution, Small 12 (2016) 1640–1648.

[384] C.-H. Li, M.-C. Li, S.-P. Liu, A.C. Jamison, D. Lee, T.R. Lee, T.-C. Lee, Plasmonically enhanced photocatalytic hydrogen production from water: the critical role of tunable surface plasmon resonance from gold–silver nanoshells, ACS Appl. Mater. Interfaces 8 (2016) 9152–9161.

[385] T. Liu, Y. Li, Plasmonic solar desalination, Nat. Photonics 10 (2016) 361–362.

[386] S.S. Patil, D.R. Patil, S.K. Apte, M.V. Kulkarni, J.D. Ambekar, C.-J. Park, S.W. Gosavi, S.S. Kolekar, B.B. Kale, Confinement of Ag 3 PO 4 nanoparticles supported by surface plasmon resonance of Ag in glass: efficient nanoscale photocatalyst for solar H 2 production from waste H 2 S, Appl. Catal. B 190 (2016) 75–84.

[387] S. Shuang, R. Lv, Z. Xie, Z. Zhang, Surface plasmon enhanced photocatalysis of Au/Pt-decorated TiO2 nanopillar arrays, Sci. Rep. 6 (2016).

[388] S.W. Verbruggen, M. Keulemans, B. Goris, N. Blommaerts, S. Bals, J.A. Martens, S. Lenaerts, Plasmonic 'rainbow' photocatalyst with broadband solar light response for environmental applications, Appl. Catal. B 188 (2016) 147–153.

[389] D. Xu, W. Shi, C. Song, M. Chen, S. Yang, W. Fan, B. Chen, In-situ synthesis and enhanced photocatalytic activity of visible-light-driven plasmonic Ag/AgCl/NaTaO 3 nanocubes photocatalysts, Appl. Catal. B 191 (2016) 228–234.

[390] C. An, S. Wang, Y. Sun, Q. Zhang, J. Zhang, C. Wang, J. Fang, Plasmonic silver incorporated silver halides for efficient photocatalysis, J. Mater. Chem. A 4 (2016) 4336–4352.

[391] P. Zhang, T. Wang, J. Gong, Mechanistic understanding of the plasmonic enhancement for solar water splitting, Adv. Mater. 27 (2015) 5328–5342.

[392] J. Shi, L. Guo, ABO3-based photocatalysts for water splitting, Prog. Nat. Sci. 22 (2012) 592–615.

[393] Y. Moriya, T. Takata, K. Domen, Recent progress in the development of (oxy)nitride photocatalysts for water splitting under visible-light irradiation, Coord. Chem. Rev. 257 (2013) 1957–1969.

[394] P. Kanhere, Z. Chen, A review on visible light active perovskite-based photocatalysts, Molecules 19 (2014) 19995–20022.

[395] W. Wang, M.O. Tadé, Z. Shao, Research progress of perovskite materials in photocatalysis- and photovoltaics-related energy conversion and environmental treatment, Chem. Soc. Rev. 44 (2015) 5371–5408.

[396] C. Huang, Z. Li, Z. Zou, A perspective on perovskite oxide semiconductor catalysts for gas phase photoreduction of carbon dioxide, MRS Commun. 6 (2016) 216–225.

[397] B. Weng, Z. Xiao, W. Meng, C.R. Grice, T. Poudel, X. Deng, Y. Yan, Bandgap engineering of barium bismuth niobate double perovskite for photoelectrochemical

water oxidation, Adv. Energy Mater. 7 (2016) 1602260.

[398] G. Zhang, G. Liu, L. Wang, J.T.S. Irvine, Inorganic perovskite photocatalysts for solar energy utilization, Chem. Soc. Rev. 45 (2016) 5951–5984.

[399] Y. Zhu, W. Zhou, Y. Zhong, Y. Bu, X. Chen, Q. Zhong, M. Liu, Z. Shao, A perovskite nanorod as bifunctional electrocatalyst for overall water splitting, Adv. Energy Mater. 7 (2016) 1602122.

[400] P. Kanhere, P. Shenai, S. Chakraborty, R. Ahuja, J. Zheng, Z. Chen, Mono- and co-doped NaTaO3for visible light photocatalysis, Phys. Chem. Chem. Phys. 16 (2014) 16085–16094.

[401] E. Grabowska, Selected perovskite oxides: characterization, preparation and photocatalytic properties—a review, Appl. Catal. B 186 (2016) 97–126.

[402] H. Zhang, G. Chen, Y. Li, Y. Teng, Electronic structure and photocatalytic properties of copper-doped CaTiO3, Int. J. Hydrogen Energy 35 (2010) 2713–2716.

[403] H.-C. Chen, C.-W. Huang, J.C.S. Wu, S.-T. Lin, Theoretical investigation of the metal-doped SrTiO3 photocatalysts for water splitting, J. Phys. Chem. C 116 (2012) 7897–7903.

[404] L. Li, Y. Zhang, A.M. Schultz, X. Liu, P.A. Salvador, G.S. Rohrer, Visible light photochemical activity of heterostructured PbTiO3–TiO2 core–shell particles, Catal. Sci. Technol. 2 (2012) 1945.

[405] Y. Qu, W. Zhou, Z. Ren, S. Du, X. Meng, G. Tian, K. Pan, G. Wang, H. Fu, Facile preparation of porous NiTiO3 nanorods with enhanced visible-light-driven photocatalytic performance, J. Mater. Chem. 22 (2012) 16471.

[406] Y. Jia, S. Shen, D. Wang, X. Wang, J. Shi, F. Zhang, H. Han, C. Li, Composite Sr2TiO4/SrTiO3(La,Cr) heterojunction based photocatalyst for hydrogen production under visible light irradiation, J. Mater. Chem. A 1 (2013) 7905.

[407] H. Kato, Y. Sasaki, N. Shirakura, A. Kudo, Synthesis of highly active rhodium-doped SrTiO3 powders in Z-scheme systems for visible-light-driven photocatalytic overall water splitting, J. Mater. Chem. A 1 (2013) 12327.

[408] L. Ni, M. Tanabe, H. Irie, A visible-light-induced overall water-splitting photocatalyst: conduction-band-controlled silver tantalate, Chem. Commun. 49 (2013) 10094.

[409] K. Maeda, Rhodium-doped barium titanate perovskite as a stable p-Type semiconductor photocatalyst for hydrogen evolution under visible light, ACS Appl. Mater. Interfaces 6 (2014) 2167–2173.

[410] X. Zhou, J. Shi, C. Li, Effect of metal doping on electronic structure and visible light absorption of SrTiO3 and NaTaO3 (Metal = Mn, Fe, and Co), J. Phys. Chem. C 115 (2011) 8305–8311.

[411] M. Li, J. Zhang, W. Dang, S.K. Cushing, D. Guo, N. Wu, P. Yin, Photocatalytic hydrogen generation enhanced by band gap narrowing and improved charge carrier mobility in AgTaO3 by compensated co-doping, Phys. Chem. Chem. Phys. 15 (2013) 16220.

[412] X. Liu, J. Lv, S. Wang, X. Li, J. Lang, Y. Su, Z. Chai, X. Wang, A novel contractive effect of KTaO3 nanocrystals via La3+ doping and an enhanced photocatalytic performance, J. Alloys Compd. 622 (2015) 894–901.

[413] M. Marchelek, B. Bajorowicz, P. Mazierski, A. Cybula, T. Klimczuk, M. Winiarski, N. Fijałkowska, A. Zaleska, KTaO3-based nanocomposites for air treatment, Catal. Today 252 (2015) 47–53.

[414] H. Shi, X. Li, H. Iwai, Z. Zou, J. Ye, 2-Propanol photodegradation over nitrogen-doped NaNbO3 powders under visible-light irradiation, J. Phys. Chem. Solids 70 (2009) 931–935.

[415] Y. Sang, L. Kuai, C. Chen, Z. Fang, B. Geng, Fabrication of a visible-light-driven plasmonic photocatalyst of AgVO3@AgBr@Ag nanobelt heterostructures, ACS Appl. Mater. Interfaces 6 (2014) 5061–5068.

[416] K.M. Parida, K.H. Reddy, S. Martha, D.P. Das, N. Biswal, Fabrication of nano-crystalline LaFeO3: an efficient sol–gel auto-combustion assisted visible light responsive photocatalyst for water decomposition, Int. J. Hydrogen Energy 35 (2010) 12161–12168.

[417] Y.-N. Feng, H.-C. Wang, Y.-D. Luo, Y. Shen, Y.-H. Lin, Ferromagnetic and photocatalytic behaviors observed in Ca-doped BiFeO3 nanofibres, J. Appl. Phys. 113 (2013) 146101.

[418] S. Thirumalairajan, K. Girija, N.Y. Hebalkar, D. Mangalaraj, C. Viswanathan, N. Ponpandian, Shape evolution of perovskite LaFeO3 nanostructures: a systematic investigation of growth mechanism, properties and morphology dependent photocatalytic activities, RSC Adv. 3 (2013) 7549.

[419] S. Thaweesak, M. Lyu, P. Peerakiatkhajohn, T. Butburee, B. Luo, H. Chen, L. Wang, Two-dimensional g-C 3 N 4 /Ca 2 Nb 2 TaO 10 nanosheet composites for efficient visible light photocatalytic hydrogen evolution, Appl. Catal. B 202 (2017) 184–190.

[420] M. Higashi, R. Abe, T. Takata, K. Domen, Photocatalytic overall water splitting under visible light using ATaO2N (A = Ca, Sr, Ba) and WO3 in a IO3 − /I − shuttle redox mediated system, Chem. Mater. 21 (2009) 1543–1549.

[421] D. Jiang, W. Ma, Y. Yao, P. Xiao, B. Wen, D. Li, M. Chen, Dion–Jacobson-type perovskite KCa2Ta3O10 nanosheets hybridized with g-C3N4 nanosheets for photocatalytic H2 production, Catal. Sci. Technol. 8 (2018) 3767–3773.

[422] Z. Chen, P. Sun, B. Fan, Z. Zhang, X. Fang, In situ template-free ion-exchange process to prepare visible-light-active g-C3N4/NiS hybrid photocatalysts with enhanced hydrogen evolution activity, J. Phys. Chem. C 118 (2014) 7801–7807.

[423] J. Wang, Z. Guan, J. Huang, Q. Li, J. Yang, Enhanced photocatalytic mechanism for the hybrid g-C3N4/MoS2 nanocomposite, J. Mater. Chem. A 2 (2014) 7960–7966.

[424] F. Shi, L. Chen, M. Chen, D. Jiang, A g-C3N4/nanocarbon/ZnIn2S4 nanocomposite: an artificial Z-scheme visible-light photocatalytic system using nanocarbon as the electron mediator, Chem. Commun. 51 (2015) 17144–17147.

[425] T. Hisatomi, J. Kubota, K. Domen, Recent advances in semiconductors for photocatalytic and photoelectrochemical water splitting, Chem. Soc. Rev. 43 (2014) 7520–7535.

[426] H. Wang, X. Yuan, H. Wang, X. Chen, Z. Wu, L. Jiang, W. Xiong, Y. Zhang, G. Zeng, One-step calcination method for synthesis of mesoporous g-C3N4/NiTiO3 heterostructure photocatalyst with improved visible light photoactivity, RSC Adv. 5 (2015) 95643–95648.

[427] X. Yang, H. Tang, J. Xu, M. Antonietti, M. Shalom, Silver phosphate/graphitic carbon nitride as an efficient photocatalytic tandem system for oxygen evolution, ChemSusChem 8 (2015) 1350–1358.

[428] D. Zheng, C. Pang, X. Wang, The function-led design of Z-scheme photocatalytic systems based on hollow carbon nitride semiconductors, Chem. Commun. 51 (2015) 17467–17470.

[429] J. Zhang, G. Zhang, X. Chen, S. Lin, L. Möhlmann, G. Dołęga, G. Lipner, M. Antonietti, S. Blechert, X. Wang, Co-monomer control of carbon nitride semiconductors to optimize hydrogen evolution with visible light, Angew. Chem. Int. Ed. 51 (2012) 3183–3187.

[430] D. Zheng, C. Pang, Y. Liu, X. Wang, Shell-engineering of hollow g-C3N4 nanospheres via copolymerization for photocatalytic hydrogen evolution, Chem. Commun. 51 (2015) 9706–9709.

[431] M. Zhang, X. Wang, Two dimensional conjugated polymers with enhanced optical absorption and charge separation for photocatalytic hydrogen evolution, Energy Environ. Sci. 7 (2014) 1902.

[432] X. Zhang, B. Peng, S. Zhang, T. Peng, Robust wide visible-light-responsive photoactivity for H2 production over a polymer/polymer heterojunction photocatalyst: the significance of sacrificial reagent, ACS Sustain. Chem. Eng. 3 (2015) 1501–1509.

[433] J. Zhang, X. Chen, K. Takanabe, K. Maeda, K. Domen, J.D. Epping, X. Fu, M. Antonietti, X. Wang, Synthesis of a carbon nitride structure for visible-light catalysis by copolymerization, Angew. Chem. Int. Ed. 49 (2009) 441–444.

[434] J. Zhang, M. Zhang, S. Lin, X. Fu, X. Wang, Molecular doping of carbon nitride photocatalysts with tunable bandgap and enhanced activity, J. Catal. 310 (2014) 24–30.

[435] Y. Sui, J. Liu, Y. Zhang, X. Tian, W. Chen, Dispersed conductive polymer nanoparticles on graphitic carbon nitride for enhanced solar-driven hydrogen evolution from pure water, Nanoscale 5 (2013) 9150.

[436] W. Chen, T.-Y. Liu, T. Huang, X.-H. Liu, G.-R. Duan, X.-J. Yang, S.-M. Chen, A novel yet simple strategy to fabricate visible light responsive C,N-TiO2/g-C3N4 heterostructures with significantly enhanced photocatalytic hydrogen generation, RSC Adv. 5 (2015) 101214–101220.

[437] X.-W. Song, H.-M. Wen, C.-B. Ma, H.-H. Cui, H. Chen, C.-N. Chen, Efficient photocatalytic hydrogen evolution with end-group-functionalized cobaloxime catalysts in combination with graphite-like C3N4, RSC Adv. 4 (2014) 18853–18861.

[438] D. Wang, Y. Zhang, W. Chen, A novel nickel–thiourea–triethylamine complex adsorbed on graphitic C3N4 for low-cost solar hydrogen production, Chem. Commun. 50 (2014) 1754.

[439] J. Zhang, Y. Wang, J. Jin, J. Zhang, Z. Lin, F. Huang, J. Yu, Efficient visible-light photocatalytic hydrogen evolution and enhanced photostability of core/shell CdS/g-C3N4 nanowires, ACS Appl. Mater. Interfaces 5 (2013) 10317–10324.

[440] L. Liu, Y. Qi, J. Hu, Y. Liang, W. Cui, Efficient visible-light photocatalytic hydrogen evolution and enhanced photostability of core@shell Cu2O@g-C3N4 octahedra, Appl. Surf. Sci. 351 (2015) 1146–1154.

[441] S.-W. Cao, Y.-P. Yuan, J. Barber, S.C.J. Loo, C. Xue, Noble-metal-free g-C3N4/Ni (dmgH)2 composite for efficient photocatalytic hydrogen evolution under visible light irradiation, Appl. Surf. Sci. 319 (2014) 344–349.

[442] J. Zhang, M. Zhang, R.-Q. Sun, X. Wang, A facile band alignment of polymeric carbon nitride semiconductors to construct isotype heterojunctions, Angew. Chem. Int. Ed. 51 (2012) 10145–10149.

[443] L. Ge, C. Han, X. Xiao, L. Guo, In situ synthesis of cobalt–phosphate (Co–Pi) modified g-C3N4 photocatalysts with enhanced photocatalytic activities, Appl. Catal. B 142-143 (2013) 414–422.

[444] R.-L. Lee, P.D. Tran, S.S. Pramana, S.Y. Chiam, Y. Ren, S. Meng, L.H. Wong, J. Barber, Assembling graphitic-carbon-nitride with cobalt-oxide-phosphate to construct an efficient hybrid photocatalyst for water splitting application, Catal. Sci. Technol. 3 (2013) 1694.

[445] Y. Zhu, Y. Xu, Y. Hou, Z. Ding, X. Wang, Cobalt sulfide modified graphitic carbon nitride semiconductor for solar hydrogen production, Int. J. Hydrogen Energy 39 (2014) 11873–11879.

[446] F. He, G. Chen, Y. Yu, Y. Zhou, Y. Zheng, S. Hao, The synthesis of condensed C-PDA–g-C3N4 composites with superior photocatalytic performance, Chem. Commun. 51 (2015) 6824–6827.

[447] X. Xia, N. Deng, G. Cui, J. Xie, X. Shi, Y. Zhao, Q. Wang, W. Wang, B. Tang, NIR light induced H2 evolution by a metal-free photocatalyst, Chem. Commun. 51 (2015) 10899–10902.

[448] X. Zhou, Z. Luo, P. Tao, B. Jin, Z. Wu, Y. Huang, Facile preparation and enhanced photocatalytic H2-production activity of Cu(OH)2 nanospheres modified porous g-C3N4, Mater. Chem. Phys. 143 (2014) 1462–1468.

[449] W. Wang, J.C. Yu, Z. Shen, D.K.L. Chan, T. Gu, g-C3N4 quantum dots: direct synthesis, upconversion properties and photocatalytic application, Chem. Commun. 50 (2014) 10148–10150.

[450] C.A. Caputo, M.A. Gross, V.W. Lau, C. Cavazza, B.V. Lotsch, E. Reisner, Photocatalytic hydrogen production using polymeric carbon nitride with a hydrogenase and a bioinspired synthetic Ni catalyst, Angew. Chem. Int. Ed. 53 (2014) 11538–11542.

[451] H. Gao, S. Yan, J. Wang, Z. Zou, Ion coordination significantly enhances the photocatalytic activity of graphitic-phase carbon nitride, Dalton Trans. 43 (2014) 8178–8183.

[452] J. Wen, X. Li, H. Li, S. Ma, K. He, Y. Xu, Y. Fang, W. Liu, Q. Gao, Enhanced visible-light H2 evolution of g-C3N4 photocatalysts via the synergetic effect of amorphous

NiS and cheap metal-free carbon black nanoparticles as co-catalysts, Appl. Surf. Sci. 358 (2015) 204–212.

[453] J. Chen, D. Zhao, Z. Diao, M. Wang, L. Guo, S. Shen, Bifunctional modification of graphitic carbon nitride with MgFe2O4 for enhanced photocatalytic hydrogen generation, ACS Appl. Mater. Interfaces 7 (2015) 18843–18848.

[454] A. Suryawanshi, P. Dhanasekaran, D. Mhamane, S. Kelkar, S. Patil, N. Gupta, S. Ogale, Doubling of photocatalytic H2 evolution from g-C3N4 via its nano-composite formation with multiwall carbon nanotubes: electronic and morpho-logical effects, Int. J. Hydrogen Energy 37 (2012) 9584–9589.

[455] P. Niu, L. Zhang, G. Liu, H.-M. Cheng, Graphene-like carbon nitride nanosheets for improved photocatalytic activities, Adv. Funct. Mater. 22 (2012) 4763–4770.

[456] X.L. Wang, W.Q. Fang, H.F. Wang, H. Zhang, H. Zhao, Y. Yao, H.G. Yang, Surface hydrogen bonding can enhance photocatalytic H2 evolution efficiency, J. Mater. Chem. A 1 (2013) 14089.

[457] J. Xu, L. Zhang, R. Shi, Y. Zhu, Chemical exfoliation of graphitic carbon nitride for efficient heterogeneous photocatalysis, J. Mater. Chem. A 1 (2013) 14766.

[458] Z. Jiang, D. Jiang, Z. Yan, D. Liu, K. Qian, J. Xie, A new visible light active mul-tifunctional ternary composite based on TiO2–In2O3 nanocrystals heterojunction decorated porous graphitic carbon nitride for photocatalytic treatment of ha-zardous pollutant and H2 evolution, Appl. Catal. B 170-171 (2015) 195–205.

[459] R. Wang, L. Gu, J. Zhou, X. Liu, F. Teng, C. Li, Y. Shen, Y. Yuan, Quasi-polymeric metal-organic framework UiO-66/g-C3N4Heterojunctions for enhanced photo-catalytic hydrogen evolution under visible light irradiation, Adv. Mater. Interfaces 2 (2015) 1500037.

[460] G. Zhao, X. Huang, F. Fina, G. Zhang, J.T.S. Irvine, Facile structure design based on C3N4 for mediator-free Z-scheme water splitting under visible light, Catal. Sci. Technol. 5 (2015) 3416–3422.

[461] Y. Hou, Y. Zhu, Y. Xu, X. Wang, Photocatalytic hydrogen production over carbon nitride loaded with WS2 as cocatalyst under visible light, Appl. Catal. B 156-157 (2014) 122–127.

[462] J. Chen, S. Shen, P. Guo, P. Wu, L. Guo, Spatial engineering of photo-active sites on g-C3N4 for efficient solar hydrogen generation, J. Mater. Chem. A 2 (2014) 4605.

[463] X. Zhang, L. Yu, C. Zhuang, T. Peng, R. Li, X. Li, Highly asymmetric phthalocya-nine as a sensitizer of graphitic carbon nitride for extremely efficient photo-catalytic H2 production under near-infrared light, ACS Catal. 4 (2013) 162–170.

[464] B. Hu, F. Cai, T. Chen, M. Fan, C. Song, X. Yan, W. Shi, Hydrothermal synthesis g-C3N4/Nano-InVO4 nanocomposites and enhanced photocatalytic activity for hy-drogen production under visible light irradiation, ACS Appl. Mater. Interfaces 7 (2015) 18247–18256.

[465] J. Chen, S. Shen, P. Wu, L. Guo, Nitrogen-doped CeOx nanoparticles modified graphitic carbon nitride for enhanced photocatalytic hydrogen production, Green Chem. 17 (2015) 509–517.

[466] Z. Hong, B. Shen, Y. Chen, B. Lin, B. Gao, Enhancement of photocatalytic H2 evolution over nitrogen-deficient graphitic carbon nitride, J. Mater. Chem. A 1 (2013) 11754.

[467] Y. Hou, A.B. Laursen, J. Zhang, G. Zhang, Y. Zhu, X. Wang, S. Dahl, I. Chorkendorff, Layered nanojunctions for hydrogen-evolution catalysis, Angew. Chem. Int. Ed. 52 (2013) 3621–3625.

[468] L. Ge, C. Han, X. Xiao, L. Guo, Synthesis and characterization of composite visible light active photocatalysts MoS2–g-C3N4 with enhanced hydrogen evolution ac-tivity, Int. J. Hydrogen Energy 38 (2013) 6960–6969.

[469] X. Ding, Y. Li, J. Zhao, Y. Zhu, Y. Li, W. Deng, C. Wang, Enhanced photocatalytic H2 evolution over CdS/Au/g-C3N4 composite photocatalyst under visible-light irradiation, APL Mater. 3 (2015) 104410.

[470] L. Ge, C. Han, J. Liu, Y. Li, Enhanced visible light photocatalytic activity of novel polymeric g-C3N4 loaded with Ag nanoparticles, Appl. Catal. A Gen. 409-410 (2011) 215–222.

[471] M. Wu, J.-M. Yan, X.-W. Zhang, M. Zhao, Q. Jiang, Ag2O modified g-C3N4 for highly efficient photocatalytic hydrogen generation under visible light irradiation, J. Mater. Chem. A 3 (2015) 15710–15714.

[472] Y. Di, X. Wang, A. Thomas, M. Antonietti, Making metal-carbon nitride hetero-junctions for improved photocatalytic hydrogen evolution with visible light, ChemCatChem 2 (2010) 834–838.

[473] J. Yu, S. Wang, B. Cheng, Z. Lin, F. Huang, Noble metal-free Ni(OH)2–g-C3N4 composite photocatalyst with enhanced visible-light photocatalytic H2-production activity, Catal. Sci. Technol. 3 (2013) 1782.

[474] J. Dong, M. Wang, X. Li, L. Chen, Y. He, L. Sun, Simple nickel-based catalyst systems combined with graphitic carbon nitride for stable photocatalytic hydrogen production in water, ChemSusChem 5 (2012) 2133–2138.

[475] Z. Yan, Z. Sun, X. Liu, H. Jia, P. Du, Cadmium sulfide/graphitic carbon nitride heterostructure nanowire loading with a nickel hydroxide cocatalyst for highly efficient photocatalytic hydrogen production in water under visible light, Nanoscale 8 (2016) 4748–4756.

[476] Y. Chen, B. Lin, W. Yu, Y. Yang, S.M. Bashir, H. Wang, K. Takanabe, H. Idriss, J.-M. Basset, Surface functionalization of g-C3N4: molecular-level design of noble-metal-free hydrogen evolution photocatalysts, Chem. Eur. J. 21 (2015) 10290–10295.

[477] G. Zhang, G. Li, X. Wang, Surface modification of carbon nitride polymers by core-shell Nickel/Nickel oxide cocatalysts for hydrogen evolution photocatalysis, ChemCatChem 7 (2015) 2864–2870.

[478] Y. Lu, D. Chu, M. Zhu, Y. Du, P. Yang, Exfoliated carbon nitride nanosheets de-corated with NiS as an efficient noble-metal-free visible-light-driven photocatalyst for hydrogen evolution, J. Chem. Soc. Faraday Trans. 17 (2015) 17355–17361.

[479] J. Hong, Y. Wang, Y. Wang, W. Zhang, R. Xu, Noble-metal-Free NiS/C3N4for ef-ficient photocatalytic hydrogen evolution from water, ChemSusChem 6 (2013) 2263–2268.

[480] Y. Zhong, J. Yuan, J. Wen, X. Li, Y. Xu, W. Liu, S. Zhang, Y. Fang, Earth-abundant NiS co-catalyst modified metal-free mpg-C3N4/CNT nanocomposites for highly efficient visible-light photocatalytic H2 evolution, J. Chem. Soc. Dalton Trans. 44 (2015) 18260–18269.

[481] L. Yin, Y.-P. Yuan, S.-W. Cao, Z. Zhang, C. Xue, Enhanced visible-light-driven photocatalytic hydrogen generation over g-C3N4 through loading the noble metal-free NiS2 cocatalyst, RSC Adv. 4 (2014) 6127.

[482] S. Obregón, G. Colón, Improved H2 production of Pt-TiO2/g-C3N4-MnOx com-posites by an efficient handling of photogenerated charge pairs, Appl. Catal. B 144 (2014) 775–782.

[483] H. Yan, Y. Huang, Polymer composites of carbon nitride and poly(3-hex-ylthiophene) to achieve enhanced hydrogen production from water under visible light, Chem. Commun. 47 (2011) 4168.

[484] S. Chu, Y. Wang, Y. Guo, J. Feng, C. Wang, W. Luo, X. Fan, Z. Zou, Band structure engineering of carbon nitride: in search of a polymer photocatalyst with high photooxidation property, ACS Catal. 3 (2013) 912–919.

[485] J. Chen, Z. Hong, Y. Chen, B. Lin, B. Gao, One-step synthesis of sulfur-doped and nitrogen-deficient g-C3N4 photocatalyst for enhanced hydrogen evolution under visible light, Mater. Lett. 145 (2015) 129–132.

[486] L. Ge, C. Han, X. Xiao, L. Guo, Y. Li, Enhanced visible light photocatalytic hy-drogen evolution of sulfur-doped polymeric g-C3N4 photocatalysts, Mater. Res. Bull. 48 (2013) 3919–3925.

[487] J. Zhang, J. Sun, K. Maeda, K. Domen, P. Liu, M. Antonietti, X. Fu, X. Wang, Sulfur-mediated synthesis of carbon nitride: band-gap engineering and improved func-tions for photocatalysis, Energy Environ. Sci. 4 (2011) 675–678.

[488] P. Niu, G. Liu, H.-M. Cheng, Nitrogen vacancy-promoted photocatalytic activity of graphitic carbon nitride, J. Phys. Chem. C 116 (2012) 11013–11018.

[489] M. Wu, J.-M. Yan, X.-n. Tang, M. Zhao, Q. Jiang, Synthesis of potassium-modified graphitic carbon nitride with high photocatalytic activity for hydrogen evolution, ChemSusChem 7 (2014) 2654–2658.

[490] H. Wang, X. Zhang, J. Xie, J. Zhang, P. Ma, B. Pan, Y. Xie, Structural distortion in graphitic-C3N4 realizing an efficient photoreactivity, Nanoscale 7 (2015) 5152–5156.

[491] S. Hu, L. Ma, J. You, F. Li, Z. Fan, G. Lu, D. Liu, J. Gui, Enhanced visible light photocatalytic performance of g-C3N4 photocatalysts co-doped with iron and phosphorus, Appl. Surf. Sci. 311 (2014) 164–171.

[492] Z. Wu, H. Gao, S. Yan, Z. Zou, Synthesis of carbon black/carbon nitride inter-calation compound composite for efficient hydrogen production, Dalton Trans. 43 (2014) 12013–12017.

[493] L. Jing, R. Zhu, D.L. Phillips, J.C. Yu, Photocatalysis: effective prevention of charge trapping in graphitic carbon nitride with nanosized red phosphorus modification for superior photo(electro)catalysis (Adv. Funct. Mater. 46/2017), Adv. Funct. Mater. 27 (2017).

[494] J. Feng, D. Zhang, H. Zhou, M. Pi, X. Wang, S. Chen, Coupling P nanostructures with P-Doped g-C3N4 As efficient visible light photocatalysts for H2 evolution and RhB degradation, ACS Sustain. Chem. Eng. 6 (2018) 6342–6349.

[495] Z.-A. Lan, G. Zhang, X. Wang, A facile synthesis of Br-modified g-C 3 N 4 semi-conductors for photoredox water splitting, Appl. Catal. B 192 (2016) 116–125.

[496] Y. Zhou, L. Zhang, W. Huang, Q. Kong, X. Fan, M. Wang, J. Shi, N-doped graphitic carbon-incorporated g-C 3 N 4 for remarkably enhanced photocatalytic H 2 evo-lution under visible light, Carbon 99 (2016) 111–117.

[497] W.J. Youngblood, S.-H.A. Lee, K. Maeda, T.E. Mallouk, Visible light water splitting using dye-sensitized oxide semiconductors, Acc. Chem. Res. 42 (2009) 1966–1973.

[498] S.G. Kumar, L.G. Devi, Review on modified TiO2Photocatalysis under UV/Visible light: selected results and related mechanisms on interfacial charge carrier transfer dynamics, J. Phys. Chem. A 115 (2011) 13211–13241.

[499] K. Maeda, M. Eguchi, W.J. Youngblood, T.E. Mallouk, Niobium oxide nanoscrolls as building blocks for dye-sensitized hydrogen production from water under visible light irradiation, Chem. Mater. 20 (2008) 6770–6778.

[500] W.-S. Han, K.-R. Wee, H.-Y. Kim, C. Pac, Y. Nabetani, D. Yamamoto, T. Shimada, H. Inoue, H. Choi, K. Cho, S.O. Kang, Hydrophilicity control of visible-light hy-drogen evolution and dynamics of the charge-separated state in Dye/TiO2/Pt hybrid systems, Chem. Eur. J. 18 (2012) 15368–15381.

[501] P.A. Sant, P.V. Kamat, Interparticle electron transfer between size-quantized CdS and TiO2 semiconductor nanoclusters dedicated to Professor Frank Wilkinson on the occasion of his retirement, J. Chem. Soc. Faraday Trans. 4 (2002) 198–203.

[502] J. Hensel, G. Wang, Y. Li, J.Z. Zhang, Synergistic effect of CdSe quantum dot sensitization and nitrogen doping of TiO2Nanostructures for photoelectrochemical solar hydrogen generation, Nano Lett. 10 (2010) 478–483.

[503] G. Wang, X. Yang, F. Qian, J.Z. Zhang, Y. Li, Double-sided CdS and CdSe quantum dot Co-sensitized ZnO nanowire arrays for photoelectrochemical hydrogen gen-eration, Nano Lett. 10 (2010) 1088–1092.

[504] Y. Wang, J. Hong, W. Zhang, R. Xu, Carbon nitride nanosheets for photocatalytic hydrogen evolution: remarkably enhanced activity by dye sensitization, Catal. Sci. Technol. 3 (2013) 1703.

[505] J. Xu, Y. Li, S. Peng, G. Lu, S. Li, Eosin Y-sensitized graphitic carbon nitride fab-ricated by heating urea for visible light photocatalytic hydrogen evolution: the effect of the pyrolysis temperature of urea, J. Chem. Soc. Faraday Trans. 15 (2013) 7657.

[506] P. Zhang, T. Wang, H. Zeng, Design of Cu-Cu 2 O/g-C 3 N 4 nanocomponent photocatalysts for hydrogen evolution under visible light irradiation using water-soluble Erythrosin B dye sensitization, Appl. Surf. Sci. 391 (2017) 404–414.

[507] P. Wang, Z. Guan, Q. Li, J. Yang, Efficient visible-light-driven photocatalytic hy-drogen production from water by using Eosin Y-sensitized novel g-C3N4/Pt/GO composites, J. Mater. Sci. 53 (2017) 774–786.

[508] P. Wang, L. Zong, Z. Guan, Q. Li, J. Yang, PtNi alloy cocatalyst modification of

eosin Y-Sensitized g-C3N4/GO hybrid for efficient visible-light photocatalytic hydrogen evolution, Nanoscale Res. Lett. 13 (2018).

[509] K. Chang, Z. Mei, T. Wang, Q. Kang, S. Ouyang, J. Ye, MoS2/Graphene cocatalyst for efficient photocatalytic H2 evolution under visible light irradiation, ACS Nano 8 (2014) 7078–7087.

[510] W. Liu, L. Cao, W. Cheng, Y. Cao, X. Liu, W. Zhang, X. Mou, L. Jin, X. Zheng, W. Che, Q. Liu, T. Yao, S. Wei, Single-site active cobalt-based photocatalyst with a long carrier lifetime for spontaneous overall water splitting, Angew. Chem. Int. Ed. 56 (2017) 9312–9317.

[511] K. Li, Z. Zeng, L. Yan, S. Luo, X. Luo, M. Huo, Y. Guo, Fabrication of platinum-deposited carbon nitride nanotubes by a one-step solvothermal treatment strategy and their efficient visible-light photocatalytic activity, Appl. Catal. B 165 (2015) 428–437.

[512] Y. Li, Y. Hu, S. Peng, G. Lu, S. Li, Synthesis of CdS nanorods by an ethylenediamine assisted hydrothermal method for photocatalytic hydrogen evolution, J. Phys. Chem. C 113 (2009) 9352–9358.

[513] W. Fan, Q. Lai, Q. Zhang, Y. Wang, Nanocomposites of TiO2 and reduced graphene oxide as efficient photocatalysts for hydrogen evolution, J. Phys. Chem. C 115 (2011) 10694–10701.

[514] D. Wang, T. Hisatomi, T. Takata, C. Pan, M. Katayama, J. Kubota, K. Domen, Core/shell photocatalyst with spatially separated co-catalysts for efficient reduction and oxidation of water, Angew. Chem. Int. Ed. 52 (2013) 11252–11256.

[515] L. Delannoy, G. Thrimurthulu, P.S. Reddy, C. Méthivier, J. Nelayah, B.M. Reddy, C. Ricolleau, C. Louis, Selective hydrogenation of butadiene over TiO2supported copper, gold and gold–copper catalysts prepared by deposition–precipitation, Phys. Chem. Chem. Phys. 16 (2014) 26514–26527.

[516] M. Wang, Z. Li, Y. Wu, J. Ma, G. Lu, Inhibition of hydrogen and oxygen reverse recombination reaction over Pt/TiO 2 by F − ions and its impact on the photocatalytic hydrogen formation, J. Catal. 353 (2017) 162–170.

[517] C. Chang, Y. Fu, M. Hu, C. Wang, G. Shan, L. Zhu, Photodegradation of bisphenol A by highly stable palladium-doped mesoporous graphite carbon nitride (Pd/mpg-C3N4) under simulated solar light irradiation, Appl. Catal. B 142-143 (2013) 553–560.

[518] Y. Bu, Z. Chen, W. Li, Using electrochemical methods to study the promotion mechanism of the photoelectric conversion performance of Ag-modified mesoporous g-C3N4 heterojunction material, Appl. Catal. B 144 (2014) 622–630.

[519] Y. Guo, L. Zhang, K. Zhou, Y. Shen, Q. Zhang, C. Gu, Selective gold recovery by carbon nitride through photoreduction, J. Mater. Chem. A 2 (2014) 19594–19597.

[520] J. Liu, Y. Yang, N. Liu, Y. Liu, H. Huang, Z. Kang, Total photocatalysis conversion from cyclohexane to cyclohexanone by C3N4/Au nanocomposites, Green Chem. 16 (2014) 4559–4565.

[521] T. Bhowmik, M.K. Kundu, S. Barman, Ultra small gold nanoparticles–graphitic carbon nitride composite: an efficient catalyst for ultrafast reduction of 4-nitrophenol and removal of organic dyes from water, RSC Adv. 5 (2015) 38760–38773.

[522] H. Tian, X.L. Zhang, J. Scott, C. Ng, R. Amal, TiO2-supported copper nanoparticles prepared via ion exchange for photocatalytic hydrogen production, J. Mater. Chem. A 2 (2014) 6432–6438.

[523] D.Y. Chung, J.W. Han, D.-H. Lim, J.-H. Jo, S.J. Yoo, H. Lee, Y.-E. Sung, Structure dependent active sites of NixSy as electrocatalysts for hydrogen evolution reaction, Nanoscale 7 (2015) 5157–5163.

[524] C. Tang, Z. Pu, Q. Liu, A.M. Asiri, X. Sun, NiS2 nanosheets array grown on carbon cloth as an efficient 3D hydrogen evolution cathode, Electrochim. Acta 153 (2015) 508–514.

[525] N. Jiang, Q. Tang, M. Sheng, B. You, D.-e. Jiang, Y. Sun, Nickel sulfides for electrocatalytic hydrogen evolution under alkaline conditions: a case study of crystalline NiS, NiS2, and Ni3S2 nanoparticles, Catal. Sci. Technol. 6 (2016) 1077–1084.

[526] H. Zhao, H. Zhang, G. Cui, Y. Dong, G. Wang, P. Jiang, X. Wu, N. Zhao, A photochemical synthesis route to typical transition metal sulfides as highly efficient cocatalyst for hydrogen evolution: from the case of NiS/g-C 3 N 4, Appl. Catal. B 225 (2018) 284–290.

[527] A.Z. Moshfegh, Nanoparticle catalysts, J. Phys. D Appl. Phys. 42 (2009) 233001.

[528] Q. Liu, Y. Chai, L. Zhang, J. Ren, W.-L. Dai, Highly efficient Pt/NaNbO 3 nanowire photocatalyst: its morphology effect and application in water purification and H 2 production, Appl. Catal. B 205 (2017) 505–513.

[529] A. Naseri, M. Samadi, A. Pourjavadi, A.Z. Moshfegh, S. Ramakrishna, Graphitic carbon nitride (g-C3N4)-based photocatalysts for solar hydrogen generation: recent advances and future development directions, J. Mater. Chem. A 5 (2017) 23406–23433.

[530] T. An, J. Tang, Y. Zhang, Y. Quan, X. Gong, A.M. Al-Enizi, A.A. Elzatahry, L. Zhang, G. Zheng, Photoelectrochemical conversion from graphitic C3N4 quantum dot decorated semiconductor nanowires, ACS Appl. Mater. Interfaces 8 (2016) 12772–12779.

[531] C.X. Guo, Y. Dong, H.B. Yang, C.M. Li, Graphene quantum dots as a green sensitizer to functionalize ZnO nanowire arrays on F-Doped SnO2Glass for enhanced photoelectrochemical water splitting, Adv. Energy Mater. 3 (2013) 997–1003.

[532] T. Wang, X. Liu, Q. Men, C. Ma, Y. Liu, Z. Liu, P. Huo, C. Li, Y. Yan, Green synthesis g-C 3 N 4 quantum dots loading h-BN for efficient and stable photocatalytic performance, J. Mol. Liq. 268 (2018) 561–568.

[533] G. Cai, J. Wang, X. Wu, Y. Zhan, S. Liang, Scalable one-pot synthesis of porous 0D/2D C 3 N 4 nanocomposites for efficient visible-light driven photocatalytic hydrogen evolution, Appl. Surf. Sci. 459 (2018) 224–232.

[534] R.C. Pawar, S. Kang, J.H. Park, J.-h. Kim, S. Ahn, C.S. Lee, Room-temperature synthesis of nanoporous 1D microrods of graphitic carbon nitride (g-C3N4) with highly enhanced photocatalytic activity and stability, Sci. Rep. 6 (2016).

[535] Z. Zeng, K. Li, L. Yan, Y. Dai, H. Guo, M. Huo, Y. Guo, Fabrication of carbon nitride nanotubes by a simple water-induced morphological transformation process and their efficient visible-light photocatalytic activity, RSC Adv. 4 (2014) 59513–59518.

[536] Y. Zeng, X. Liu, C. Liu, L. Wang, Y. Xia, S. Zhang, S. Luo, Y. Pei, Scalable one-step production of porous oxygen-doped g-C 3 N 4 nanorods with effective electron separation for excellent visible-light photocatalytic activity, Appl. Catal. B 224 (2018) 1–9.

[537] Z. You, Y. Su, Y. Yu, H. Wang, T. Qin, F. Zhang, Q. Shen, H. Yang, Preparation of g-C 3 N 4 nanorod/InVO 4 hollow sphere composite with enhanced visible-light photocatalytic activities, Appl. Catal. B 213 (2017) 127–135.

[538] L. Yao, D. Wei, Y. Ni, D. Yan, C. Hu, Surface localization of CdZnS quantum dots onto 2D g -C 3 N 4 ultrathin microribbons: highly efficient visible light-induced H 2 -generation, Nano Energy 26 (2016) 248–256.

[539] D. Jiang, J. Li, C. Xing, Z. Zhang, S. Meng, M. Chen, Two-dimensional CaIn2S4/g-C3N4 heterojunction nanocomposite with enhanced visible-light photocatalytic activities: interfacial engineering and mechanism insight, ACS Appl. Mater. Interfaces 7 (2015) 19234–19242.

[540] K. Zhang, Y. Zhang, W. Zhang, Ultrathin hexagonal SnS2 nanosheets coupled with tetragonal CuInS2 nanosheets as 2D/2D heterojunction photocatalysts toward high visible-light photocatalytic activity and stability, Catal. Letters 148 (2018) 1990–2000.

[541] T.-F. Yeh, J.-M. Syu, C. Cheng, T.-H. Chang, H. Teng, Graphite oxide as a photocatalyst for hydrogen production from water, Adv. Funct. Mater. 20 (2010) 2255–2262.

[542] R. Cheng, L. Zhang, X. Fan, M. Wang, M. Li, J. Shi, One-step construction of FeO x modified g-C 3 N 4 for largely enhanced visible-light photocatalytic hydrogen evolution, Carbon 101 (2016) 62–70.

[543] M. Li, L. Zhang, X. Fan, M. Wu, Y. Du, M. Wang, Q. Kong, L. Zhang, J. Shi, Dual synergetic effects in MoS 2 /pyridine-modified g-C 3 N 4 composite for highly active and stable photocatalytic hydrogen evolution under visible light, Appl. Catal. B 190 (2016) 36–43.

[544] H. Liu, Z. Xu, Z. Zhang, D. Ao, Highly efficient photocatalytic H 2 evolution from water over CdLa 2 S 4 /mesoporous g-C 3 N 4 hybrids under visible light irradiation, Appl. Catal. B 192 (2016) 234–241.

[545] H. Liu, Z. Xu, Z. Zhang, D. Ao, Novel visible-light driven Mn 0.8 Cd 0.2 S/g-C 3 N 4 composites: preparation and efficient photocatalytic hydrogen production from water without noble metals, Appl. Catal. A Gen. 518 (2016) 150–157.

[546] R. Ye, H. Fang, Y.-Z. Zheng, N. Li, Y. Wang, X. Tao, Fabrication of CoTiO3/g-C3N4 hybrid photocatalysts with enhanced H2 evolution: Z-scheme photocatalytic mechanism insight, ACS Appl. Mater. Interfaces 8 (2016) 13879–13889.

[547] D. Zheng, G. Zhang, Y. Hou, X. Wang, Layering MoS 2 on soft hollow g-C 3 N 4 nanostructures for photocatalytic hydrogen evolution, Appl. Catal. A Gen. 521 (2016) 2–8.

[548] T. Chen, C. Song, M. Fan, Y. Hong, B. Hu, L. Yu, W. Shi, In-situ fabrication of CuS/g-C 3 N 4 nanocomposites with enhanced photocatalytic H 2 -production activity via photoinduced interfacial charge transfer, Int. J. Hydrogen Energy 42 (2017) 12210–12219.

[549] F. Cheng, H. Yin, Q. Xiang, Low-temperature solid-state preparation of ternary CdS/g-C 3 N 4 /CuS nanocomposites for enhanced visible-light photocatalytic H 2 -production activity, Appl. Surf. Sci. 391 (2017) 432–439.

[550] X. Fang, J. Song, H. Shi, S. Kang, Y. Li, G. Sun, L. Cui, Enhanced efficiency and stability of Co 0.5 Cd 0.5 S/g-C 3 N 4 composite photo-catalysts for hydrogen evolution from water under visible light irradiation, Int. J. Hydrogen Energy 42 (2017) 5741–5748.

[551] Q.-Z. Huang, J.-C. Wang, P.-P. Wang, H.-C. Yao, Z.-J. Li, In-situ growth of mesoporous Nb 2 O 5 microspheres on g-C 3 N 4 nanosheets for enhanced photocatalytic H 2 evolution under visible light irradiation, Int. J. Hydrogen Energy 42 (2017) 6683–6694.

[552] D. Li, F. Shi, D. Jiang, M. Chen, W. Shi, CdIn2S4/g-C3N4 heterojunction photocatalysts: enhanced photocatalytic performance and charge transfer mechanism, RSC Adv. 7 (2017) 231–237.

[553] Z. Mao, J. Chen, Y. Yang, D. Wang, L. Bie, B.D. Fahlman, Novel g-C3N4/CoO nanocomposites with significantly enhanced visible-light photocatalytic activity for H2 evolution, ACS Appl. Mater. Interfaces 9 (2017) 12427–12435.

[554] B. Wang, J. Zhang, F. Huang, Enhanced visible light photocatalytic H 2 evolution of metal-free g-C 3 N 4 /SiC heterostructured photocatalysts, Appl. Surf. Sci. 391 (2017) 449–456.

[555] J. Zhang, S. Liu, J. Yu, M. Jaroniec, A simple cation exchange approach to Bi-doped ZnS hollow spheres with enhanced UV and visible-light photocatalytic H2-production activity, J. Mater. Chem. 21 (2011) 14655.

[556] J. Zhang, J. Yu, Y. Zhang, Q. Li, J.R. Gong, Visible light photocatalytic H2-production activity of CuS/ZnS porous nanosheets based on photoinduced interfacial charge transfer, Nano Lett. 11 (2011) 4774–4779.

[557] J. Zhang, J. Yu, M. Jaroniec, J.R. Gong, Noble metal-free reduced graphene oxide-ZnxCd1−xS nanocomposite with enhanced solar photocatalytic H2-Production performance, Nano Lett. 12 (2012) 4584–4589.

[558] Q. Li, X. Li, S. Wageh, A.A. Al-Ghamdi, J. Yu, CdS/graphene nanocomposite photocatalysts, Adv. Energy Mater. 5 (2015) 1500010.

[559] E. Huang, X. Yao, W. Wang, G. Wu, N. Guan, L. Li, SnS2Nanoplates with specific facets exposed for enhanced visible-light-driven photocatalysis, ChemPhotoChem 1 (2016) 60–69.

[560] L. Jing, Y. Xu, Z. Chen, M. He, M. Xie, J. Liu, H. Xu, S. Huang, H. Li, Different morphologies of SnS2 supported on 2D g-C3N4 for excellent and stable visible light photocatalytic hydrogen generation, ACS Sustain. Chem. Eng. 6 (2018) 5132–5141.

[561] Y. Li, R. Jin, Y. Xing, J. Li, S. Song, X. Liu, M. Li, R. Jin, Macroscopic foam-like holey ultrathin g-C3N4Nanosheets for drastic improvement of visible-light pho-tocatalytic activity, Adv. Energy Mater. 6 (2016) 1601273.

[562] S. Yang, Y. Gong, J. Zhang, L. Zhan, L. Ma, Z. Fang, R. Vajtai, X. Wang, P.M. Ajayan, Exfoliated graphitic carbon nitride nanosheets as efficient catalysts for hydrogen evolution under visible light, Adv. Mater. 25 (2013) 2452–2456.

[563] J. Tong, L. Zhang, F. Li, K. Wang, L. Han, S. Cao, Rapid and high-yield production of g-C3N4 nanosheets via chemical exfoliation for photocatalytic H2 evolution, RSC Adv. 5 (2015) 88149–88153.

[564] Q. Han, B. Wang, J. Gao, Z. Cheng, Y. Zhao, Z. Zhang, L. Qu, Atomically thin mesoporous nanomesh of graphitic C3N4 for high-efficiency photocatalytic hy-drogen evolution, ACS Nano 10 (2016) 2745–2751.

[565] T. Rodenas, I. Luz, G. Prieto, B. Seoane, H. Miro, A. Corma, F. Kapteijn, F.X. Llabrés i Xamena, J. Gascon, Metal–organic framework nanosheets in polymer composite materials for gas separation, Nat. Mater. 14 (2014) 48–55.

[566] T. Wang, X. Meng, P. Li, S. Ouyang, K. Chang, G. Liu, Z. Mei, J. Ye, Photoreduction of CO 2 over the well-crystallized ordered mesoporous TiO 2 with the confined space effect, Nano Energy 9 (2014) 50–60.

[567] J. Lin, Z. Pan, X. Wang, Photochemical reduction of CO2 by graphitic carbon ni-tride polymers, ACS Sustain. Chem. Eng. 2 (2013) 353–358.

[568] J. Wang, C. Zhang, Y. Shen, Z. Zhou, J. Yu, Y. Li, W. Wei, S. Liu, Y. Zhang, Environment-friendly preparation of porous graphite-phase polymeric carbon ni-tride using calcium carbonate as templates, and enhanced photoelectrochemical activity, J. Mater. Chem. A 3 (2015) 5126–5131.

[569] D. Zheng, X.-N. Cao, X. Wang, Precise formation of a hollow carbon nitride structure with a Janus surface to promote water splitting by photoredox catalysis, Angew. Chem. Int. Ed. 55 (2016) 11512–11516.